(12) INTERNATIONAL APPLICATION PUBLISHED UNDER THE PATENT COOPERATION TREATY (PCT)

(19) World Intellectual Property Organization
International Bureau

(43) International Publication Date
08 August 2024 (08.08.2024)

WIPO | PCT

(10) International Publication Number
WO 2024/163543 A1

(51) International Patent Classification:
B01J 20/22 (2006.01) *C01B 3/50* (2006.01)
B01D 53/02 (2006.01) *C07F 5/06* (2006.01)
B01J 20/28 (2006.01) *F17C 11/00* (2006.01)
C01B 3/00 (2006.01) *B01D 59/00* (2006.01)

(21) International Application Number:
PCT/US2024/013659

(22) International Filing Date:
31 January 2024 (31.01.2024)

(25) Filing Language: English

(26) Publication Language: English

(30) Priority Data:
63/442,398 31 January 2023 (31.01.2023) US

(71) Applicant: **GOVERNMENT OF THE UNITED STATES OF AMERICA, AS REPRESENTED BY THE SECRETARY OF COMMERCE** [US/US]; National Institute of Standards and Technology, 100 Bureau Drive, MS 1052, Gaithersburg, Maryland 20899 (US).

(72) Inventors: **EVANS, Hayden Aled**; National Institute of Standards and Technology, 100 Bureau Drive, MS 1052, Gaithersburg, Maryland 20899 (US). **YILDIRIM, Taner**; National Institute of Standards and Technology, 100 Bureau Drive, MS 1052, Gaithersburg, Maryland 20899 (US). **BROWN, Craig Martin**; National Institute of Standards and Technology, 100 Bureau Drive, MS 1052, Gaithersburg, Maryland 20899 (US).

(74) Agent: **HAIN, Toby D.**; National Institute of Standards and Technology, 100 Bureau Drive, MS 1052, Gaithersburg, Maryland 20899 (US).

(81) Designated States *(unless otherwise indicated, for every kind of national protection available)*: AE, AG, AL, AM, AO, AT, AU, AZ, BA, BB, BG, BH, BN, BR, BW, BY, BZ, CA, CH, CL, CN, CO, CR, CU, CV, CZ, DE, DJ, DK, DM, DO, DZ, EC, EE, EG, ES, FI, GB, GD, GE, GH, GM, GT, HN, HR, HU, ID, IL, IN, IQ, IR, IS, IT, JM, JO, JP, KE, KG, KH, KN, KP, KR, KW, KZ, LA, LC, LK, LR, LS, LU, LY, MA, MD, MG, MK, MN, MU, MW, MX, MY, MZ, NA, NG, NI, NO, NZ, OM, PA, PE, PG, PH, PL, PT, QA, RO, RS, RU, RW, SA, SC, SD, SE, SG, SK, SL, ST, SV, SY, TH, TJ, TM, TN, TR, TT, TZ, UA, UG, US, UZ, VC, VN, WS, ZA, ZM, ZW.

(84) Designated States *(unless otherwise indicated, for every kind of regional protection available)*: ARIPO (BW, CV, GH, GM, KE, LR, LS, MW, MZ, NA, RW, SC, SD, SL, ST,

(54) Title: HYDROGEN FUEL MEMBER COMPRISING A MOF FOR STORING MOLECULAR HYDROGEN

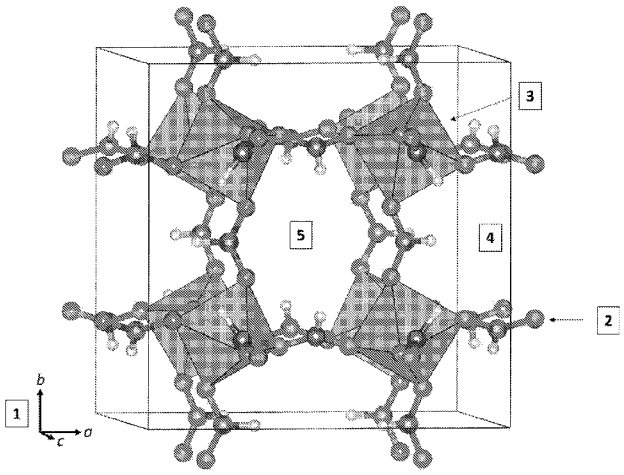

FIG. 1

(57) Abstract: A metal-organic framework includes a porous ReO_3-type aluminum formate, a congener of the porous ReO_3-type aluminum formate, or a combination comprising at least one of the foregoing metal-organic frameworks.

[Continued on next page]

WO 2024/163543 A1

SZ, TZ, UG, ZM, ZW), Eurasian (AM, AZ, BY, KG, KZ, RU, TJ, TM), European (AL, AT, BE, BG, CH, CY, CZ, DE, DK, EE, ES, FI, FR, GB, GR, HR, HU, IE, IS, IT, LT, LU, LV, MC, ME, MK, MT, NL, NO, PL, PT, RO, RS, SE, SI, SK, SM, TR), OAPI (BF, BJ, CF, CG, CI, CM, GA, GN, GQ, GW, KM, ML, MR, NE, SN, TD, TG).

Published:

— *with international search report (Art. 21(3))*

— *before the expiration of the time limit for amending the claims and to be republished in the event of receipt of amendments (Rule 48.2(h))*

HYDROGEN FUEL MEMBER COMPRISING A MOF FOR STORING MOLECULAR HYDROGEN

STATEMENT REGARDING FEDERALLY SPONSORED RESEARCH

[0001] This invention was made with United States Government support from the National Institute of Standards and Technology (NIST), an agency of the United States Department of Commerce. The Government has certain rights in this invention.

CROSS REFERENCE TO RELATED APPLICATIONS

[0002] This application claims the benefit of U.S. Provisional Patent Application Serial No. 63/442,398 (filed January 31, 2023), which is herein incorporated by reference in its entirety.

BRIEF DESCRIPTION

[0003] Disclosed is a metal-organic framework comprising a porous ReO_3-type aluminum formate, a congener of the porous ReO_3-type aluminum formate, or a combination comprising at least one of the foregoing metal-organic frameworks.

[0004] Disclosed is a hydrogen fuel member for storing molecular hydrogen, the hydrogen fuel member comprising: a molecular hydrogen physisorber that comprises a metal-organic framework; and a storage container in which is disposed the molecular hydrogen physisorber.

[0005] Disclosed is a process for storing molecular hydrogen, the process comprising: adsorbing molecular hydrogen in hydrogen fuel member, wherein the hydrogen fuel member comprises: a molecular hydrogen physisorber that comprises a metal-organic framework; and a storage container in which is disposed the molecular hydrogen physisorber.

BRIEF DESCRIPTION OF THE DRAWINGS

[0006] The following description cannot be considered limiting in any way. Various objectives, features, and advantages of the disclosed subject matter can be more fully appreciated with reference to the following detailed description of the

disclosed subject matter when considered in connection with the following drawings, in which like reference numerals identify like elements.

[0007] FIG. 1 shows a structure of ALF prior to adsorption. It is representative of the crystal structure the material class has at all relevant temperatures, according to some embodiments. The structure is defined by octahedrally coordinated metal centers that bond/associate with ligands and create a cage like structure. This structure type is known in the literature as ReO_3-type and is related to the perovskite structure. The exact symmetry/unit cell/orientation of octahedra or ligand may change based on chemical substitution, but on average this cage structure arrangement is maintained, then the structure description is appropriate. This material is porous. Numerical labels refer to [1] unit cell coordinate directions for the [2] formate anion, oxygen = red, carbon = brown, hydrogen = beige. [3] octahedrally coordinated (6 coordinate) metal center that bonds to the oxygens of the formate ligands, metal center = blue. [4] example location of small cavity within unit cell. [5] Example location of large cavity within unit cell.

[0008] FIG. 2 shows a skeleton structure of ALF prior to adsorption, according to some embodiments. It is representative of the crystal structure the material class has at all relevant temperatures, according to some embodiments. The structure is defined by octahedrally coordinated metal centers that bond/associate with ligands and create a cage like structure. This structure type is known in the literature as ReO_3-type and is related to the perovskite structure. The exact symmetry/unit cell/orientation of octahedra or ligand may change based on chemical substitution, but on average this cage structure arrangement is maintained, then the structure description is appropriate. This material is porous. Numerical labels refer to [1] unit cell coordinate directions for the [2] formate anion, oxygen = red, carbon = brown, hydrogen = beige. [3] octahedrally coordinated (6 coordinate) metal center that bonds to the oxygens of the formate ligands, metal center = blue. [4] Example location of small cavity within unit cell. [5] Example location of large cavity within unit cell.

[0009] FIG. 3 shows a full structure of ALF after D_2 adsorption at 160 K with 90 bar of D_2 gas, according to some embodiments. The structure shows what the structure of ALF is after D_2 adsorption e.g. (ALF-H_2 or ALF-D_2). D_2 super atoms were used to resolve the location of D_2 molecules, as is done commonly for D_2 structure

solutions.[references 1,2,3] Numerical labels refer to [1] unit cell coordinate directions for the [2] formate anion, oxygen = red, carbon = brown, hydrogen = beige. [3] octahedrally coordinated (6 coordinate) metal center that bonds to the oxygens of the formate ligands, metal center = blue. [4] D_2 super atom within a small cavity within unit cell. [5] Example of modeling of disordered D_2 super atoms in the large cavity within unit cell.

[0010] FIG. 4 shows a full skeleton structure of ALF after D_2 adsorption at 160 K with 90 bar of D_2 gas, according to some embodiments. The structure shows what the structure of ALF is after D_2 adsorption e.g. (ALF-H_2 or ALF-D_2). D_2 super atoms were used to resolve the location of D_2 molecules, as is done commonly for D_2 structure solutions.[references 1,2,3] Numerical labels refer to [1] unit cell coordinate directions for the [2] formate anion, oxygen = red, carbon = brown, hydrogen = beige. [3] octahedrally coordinated (6 coordinate) metal center that bonds to the oxygens of the formate ligands, metal center = blue. [4] D_2 super atom within a small cavity within unit cell. [5] Example of modeling of disordered D_2 super atoms in the large cavity within unit cell.

[0011] FIG. 5 shows a small cavity within the crystal structure of ALF after D_2 adsorption at 160 K with 90 bar of D_2 gas, according to some embodiments. The structure shows how the small cavity is modeled after D_2 adsorption (e.g., the structure of the small cavity of ALF-H_2 or ALF-D_2). D_2 super atoms were used to resolve the location of D_2 molecules, as is done commonly for D_2 structure solutions.[references 1,2,3] numbers within the figure refer to [1] small cavity within ALF. In this specific symmetry form of the crystal structure, when viewed on average, 4 of the 12 possible formate hydrogens point inward towards the center of the cavity. Chemical modifications may alter the exact symmetry, unit cell, space group, and orientation of how formates and their hydrogens arrange within the crystal structure. [2] D_2 super atom modeled within the small cavity of the ALF structure. [3] Octahedrally coordinated (6 coordinate) metal center that bonds to the oxygens of the formate ligands. [4] Formate anion ligand that coordinates to the metal centers.

[0012] FIG. 6 shows a large cavity within the crystal structure of ALF after D_2 adsorption at 160 K with 90 bar of D_2 gas, according to some embodiments. The structure shows how the large cavity is modeled after D_2 adsorption (e.g., the structure

of the large cavity of ALF-H_2 or ALF-D_2). D_2 super atoms were used to resolve the location of D_2 molecules, as is done commonly for D_2 structure solutions.[references 1,2,3] numbers within figure refer to [1] Large cavity within ALF. In this specific symmetry form of the crystal structure, when viewed on average, all possible formate hydrogens point away from the center of the cavity. Chemical modifications may alter the exact symmetry, unit cell, space group, and orientation of how formates and their hydrogens arrange within the crystal structure. [2] Disordered distribution of D_2 superatoms within the large cavity of ALF. The disordered distribution suggests the D_2 super atoms are more closely association with the formate oxygen-carbon framework. [3] Octahedrally coordinated (6 coordinate) metal center that bonds to the oxygens of the formate ligands. [4] Formate anion ligand that coordinates to the metal centers.

[0013] FIG. 7 shows a Rietveld refinement fit of neutron powder diffraction data of ALF measured at 160 K, under 90 bar of D_2 [POWGEN, ORNL, bank 2]. R_{wp} = 3.92 %, R_p = 3.37 %. Space group = 204 Im-3, according to some embodiments. Lattice parameters, $a = b = c$ = 11.3669(1) Å. The x-axis is shown in Q (inverse angstroms, $Å^{-1}$. Q is related to the common 2-theta (2θ) scattering angle by $Q = (4\pi/\lambda)\sin(2\theta/2)$ and has the same scale no matter the wavelength (λ) of the experiment. Aluminum hkl's refer to solid Al sample holder used for experiment, not Al metal within the sample. Error bars denote 1 sigma. Inset is a magnified version of figure between 6 $Å^{-1}$to 12 $Å^{-1}$ in Q.

[0014] FIG. 8 shows atomic information for Rietveld refinement fit of ALF under 90 bar of D_2 shown in FIG. 7, according to some embodiments. Space group = 204 Im-3, $a = b = c$ = 11.3669(1) Å, wherein x, y, and z refer to position within the unit cell. Occ refers to crystallographic occupancy. B refers to Debye Waller factor ($Å^2$). Site refers to Wycoff position in the unit cell based on the space group. Sym. Refers to specific symmetry operator of the Wycoff site. Values in parentheses denote 1 sigma.

[0015] FIG. 9 shows a Rietveld refinement fit neutron powder diffraction data of ALF measured at 160 K, under 50 bar of D_2 [POWGEN, ORNL, bank 2], according to some embodiments. R_{wp} = 4.07 %, R_p = 3.45 %. Space group = 204 Im-3. Lattice parameters, $a = b = c$ = 11. 3627(1) Å. The x-axis is shown in Q (inverse angstroms, $Å^{-1}$). Aluminum hkl's refer to solid Al sample can used for experiment, not Al metal

within the sample. Error bars denote 1 sigma. Inset is a magnified version of figure between 6 $Å^{-1}$to 12 $Å^{-1}$ in Q.

[0016] FIG. 10 shows atomic information for Rietveld refinement fit of ALF under 50 bar of D_2 shown in FIG. 9, according to some embodiments. Space group = 204 Im-3, $a = b = c$ = 11.3627(1) Å, and x, y, and z refer to position within the unit cell. Occ refers to crystallographic occupancy. B refers to Debye Waller factor ($Å^2$). Site refers to Wycoff position in the unit cell based on the space group. Sym. Refers to specific symmetry operator of the Wycoff site. Values in parentheses denote 1 sigma.

[0017] FIG. 11 shows a Rietveld refinement fit of neutron powder diffraction data of ALF measured at 160 K, under 20 bar of D_2 [POWGEN, ORNL, bank 2], according to some embodiments. R_{wp} = 4.10 %, R_p = 3.53 %. Space group = 204 Im-3. Lattice parameters, $a = b = c$ = 11.3616 (1) Å. The x-axis is shown in Q (inverse angstroms, $Å^{-1}$). Aluminum hkl's refer to solid Al sample can used for experiment, not Al metal within the sample. Error bars denote 1 sigma. Inset is a magnified version of figure between 6 $Å^{-1}$to 12 $Å^{-1}$ in Q.

[0018] FIG. 12 shows atomic information for Rietveld refinement fit of ALF under 20 bar of D_2 shown in FIG. 11, according to some embodiments. Space group = 204 Im-3, $a = b = c$ = 11.3616(1) Å, and x, y, and z refer to position within the unit cell. Occ refers to crystallographic occupancy. B refers to Debye Waller factor ($Å^2$). Site refers to Wycoff position in the unit cell based on the space group. Sym. Refers to specific symmetry operator of the Wycoff site. Values in parentheses denote 1 sigma.

[0019] FIG. 13 shows a Rietveld refinement fit of neutron powder diffraction data of ALF measured at 160 K, under 10 bar of D_2 [POWGEN, ORNL, bank 2], according to some embodiments. R_{wp} = 4.02 %, R_p = 3.02 %. Space group = 204 Im-3. Lattice parameters, $a = b = c$ = 11.3599(1) Å. The x-axis is shown in Q (inverse angstroms, $Å^{-1}$).Aluminum hkl's refer to solid Al sample can used for experiment, not Al metal within the sample. Error bars denote 1 sigma. Inset is a magnified version of figure between 6 $Å^{-1}$to 12 $Å^{-1}$ in Q.

[0020] FIG. 14 shows atomic information for Rietveld refinement fit of ALF under 10 bar of D_2 shown in FIG. 13, according to some embodiments. Space group

= 204 Im-3, $a = b = c$ = 11.3599(1) Å, and x, y, and z refer to position within the unit cell. Occ. refers to crystallographic occupancy. B refers to Debye Waller factor (Å^2). Site refers to Wycoff position in the unit cell based on the space group. Sym. Refers to specific symmetry operator of the Wycoff site. Values in parentheses denote 1 sigma.

[0021] FIG. 15 shows a Rietveld refinement fit of activated neutron powder diffraction data of ALF measured at 160 K prior to D_2 exposure [POWGEN, ORNL, bank 2], according to some embodiments. R_{wp} = 4.52 %, R_p = 3.38 %. Space group = 204 Im-3. Lattice parameters, $a = b = c$ = 11.3623(4) Å. The x-axis is shown in Q (inverse angstroms, Å^{-1}). Aluminum hkl's refer to solid Al sample can used for experiment, not Al metal within the sample. Error bars denote 1 sigma. Inset is a magnified version of figure between 6 Å^{-1}to 12 Å^{-1} in Q.

[0022] FIG. 16 shows atomic information for Rietveld refinement fit of activated ALF at 160 K prior to D_2 exposure as shown in FIG. 15, according to some embodiments. Space group = 204 Im-3, $a = b = c$ = 11.3623(4) Å, and x, y ,and z refer to position within the unit cell. Occ refers to crystallographic occupancy. B refers to Debye Waller factor (Å^2). Site refers to Wycoff position in the unit cell based on the space group. Sym. Refers to specific symmetry operator of the Wycoff site. Values in parentheses denote 1 sigma.

[0023] FIG. 17 shows, according to some embodiments, a hydrogen fuel member 200 in which molecular hydrogen 203 is physisorbed in a metal-organic framework 204 that is disposed in storage container 207.

[0024] FIG. 18 shows excess H_2 gas adsorption/desorption isotherm measurements on ALF between 120 K and 296 K. Closed symbols = adsorption, open symbols = desorption.

[0025] FIG. 19 shows H_2 excess uptake using ALF at temperatures between 77 K and 296 K, presented in two different metrics. mmol H_2 / g ALF and g H_2 / kg ALF, according to some embodiments.

[0026] FIG. 20 shows H_2 total uptake using ALF at temperatures between 77 K and 296 K, presented in two different metrics. mmol H_2 / g ALF and g H_2 / kg

ALF. The total uptake was calculated using the pore volume 0.195 cc/g, according to some embodiments.

[0027] FIG. 21 shows total adsorption data of H_2 in ALF, plotted versus g H_2 per L ALF. Solid symbols are adsorption data, open symbols are desorption data.

[0028] FIG. 22 shows Non-linear single site Langmuir fits of excess adsorption data of H_2 in ALF. Solid circles are data, black lines are fits.

[0029] FIG. 23 shows, from in-situ neutron diffraction results on ALF at 160 K under D_2 pressure for data shown in FIGs. 8, 10, 12, 14, and 16, refined values of D_2 occupancy found within ALF from the 160 K data sets for each cavity, converted into equivalent grams of H_2 per kg of ALF (using molecular mass of 2 g/mol instead of 4 g/mol (D_2)) for direct comparison with FIG. 18. Some results are also shown in FIG. 37 as a function of mmol D_2 / g ALF and g D_2 / kg ALF. Error bars and values denote 1 sigma.

[0030] FIG. 24 shows technoeconomic analysis (TEA) and system-level performance of ALF versus compressed gas and other MOFs. a) Modeled installed capital cost for ALF at different temperatures and pressures, when charging rate is the same as discharge rate. The red line shows the installed cost if ALF was priced at 10 $/kg. Compressed hydrogen gas installed costs at 350 bar are shown by the light blue bar. b) Comparison of system-level energy density of ALF with compressed hydrogen storage under 350 bar (293 K), calculated based on the amount of hydrogen stored in a tank and the tank's outer volume. c) Comparison of ALF with a top-performing contemporary MOF (Ni_2(*m*-dobdc)) under optimum cost and pressures under different manufacturing costs and operating conditions (low-cost value – 2 $/kg with moderate charging (charge = discharge) and high-cost value – 10 $/kg with fast charging (charge = 4 times faster than the discharge) for both MOFs). The green area denotes ideal delivery pressure range (10 bar – 20 bar) for stationary applications when coupled with fuel cells. Dashed lines between the two data points for ALF and Ni_2(*m*-dobdc) are used for easier comparison between the ranges. The shaded region behind the line denotes that values between the two ranges can vary. d) A schematic diagram depicting the optimum range of temperature and pressure conditions for different types of MOFs.

[0031] FIG. 25 shows a theoretical comparison of usable hydrogen obtained from a pressure and temperature swing process for ALF-H_2 vs compressed hydrogen cycling between 25 bar at given temperature (x-axis) to 5 bar and 296 K, according to some embodiments. The Y-axis is in terms of volumetric capacity. Values for ALF usable volumetric capacity is derived from total adsorption isotherm values at the specific temperature and pressures listed. The compressed hydrogen volumetric capacities are derived from standard volumetric densities of isothermal properties for compressed hydrogen from the NIST Chemistry webbook.

[0032] FIG. 26 shows a theoretical comparison of usable hydrogen obtained from a pressure and temperature swing process for ALF-H_2 vs compressed hydrogen cycling between 50 bar at given temperature (x-axis) to 5 bar and 296 K, according to some embodiments. The Y-axis is in terms of volumetric capacity. Values for ALF usable volumetric capacity is derived from total adsorption isotherm values at the specific temperature and pressures listed. The compressed hydrogen volumetric capacities are derived from standard volumetric densities of isothermal properties for compressed hydrogen from the NIST Chemistry webbook.

[0033] FIG. 27 shows a theoretical comparison of usable hydrogen obtained from a pressure and temperature swing process for ALF-H_2 vs compressed hydrogen cycling between 100 bar at given temperature (x-axis) to 5 bar and 296 K, according to some embodiments. The Y-axis is in terms of volumetric capacity. Values for ALF usable volumetric capacity is derived from total adsorption isotherm values at the specific temperature and pressures listed. The compressed hydrogen volumetric capacities are derived from standard volumetric densities of isothermal properties for compressed hydrogen from the NIST Chemistry webbook.

[0034] FIG. 28 shows CH_4 discrimination from isotherm measurements, wherein in the isotherm of CH_4 with ALF (excess uptake) the material does not adsorb CH_4 at any appreciable pressure. The graph has negative values at higher pressures due to a correction established when calculating excess uptake at pressures above 2 bar but indicates here that no CH_4 is entering inside the pores of ALF.

[0035] FIG. 29 shows q_{max} and b values from non-linear single site Langmuir fits shown in FIG. 22.

[0036] FIG. 30 shows calculated pore volume and surface area using He probe for the data shown in FIG. 31.

[0037] FIG. 31 shows He-probe pore size diameter/volume results. (left) Pore size distribution (orange trace), cumulative pore volume normalized to unity (blue trace). (right) Figure illustrating how in the conventional unit cell that there are large cavity volumes centred at (0,0,0) and (1/2,1/2,1/2) (light green spheres) and small cavity volumes (blue spheres) centred at (1/2,0,0),(0,1/2,0), (0,0,1/2), (1/2,1/2,0),(1/2,0,1/2), and (0,1/2,1/2).

[0038] FIG. 32 shows pore volume examination using CO_2 at 270 K. Given kinetic considerations at this temperature, the pore volume is the lower limit estimation at 0.09 cc/g, compared to 0.195 cc/g when using He. Closed symbols = adsorption, open symbols = desorption.

[0039] FIG. 33 shows total adsorption dual site Langmuir fitting using upper bound pore volume of 0.195 cc/g. (left) Isotherm fitting. (right) Obtained Q_{st} as a function of H_2 loading. Dual site equation parameters listed in FIG. 34. Error bars denote 1 sigma.

[0040] FIG. 34 shows dual site Langmuir equation parameters from fits in FIG. 33. Pore volume used was 0.195 cc/g.

[0041] FIG. 35 shows total adsorption dual site Langmuir fitting using lower bound pore volume of 0.09 cc/g. (left) Isotherm fitting. (right) Obtained Q_{st} as a function of H_2 loading. Dual site equation parameters listed in FIG. 36. Error bars denote 1 sigma.

[0042] FIG. 36 shows dual site Langmuir equation parameters from fits in FIG. 37. Pore volume used was 0.09 cc/g.

[0043] FIG. 37 shows Rietveld refined values of D_2 occupancy (total, and as a function of cavity) found within ALF from the in-situ neutron diffraction experiment.

[0044] FIG. 38 shows position energy (in kJ/mol) of a single H_2 molecule in the small and large cavities of ALF. The energy minimum for H_2 is centred in small cavity, whereas in large cavity, it is with a slight offset (≈ 0.8 Å - 1 Å) from the centre.

The results suggest that the small cavity provides a more favourable environment for H_2 binding.

[0045] FIG. 39 shows optimized lattice parameters and the atomic positions of the structure used for phonon calculations using Quantum Espresso. *a* = 11.4907 Å (calc.), *a* = 11.3624 (exp.), error = 1.1 %. Values listed are calculated, and values in parenthesis are empirical.

[0046] FIG. 40 shows pie charts representing overall installed cost of H_2 storage at a MOF material cost of (left) $10/kg and (right) 2 dollar per kg. LISCH = combined contribution of land, insulation, storage tank, compressor, heater.

[0047] FIG. 41 shows q_{max} and b values from Langmuir fits.

[0048] FIG. 42 shows a summary of market listing found for the key compounds used in the synthesis of MOFs.

[0049] FIG. 43 shows average experimental heat capacity (C_p) of ALF between 190 K and 297 K from DSC (3 runs), plotted alongside DFT derived C_p. Error bars denote 1 sigma.

[0050] FIG. 44 shows thermogravimetric analysis (TGA, top panel) and Differential Scanning Calorimetry (DSC, bottom panel, exo down) of ALF through degradation. ALF undergoes no phase change upon heating, where the peak endothermic energy maximum for degradation is centered just above 600 K. Heating rate 5 K/min.

DETAILED DESCRIPTION

[0051] A detailed description of one or more embodiments is presented herein by way of exemplification and not limitation.

[0052] Hydrogen storage is a contemporaneous issue that has faced technological obstacles for use as an on-demand energy supply via hydrogen chemistry. For zeolites, hydrogen storage capacity of zeolites is less than 2 wt.% at cryogenic temperatures and less than 0.3 wt.% at room temperature and above. See, e.g., “Zeolites as media for hydrogen storage,” International Journal of Hydrogen

Energy 20, 967 (1995), which is incorporated by reference in its entirety. Additionally, carbon-based sorbent systems have interesting properties (e.g., light weight, high surface areas, and chemical stabilities), but the hydrogen adsorption capacities at ambient temperature on all known sorbents are below 0.6–0.8 wt.% at 298 K and 30 bar. See, e.g., "Oxygen-rich microporous carbons with exceptional hydrogen storage capacity," Nat. Commun. 8, 1545 (2017), which is incorporated by reference in its entirety. A class of materials that might store molecular hydrogen through a catalytic process at ~4 wt.% is described in "New sorbents for hydrogen storage by hydrogen spillover," Energy Environ. Sci. 1, 268 (2008), which is incorporated by reference in its entirety. However, the Department of Energy (Gennett, Thomas. Position Paper: Hydrogen Spillover Limitations for Onboard Hydrogen Storage. United States: N. p., 2019. Web. doi:10.2172/1489894, which is incorporated by reference in its entirety) states, "…even though there are validated results in the literature that the hydrogen spillover process may result in an observed 10% to 50% increase in hydrogen sorption capacities, it has only been verified for well-defined, low surface area materials with inherently low gravimetric capacity. . . . Thus, although there is now definitive spectroscopic evidence in the literature (DRIFTS, NMR, RAMAN, Neutron Scattering) of studies that confirm reversible hydrogen adsorption/desorption spillover behavior, these confirmations have only been observed for materials with low initial hydrogen capacity."

[0053] Technoeconomic analysis for using metal-organic frameworks (MOFs) as a hydrogen transport medium for backup energy H_2 storage relies on the unachieved assumption that MOFs will reach $10/kg to manufacture. See Technoeconomic analysis of metal–organic frameworks for bulk hydrogen transportation, Energy Environ. Sci. 14, 1083 (2021), which is incorporated by reference in its entirety. Certain MOFs for such applications can be made between $25/kg – $100/kg. The majority of hydrogen storage information and data for MOFs are collected at liquid-N_2 cryogenic temperatures of 77 K. The highest published deliverable volumetric capacity is reported for Ni_2(*m*-dobdc), "Record High Hydrogen Storage Capacity in the Metal–Organic Framework Ni2(m-dobdc) at Near-Ambient Temperatures," Chem. Mater. 30, 8179 (2018), which is incorporated by reference in its entirety. This article indicates that lack of gravimetric capacity in these type of systems with a reported *TOTAL* gravimetric capacity of ~1.4 wt.% at -75 °C that falls

to ~0.75 wt.% at 25 °C (see Fig. S1 of the article). The excess capacity at 100 bar is expected to be on the order of half this total capacity judging from the published data (see Fig S3 of the article).

[0054] Hydrogen is the lightest element, and adsorption of hydrogen in a porous material has considerable challenges because the interaction of molecular hydrogen (such as H_2 or another isotope of hydrogen) with solid surfaces is weak as an outcome of the properties of molecular hydrogen. Such properties of molecular hydrogen include charge neutrality, no electric dipole moment, a relatively weak quadrupole moment, and small molecular polarizability. As a result, conventional adsorbents often adsorb molecular hydrogen at cryogenic temperatures, e.g., less than 77 K. Moreover, adequate storage quantities of hydrogen by conventional adsorbents often requires high pressures, e.g., exceeding 100 bar. For high temperature or lower pressure cryogenic adsorption of hydrogen, some adsorbents use undercoordinated metal centers or cations to induce polarizability of molecular hydrogen. Other adsorbents physisorb molecular hydrogen via interactions between molecular hydrogen and the host framework.

[0055] Unlike difficulties that adsorbents face for adsorption of molecular hydrogen, many adsorbents adsorb other gases such as O_2 or CO_2 that include heavier elements than hydrogen and that have an attribute (e.g., charge non-neutrality, non-zero electric dipole moment, a quadrupole moment, or molecular polarizability) that favors adsorption in porous materials. Indeed, activated aluminum formate adsorbs O_2 and CO_2 over a range of temperatures and pressures. See "An earth-abundant, scalable, and highly selective material for CO_2 capture," Science Advances 8, eade1473 (2022); and international patent application PCT/SG2022/050383 (filed June 6, 2022, published as WO2022260592), the disclosure of each of which is incorporated herein by reference in its entirety. However, adsorption of molecular hydrogen by activated aluminum formate is not reasonably expected to occur above cryogenic temperatures or below high pressure. Past experimental evidence shows that molecular hydrogen fails to adsorb above cryogenic temperatures or below high pressure on conventional adsorbents without exposed metal centers (such as metal organic frameworks (e.g., manganese (II) formate), many zeolites, activated carbons, or high surface area porous materials). It

should be appreciated that activated aluminum formate does not include an exposed metal center and is chemically distinct from conventional adsorbents with under-coordinated metal centers (such as metal organic frameworks known as Ni_2(m-dobdc), $V_2Cl_{2.8}$(btdd), Cu-MFU-4*l*, or HKUST-1). Without wishing to be bound by theory, it is believed that embodiments of the present invention overcome the lack of hydrogen adsorption of conventional adsorbents due to a size of pores in activated aluminum formate and interaction of metal organic framework of activated aluminum formate with molecular hydrogen that arises from thermal activation of phonons that opens pores and receives molecular hydrogen in the pores. Such properties are absent in conventional adsorbents with respect to the temperature and pressure conditions disclosed herein for adsorption of molecular hydrogen by activated aluminum formate and other ReO_3-type species.

[0056] Although the long-sought after hydrogen economy desires a stable, low cost, non-cryogenic, lower pressure way to store hydrogen, prior attempts to achieve this end with the immediately listed conventional adsorbents failed. Embodiments of the invention disclosed herein overcome this technical deficiency and achieve hydrogen adsorption by activated aluminum formate and related ReO_3-type adsorbents even though this result is unexpected and not present in the prior art. Further, this unexpected behavior is not described or suggested in literature that describes O_2 or CO_2 adsorption on activated aluminum formate cited above, namely Science Advances 8, eade1473 (2022) and PCT/SG2022/050383.

[0057] It has been discovered that a hydrogen fuel member 200 and storing molecular hydrogen by activated metal organic framework 201 provide a dense store of an isotope of molecular hydrogen. As used herein, molecular hydrogen (also referred to herein as simply hydrogen) can be H_2 gas, D_2 gas, T_2 gas, HD gas, HT gas, DT gas, or a combination of any of the foregoing isotopes of molecular hydrogen. Hydrogen fuel member 200 can include a ReO_3-type aluminum formate for storing molecular hydrogen. Embodiments provide excellent mass/mass and mass/volume adsorption of molecular hydrogen 203 over a broad range of temperatures. Hydrogen fuel member 200 and storing molecular hydrogen by activated metal organic framework 201 provide one of the largest mass storage per unit cost of an isotope of hydrogen compared with conventional metal-organic frameworks at a temperature

greater than or equal to 77 K. Embodiments can be used for storing molecular hydrogen 203 in an electric storage grid or on-demand delivery of stored hydrogen such as for automotive modalities, e.g., cars and freight transport vehicles including trucks and trains. Hydrogen fuel member 200 and storing molecular hydrogen by activated metal organic framework 201 can selectively separate molecular hydrogen 203 present in a composition that includes other gases such as hydrocarbons, e.g., methane or a larger chain hydrocarbon, CO, CO_2, N_2, noble gases, and the like.

[0058] In an embodiment, hydrogen fuel member 200 includes aluminum formate (referred to as ALF) that adsorbs molecular hydrogen 203 at temperatures from 0 K to at least 300 K, specifically from 90 K to at least 298 K. A pressure can be from 0 to 120 bar. Accordingly, hydrogen fuel member 200 has a high density of ALF, provides excellent weight/weight and weight/volume adsorption of molecular hydrogen 203 at these temperatures. Moreover, hydrogen fuel member 200 holds the highest weight of molecular hydrogen 203 stored per dollar of any metal-organic framework at above 77 K. Advantageously, hydrogen fuel member 200 can be used as a fuel source for the electric grid or as a large stationary storage of hydrogen gas for hydrogen energy-based devices.

[0059] In an embodiment, aluminum formate is made porous to form activated ALF that is subsequently exposed to molecular hydrogen. According to an embodiment, the pressure of molecular hydrogen is from 0 bar to 120 bar. According to an embodiment, the temperature during exposure to molecular hydrogen is from greater than or equal to 77 K to 298 K. In response to being exposed to molecular hydrogen the activated ALF adsorbs molecular hydrogen in the pores of the activated ALF to form hydrogen fuel member 200.

[0060] The hydrogen fuel member 200 can be subjected to heating or reduced pressure (e.g., a vacuum) to remove the molecular hydrogen from hydrogen fuel member 200. The activated ALF or hydrogen fuel member 200 can be subjected to higher pressures and store more molecular hydrogen. Although ALF reportedly adsorbs CO_2 and O_2 gas, a person having ordinary skill in the art would not expect ALF to adsorb molecular hydrogen under the temperature or pressure described herein. Instead, molecular hydrogen is received and disposed in pores of ALF above 77 K, and cooler than 77 K the thermal motion of ALF prevents fast permeation and

receipt of molecular hydrogen in the pores, effectively blocking disposition of molecular hydrogen in the pores of ALF on a reasonable timescale. Other conventional metal organic frameworks (excluding ALF) that adsorb molecular hydrogen are expensive, have large void spaces, and are highly sensitive to moisture or O_2 gas. Beneficially, ALF is comparatively cheap, dense, and robust against moisture or O_2 gas. ALF has a kinetic rate of adsorption or desorption that includes temperatures below ≈200 K.

[0061] In an embodiment, hydrogen fuel member 200 includes a porous material that adsorbs molecular hydrogen in pores of the matrerial. According to an embodiment, the porous material is porous ReO_3-type formate materials such as aluminum formate ($Al(HCOO)_3$; ALF), a resilient MOF-like material. Such porous material is a physisorbent material that store molecular hydrogen. ALF exhibits high excess and total H_2 adsorption from 77 K to 298 K, specifically from 77 K to 150 K, and more specifically from 100 K to 150K, and from 0 bar to 120 bar. A cage-like structure like that of ALF is structurally reminiscent of rhenium oxide. This family of structurally related materials is described in "Perovskite-related ReO3-type structures,". Nat. Rev. Mater. 5, 196 (2020), which is incorporated by reference herein in its entirety.

[0062] It should be appreciated that a ReO_3-type structure is a variant of the perovskite structure, with the general formula ML_3, where M is a transition metal, and L is a ligand such as formate. The structure is characterized by octahedrally coordinated metal atoms, with the G group atoms are arranged in a trigonal prismatic geometry around each metal atom. The ReO_3-type structure is found in a number of transition metal oxides, including ReO_3, OsO_3, IrO_3, and RuO_3. The ReO_3-type structure is similar to the perovskite structure, but with the difference that the metal atoms are octahedrally coordinated, rather than tetrahedrally coordinated. This difference in coordination geometry is due to the larger size of ligands in the ReO_3-type structure. The large ligands are able to accommodate the larger metal atoms in an octahedral geometry. The ReO_3-type structure is characterized by a high degree of covalent bonding, due to the large difference in electronegativity between the metal and ligands. This high degree of covalent bonding contributes to the stability of the ReO_3-type structure. The ReO_3-type structure is a versatile structure that can be used to store molecular hydrogen.

[0063] With reference to FIG. 1 to FIG. 16, ReO_3-type formate materials have a porous structure (crystal structure of ALF shown, e.g., in FIG. 1) that receives molecular hydrogen in pores at higher temperatures or low pressures. These materials may adsorb molecular hydrogen at lower energy and infrastructure costs for storage than is required to liquify or pressurize similar amounts of molecular hydrogen, particularly at lower pressures (e.g., 0 bar to 50 bar). For hydrogen storage, porous formate materials can be disposed in a storage tank as an energy reservoir. Although some materials such as Ni_2(*m*-dobdc), $V_2Cl_{2.8}$(btdd), Cu-MFU-l, or activated carbons can adsorb hydrogen or deuterium, ALF is distinct from these other materials because ALF is air stable and cheaper to produce so that ALF provides grid-scale H_2 storage.

[0064] H_2 adsorption is a difficult and different process compared to CO_2 and O_2 adsorption, and many metal-organic framework (MOF) materials do not strongly adsorb hydrogen at temperatures above 100 K even though they may adsorb O_2 or CO_2. If they do, they commonly leverage "open-metal sites" which allow a metal's uncoordinated orbitals to interact the H_2 molecules. ALF has no such open metal sites and is a different category of adsorbent referred to as ultramicroporous. Without wishing to be bound by theory, it is believed that the adsorption mechanism for H_2 storage in metal organic frameworks (such as MOFs Ni_2(*m*-dobdc), $V_2Cl_{2.8}$(btdd), or Cu-MFU-l) is not what is occurring in ALF and is not expected to work based on published literature. Materials that lack open metal sites and are leveraging framework physisorption for H_2 adsorption usually adsorb at low temperatures and have extended conjugated carbon/nitrogen ring systems that are a part of the organic compounds that link the metal centers in the MOFs, which are absent in ALF and therefore cannot provide adsorption of molecular hydrogen in ALF.

[0065] ALF is an ultramicroporous material based on how wide the open windows into the chemical structure are. As used herein, ultramicroporous refers to a material with pores smaller than 0.7nm (7 angstroms). Ultramicroporous materials are often only tested near 77 K with H_2, given adsorption of gases thermodynamically should increase as temperature is decreased. ALF and porous ReO_3-type framework formate materials do not display similar behavior to what is observed (poor H_2/D_2 adsorption at less than 77 K due to kinetic limitations) and can limit the logical assumption that ALF would adsorb H_2 at temperatures towards room temperature.

Typical laboratory procedures to characterize porous materials for H_2 storage include a 77 K N_2 surface area measurement and a similar isotherm for H_2 at 77 K or below. Some literature further details the decrease in H_2 adsorption capacity as temperatures are increased, and fewer publications go to lower temperatures where H_2 capacities further increase.

[0066] ALF stores sizeable amounts of molecular hydrogen at non-cryogenic temperatures, wherein the molecular hydrogen is received and disposed in the porous structure of the material. ALF can store molecular hydrogen at non-cryogenic temperatures even though ALF is made cheaply.

[0067] According to an embodiment, a process for selectively adsorbing molecular hydrogen includes contacting ALF with a composition including molecular hydrogen and a contaminant (e.g., methane or a higher alkane, alkene, or alkyne); and adsorbing the molecular hydrogen in an absence of adsorption of the contaminant. The contaminant can be a combination of non-adsorbing species or a single non-adsorbing species. In an embodiment, ALF adsorbs molecular hydrogen while not adsorbing methane (see, e.g., FIG. 28). As a result, ALF separates hydrogen from hydrocarbons, e.g., methane or longer carbon chain hydrocarbons than methane.

[0068] With regard to gas adsorption by an adsorbent, it should be appreciated that excess adsorption can be a difference between an amount of gas in an adsorbent due to adsorption compared with an amount of gas in the adsorbent in absence of adsorption at the same temperature and pressure. Recoverable hydrogen can be an amount of workable gas that can be removed from the adsorbent. If the working pressures of the adsorbent are 5 bar to 100 bar, gas can be present in the adsorbent at 5 bar such that this amount is subtracted from the amount adsorbed at 100 bar to get a recoverable quantity. Accordingly, excess adsorption can be used to plot data and account for a correction of non-accessible volume. At higher pressures, this overcompensates with a deviation that can be an artifact of this correction. Total adsorption is how much actual gas can be stored by an adsorbent with knowledge of pore volume of the adsorbent.

[0069] In an embodiment, a metal-organic framework 204 includes a porous ReO_3-type aluminum formate 205, a congener 206 of the porous ReO_3-type aluminum

formate 205, or a combination comprising at least one of the foregoing metal-organic framework 204. In an embodiment, the metal-organic framework 204 has an X-ray powder diffraction pattern that comprises 2θ peaks at 10.98°, 15.55°, 19.07°, 22.05°, 24.70°, 27.10°, 29.31°, 31.89°, 33.35°, and 35.21 at 300 K with a unit cell lattice parameter of 11.39 Å, space group Im-3 (204) for X-rays at a wavelength 1.5406 Å.

[0070] In an embodiment, the metal-organic framework 204 is $X_{1-n}Y_nZ_3$, wherein: X is a metal; Y is a metal, and Y is different than X; Z is selected from the group consisting of HCOO-* (formate), RCOO-*, H_2PO_2, and NO_2, wherein * is a point of atachment; R is a C1 to C6 alkyl group; and n is a real number from 0 to 1. In an embodiment, X has a +3 oxidation state. In an embodiment, X comprises Al, Fe, Mn, Y, Sc, Ga, In, Ti, Fe, Mn, V, Cr, Co, Tl, Bi, Ru, Os, Re, Ir, Rh, Ce, La, Pr, Nd, Sm, Eu, Gd, Tb, Dy, Ho, Er, Tm, Yb, Lu, or a combination comprising at least one of the foregoing metals. In an embodiment, X comprises a plurality of different metals. In an embodiment, X is Al.

[0071] In an embodiment, wherein Y has a +3 oxidation state. In an embodiment, Y comprises Al, Fe, Mn, Y, Sc, Ga, In, Ti, Fe, Mn, V, Cr, Co, Tl, Bi, Ru, Os, Re, Ir, Rh, Ce, La, Pr, Nd, Sm, Eu, Gd, Tb, Dy, Ho, Er, Tm, Yb, Lu, or a combination comprising at least one of the foregoing metals. In an embodiment, Y includes a plurality of different metals. In an embodiment, Y is Fe.

[0072] In an embodiment, Z is HCOO-*.

[0073] In an embodiment, n is from 0 to 0.99. In an embodiment, n is from 0.25 to 0.85.

[0074] In an embodiment, metal-organic framework 204 is selected from the group consisting of $Al(HCOO)_3$, $Al_{0.75}Fe_{0.25}(HCOO)_3$; $Al_{0.5}Fe_{0.5}(HCOO)_3$; $Al_{0.25}Fe_{0.75}(HCOO)_3$; $Al_{0.15}Fe_{0.85}(HCOO)_3$; $V(HCOO)_3$; and $V_{0.3}Al_{0.7}(HCOO)_3$. In an embodiment, the metal-organic framework 204 absorbs molecular hydrogen 203 at a temperature from 0 K to 300 K at a pressure from 0 bar to 700 bar. In an embodiment, metal-organic framework 204 selectively adsorbs molecular hydrogen 203 in a composition comprising the molecular hydrogen 203 and a polyatomic component, such that the metal-organic framework 204 adsorbs the molecular hydrogen 203 in an absence of adsorbing other components of the composition. In an embodiment, the

polyatomic component comprises a hydrocarbon, CO_2, or a combination comprising at least one of the foregoing polyatomic components. In an embodiment, the hydrocarbon comprises methane.

[0075] It should be appreciated that a molecular hydrogen physisorbent that includes a metal-organic framework (MOF) is a material that can absorb molecular hydrogen by physisorption. MOFs are a class of porous materials that are composed of metal ions or clusters coordinated to organic ligands. The pores in MOFs can be tailored to have a specific size and shape, which can be used to selectively adsorb certain molecules. In the case of H_2, the pores in MOFs can be designed to be large enough to accommodate the H_2 molecules, but small enough to prevent them from escaping.

[0076] MOFs are a promising material for molecular hydrogen storage because they can have high molecular hydrogen adsorption capacities and are relatively lightweight. However, the molecular hydrogen adsorption capacity of MOFs is typically limited by the weak van der Waals interactions between the molecular hydrogen molecules and the MOF surface. To improve the molecular hydrogen adsorption capacity, MOFs can be functionalized with groups that can interact more strongly with molecular hydrogen.

[0077] A molecular hydrogen physisorbent that includes a congener of porous ReO_3-type aluminum formate is a material that can absorb molecular hydrogen by physical means. The material is composed of a congener of porous ReO_3-type aluminum formate, which is a type of metal-organic framework (MOF). The congener of porous ReO_3-type aluminum formate used in this material is a MOF that is composed of metal ions and ligands. The congener of porous ReO_3-type aluminum formate has a high molecular hydrogen adsorption capacity. This is because the pores in the MOF are large enough to accommodate molecular hydrogen, but small enough to prevent them from escaping. The MOF also has a high molecular hydrogen desorption capacity because molecular hydrogen can easily diffuse out of the pores in the MOF. This makes it ideal for use in applications where molecular hydrogen storage is required, such as fuel cells and hydrogen-powered vehicles.

[0078] It should be appreciated that a congener is a compound that is similar to another compound in structure and properties. In the context of this material, a congener of porous ReO_3-type aluminum formate is a MOF that has a similar structure and properties to porous ReO_3-type aluminum formate. The congener may have different metal ions or ligands, or it may have a different pore size or shape. However, it will still have the same basic structure and properties as porous ReO_3-type aluminum formate.

[0079] With respect to the structure of metal-organic framework 204, e.g., ALF, as related to FIG. 1 to FIG. 16, diffraction patterns of ALF includes an x-axis labeled as Q (momentum transfer or wave vector), particularly in FIG. 7, FIG. 9, FIG. 11, FIG. 13, and FIG. 15. Diffraction patterns also can be presented with the x-axis labelled as a function of 2θ. However, given that 2θ is dependent on the wavelength used to obtain any diffraction pattern, displaying diffraction patterns as a function of Q is useful as it eliminates ambiguity and will be the same regardless of what wavelength is used to obtain the data. Q and 2θ can be converted according to

$$\mathrm{Q} = \frac{4\pi}{\lambda} \sin\left(\frac{2\theta}{2}\right).$$

[0080] The first 10 allowed diffraction peaks for ALF at room temperature as a function of 2θ when using the common lab diffractometer source, Cu Kα, λ = 1.5406 Å are listed in Table 1, which lists the first 10 expected diffraction peaks of ALF at ≈ 300 K with unit cell lattice parameter = 11.39051 Å, space group *Im*-3 (204) as a function of 2θ. When using X-rays with the wavelength 1.5406 Å, the most intense peak appears at 15.5465° for data acquired.

Table 1.

2θ (degrees)
10.9761
15.5465
19.0700
22.0546
24.6966
27.0966

29.3144
31.8870
33.3467
35.2078

[0081] When ALF is at a temperature that is cooler than room temperature (≈ 300 K), ALF's unit cell lattice parameter contracts relative that at 300 K. From neutron diffraction experiments conducted on POWGEN at Oak Ridge National Laboratory, activated ALF (no guest species present) had a unit cell lattice parameter of 11.3624(4) Å, space group Im-3 (204) at 160 K. When dosed with D_2 gas at varying pressures (10 bar to 90 bar), this lattice parameter can change (become smaller/bigger), as D_2 gas interacts with the framework material, and the material accommodates gas entering its porous framework. The crystal structure of ALF (ReO_3-type structure) does not change, per figures of the refined crystal structures with D_2 inside of the porous structure. The relative intensities of the diffraction peaks are different if the source is X-rays or neutrons since neutrons probe the nucleus of atoms, but X-rays are sensitive to the number of electrons around atoms. Further, once dosed with H_2 or D_2 gas, the peak intensities vary slightly with X-rays (only 2 electrons per gas molecule). Neutrons have a larger variation between the intensities of activated ALF and D_2 adsorbed ALF. Neutron diffraction results in different changes in intensities if H_2 is adsorbed.

[0082] In an embodiment, hydrogen fuel member 200 stores molecular hydrogen, and the hydrogen fuel member 200 includes: molecular hydrogen physisorber 202 that comprises metal-organic framework 204; and storage container 207 in which is disposed molecular hydrogen physisorber 202. In an embodiment, with reference to FIG. 17, hydrogen fuel member 200 includes storage container 207, wherein storage container 207 is a vessel that interconnects to a fluid supply that provides fluid supply flow 211 and includes molecular hydrogen 203 that flows into storage container 207 via inlet fluid line 209 and is isolatable via valve 208. Further, fluid delivery flow 212 can include molecular hydrogen 203 desorbed from metal-organic framework 204 in storage container 207 via outlet fluid line 210 that can be isolated by valve 208. The temperature of storage container 207 can be moderated by a heater or cooler (e.g., cryogenic jacket, closed loop coolant system, and the like).

[0083] Hydrogen fuel member 200 and ALF can be made of various elements and components. Elements of hydrogen fuel member 200 can be various sizes. Elements of hydrogen fuel member 200 can be made of a material that is physically or chemically resilient in an environment in which hydrogen fuel member 200 is disposed. Exemplary materials include a metal, ceramic, thermoplastic, glass, semiconductor, and the like. The elements of hydrogen fuel member 200 can be made of the same or different material and can be monolithic in a single physical body or can be separate members that are phsycially joined. It is contemplated that ALF is disposed in a storage container that can connected to a gas manifold such that the storage container can be sealed against gas loss. Various gas handling components, e.g., tubing, valves, pressure regulators, and the like, can be connected to the container for storage of molecular hydrogen by the ALF in the storage container and delivery of molecular hydrogen adsorbed on the ALF in the storage container.

[0084] Preparation of as-made aluminum formate

[0085] As-made $Al(HCOO)_3$, the precursor to ALF, is synthesized by combining formic acid (50 ml) and aluminum hydroxide (0.6 g, 0.0075 mol) and refluxing in an appropriate sized vessel, such as 125-ml three-neck round-bottom flask, at ≈100°C (≈373 K) for 48 hours. After the reaction is complete, the excess formic acid can be removed by centrifugation. The reaction product, a white solid, is rinsed with ethanol. This material is as-made aluminum formate. The as-made aluminum formate can be separated from any residual solvent using vacuum filtration.

[0086] Preparation of ALF, porous aluminum formate

[0087] To synthesize ALF, the porous version of aluminum formate, the solid obtained from the prior step (dried as-made aluminum formate) is heated to ≈150°C (≈423 K) for 24 hours under high vacuum (1×10^{-4} mmHg) or alternatively, heated in air/ambient conditions at 180°C (453 K) for 24 hours, yielding quantitative amounts of the guest-free ALF.

[0088] Preparation of ALF- X H2 or ALF- X D2, where X ranges between 0 and 1

[0089] To synthesize ALF-X H_2 or ALF-X D_2, where X ranges between 0 and 1, porous aluminum formate (ALF) is exposed to molecular hydrogen (H_2 gas, D_2 gas, T2 gas, HD gas, HT gas, DT gas, or a combination of any of the foregoing isotopes of molecular hydrogen) at a temperature, e.g., from 0 K to 300 K, and a pressure of D_2 or H_2 greater than 0 bar, specifically from 0.0001 bar to 5000 bar, and more specifically from 5 bar to 300 bar, or at a commercially viable pressure.

[0090] In an embodiment, exposure of ALF to molecular hydrogen 50 bar (cooled to some temp) to 5 bar 296 K temperature swings, given that the material is so dense and as higher pressures of H2 get closer and closer to compressed hydrogen volumetric capacities. See FIG. 12, FIG. 13, and FIG. 14.

H_2 isotherms of ALF

[0091] Gas isotherm measurements of H_2 gas at various pressures using a sample of ALF are shown in FIG. 18 and FIG. 21. Here, the material was activated (emptied of guest species) prior to measurement. FIG. 19 and FIG. 20 show excess and total uptake isotherms that show how much gas is adsorbed at equilibrium at specific pressures/temperatures. Excess uptake is the conservate evaluation of how much gas is adsorbed, total uptake accounts for a pore volume of the material.

[0092] The isotherms illustrate of the capacity for hydrogen storage by the metal-organic framework (e.g., ALF) as the experiment measures how much gas can be stored inside of the material at different temperatures. The separation capacity between H_2/CH_4 and other hydrocarbons has no examples outside of the isotherms that show H_2 adsorption and lack of CH_4 adsorption at comparable temperatures. Diffraction experiments confirm that H_2/D_2 gas is adsorbed within the crystal structure of ALF.

[0093] Confirmation of ALF adsorption of D2 gas using neutron diffraction

[0094] Experimental confirmation using neutron powder diffraction and subsequent Rietveld refinement of obtained data show that $Al(HCOO)_3$ (ALF) adsorbs D_2 inside of its porous structure. This was confirmed at 160 K various pressures between 0 and 90 bar. The crystal structure of ALF with D_2 present inside of its cavities is shown in FIG. 1. The crystal structure shown was resolved from Rietveld refinements of neutron diffraction data taken at 160 K under 90 bar D2 atmosphere.

The structure solution from the 160 K and 90 bar D_2 dataset is consistent with other data sets taken at different temperatures and pressures and indicates that both crystallographically distinct cavities within ALF fill with D_2 during adsorption.

[0095] ALF was preactivated prior to the in-situ diffraction experiment. Given the high pressures used for the experiment an aluminum sample can was used, which added elemental aluminum diffraction peaks into the pattern. These elemental aluminum peaks were Pawley fit simultaneously during the Rietveld refinements shown. For the 160 K dosing experiment, ALF was measured prior to D_2 exposure, then exposed to increasing pressures of D_2 gas (10 bar, 20 bar, 50 bar, 90 bar). The refined quantities of D_2 are consistent with the isotherm data presented (FIG. 19 and FIG. 20). Rietveld refinements were performed in the TOPAS software suite.

[0096] With reference to FIG. 1, numbers in the figure refer to [1] fractional coordinates for structure. Unit cell of and space group of models derived for ALF without any guest species at 160 K is space group 204 Im-3, $a = b = c = 11.3623(4)$ Å. Error bars denote 1 sigma. Chemical modifications may alter the exact symmetry, space group, and unit cell of the ALF structure, but the ALF structure is defined by a cage like network built out of 6-coordinate octahedral metal atoms and ligands that bond to create an ReO_3-type, perovskite related, cage-like structure as described in Evans, H.A., Wu, Y., Seshadri, R. et al. Perovskite-related ReO_3-type structures. Nat Rev Mater 5, 196–213 (2020), which is incorporated by reference herein in its entirety. [2] Formate ligands that bond/associate to metal center can be replaced with ligands that chemically bond similarly. [3] Octahedrally coordinated (6 coordinate) metal center that bond to the oxygens of the formate ligands, or other atoms of related ligands. [4] Small cavity within ALF that is defined, on average, by having 4 of the 12 possible formate hydrogens pointing inwards towards the center of the cavity. Chemical modifications outside of ALF ($Al(HCOO)_3$ of the family may alter exact character of how formate hydrogens arrange. [5] Large cavity within ALF. It is defined by its, on average, lack of formate hydrogens pointing inward. Chemical modifications of the family may alter exact character.

[0097] With reference to FIG. 2, numbers in refer to [1] fractional coordinates for structure. Unit cell of and space group of models derived for ALF without any guest species at 160 K is space group 204 Im-3, $a = b = c = 11.3623(4)$ Å. Error bars denote

1 sigma. Chemical modifications may alter the exact symmetry, space group, and unit cell of the ALF structure, but the ALF structure is defined by a cage like network built out of 6-coordinate octahedral metal atoms and ligands that bond to create an ReO_3-type, perovskite related, cage-like structure. [2] Formate ligands that bond/associate to metal center. Can potentially be replaced with ligands that chemically bond and similarly. [3] Octahedrally coordinated (6 coordinate) metal center that bond to the oxygens of the formate ligands, or other atoms of related ligands. [4] Small cavity within ALF. It is defined, on average, by having 4 of the 12 possible formate hydrogens pointing inwards towards the center of the cavity. Chemical modifications outside of ALF ($Al(HCOO)_3$ of the family may alter exact character of how formate hydrogens arrange. [5] Large cavity within ALF. It is defined by its, on average, lack of formate hydrogens pointing inward. Chemical modifications of the family may alter exact character.

[0098] With reference to FIG. 3, numbers refer to [1] Fractional coordinates for figure. Unit cell of and space group of models derived for 160 K with 90 bar of D_2 gas is space group 204 Im-3, $a=b=c=$ 11.36687(9) Å. Error bars denote 1 sigma. Chemical modifications to the framework may alter the exact symmetry, space group, and unit cell of the ALF structure, but the ALF structure is defined by a cage like network built out of 6-coordinate octahedral metal atoms and ligands that bond to create an ReO_3-type, perovskite related, cage like structure. [2] Formate anion ligand that coordinates to the metal centers. [3] octahedrally coordinated (6 coordinate) metal center that bonds to the oxygens of the formate ligands. [4] D_2 super atom modeled within the small cavity of the ALF structure. [5] Disordered distribution of D_2 superatoms within the large cavity of ALF. The structure is representative of how ALF fills with D_2 at all relevant temperatures and pressures, namely, that both pores fill simultaneously as the compound adsorbs H_2/D_2 gas. This is confirmed via structural models derived at 160 K at multiple dosing pressures.

[0099] With reference to FIG. 4, numbers refer to [1] Fractional coordinates for figure. Unit cell of and space group of models derived for 160 K with 90 bar of D_2 gas is space group 204 Im-3, $a=b=c=$ 11.36687(9) Å. Error bars denote 1 sigma. Chemical modifications to the framework may alter the exact symmetry, space group, and unit cell of the ALF structure, but the ALF structure is defined by a cage like

network built out of 6-coordinate octahedral metal atoms and ligands that bond to create an ReO_3-type, perovskite related, cage like structure. [2] Formate anion ligand that coordinates to the metal centers. [3] octahedrally coordinated (6 coordinate) metal center that bonds to the oxygens of the formate ligands. [4] D_2 super atom modeled within the small cavity of the ALF structure. [5] Disordered distribution of D_2 superatoms within the large cavity of ALF. The structure is representative of how ALF fills with D_2 at all relevant temperatures and pressures, namely, that both pores fill simultaneously as the compound adsorbs H_2/D_2 gas. This is confirmed via structural models derived at 160 K at multiple dosing pressures.

[00100] Hydrogen fuel member 200 has numerous advantageous and unexpected benefits and uses. In an embodiment, , a process for storing molecular hydrogen includes: adsorbing molecular hydrogen 203 in hydrogen fuel member 200, wherein the hydrogen fuel member 200 comprises: a molecular hydrogen physisorber 202 that comprises a metal-organic framework 204; and a storage container 207 in which is disposed the molecular hydrogen physisorber 202. The process of claim can include separating the molecular hydrogen 203 in a composition comprising the molecular hydrogen 203 and a polyatomic component, such that the metal-organic framework 204 selectively adsorbs the molecular hydrogen 203 in an absence of adsorbing other components of the composition. In the process, separating the molecular hydrogen 203 in the composition comprises contacting the metal-organic framework 204 with the composition and selectively adsorbing the molecular hydrogen 203 over the other components of the composition. In an embodiment, the polyatomic component comprises a hydrocarbon, CO_2, or a combination comprising at least one of the foregoing polyatomic components. In an embodiment, the hydrocarbon comprises methane. In an embodiment, contacting the metal-organic framework 204 with the composition comprises subjecting the metal-organic framework 204 to a flow of gas of the composition that includes an isotope of molecular hydrogen 203. In an embodiment, the isotope of the molecular hydrogen 203 comprises hydrogen, deuterium, or a combination comprising at least one of the foregoing isotopes. In an embodiment, the process includes activating or reducing an amount of molecular hydrogen 203 adsorbed on the metal-organic framework 204 by subjecting the metal-organic framework 204 to a temperature from 90 K to 450 K or a reduced pressure (e.g., from 0 to 20 bar) for a period of time (e.g., e.g., from 1 to 2 hours) sufficient to

release a selected amount of the molecular hydrogen 203. In an embodiment, the process includes desorbing molecular hydrogen 203 from the metal-organic framework 204 in the storage container 207 to obtain free molecular hydrogen 203; and releasing the free molecular hydrogen 203 from the storage container 207. In an embodiment, the process includes activating the metal-organic framework 204 by: providing unactivated metal-organic framework; and subjecting the unactivated metal-organic framework to a selected temperature under reduced pressure for a selected period of time to obtain an activated metal-organic framework 204.

[00101] Hydrogen fuel member 200 and processes disclosed herein have numerous beneficial uses, including high-density storage of molecular hydrogen over a broad range of temperatures and a broad range of pressures in a molecular hydrogen physisorber 202 such as metal-organic framework 204. It is well known that hydrogen is the lightest element, and adsorption of hydrogen in a porous material has considerable challenges because the interaction of molecular hydrogen with solid surfaces is weak as an outcome of the properties of molecular hydrogen. Such properties of molecular hydrogen include charge neutrality, no electric dipole moment, a relatively weak quadrupole moment, and small molecular polarizability. As a result, conventional adsorbents often adsorb molecular hydrogen at cryogenic temperatures, e.g., less than 77 K. Moreover, adequate storage quantities of hydrogen by conventional adsorbents often require high pressures, e.g., exceeding 100 bar. For high temperature or lower pressure cryogenic adsorption of hydrogen, some conventional adsorbents use undercoordinated metal centers or cations to induce polarizability of molecular hydrogen. Other conventional adsorbents physisorb molecular hydrogen via interactions between molecular hydrogen and the host framework.

[00102] Unlike difficulties that adsorbents face for adsorption of molecular hydrogen, many adsorbents adsorb other gases, such as O_2 or CO_2, that include heavier elements than hydrogen and that have an attribute (e.g., charge non-neutrality, non-zero electric dipole moment, a quadrupole moment, or molecular polarizability) that favors adsorption in porous materials. Indeed, activated aluminum formate adsorbs O_2 and CO_2 over a range of temperatures and pressures as discussed above. However, adsorption of molecular hydrogen by activated aluminum

formate is not reasonably expected to occur above cryogenic temperatures or below high pressure. Past experimental evidence shows that molecular hydrogen fails to adsorb well-above cryogenic temperatures or below high pressure on conventional adsorbents without exposed metal centers (such as metal organic frameworks (e.g., manganese (II) formate), many zeolites, activated carbons, or high surface area porous materials). Activated aluminum formate does not include an exposed metal center and is chemically distinct from conventional adsorbents with under-coordinated metal centers (such as metal organic frameworks known as Ni_2(m-dobdc), $V_2Cl_{2.8}$(btdd), Cu-MFU-4*l*, or HKUST-1).

[00103] Although the long-sought after hydrogen economy desires a stable, low cost, non-cryogenic, lower pressure way to store hydrogen, past attempts to achieve this end with the conventional adsorbents failed. Embodiments of the invention of adsorption of molecular hydrogen on molecular hydrogen physisorber 202, e.g., aluminum formate, as described in this patent application, provide hydrogen adsorption by activated aluminum formate and other ReO_3-type adsorbents even though this result is unexpected and not present in the prior art.

[00104] The articles and processes herein are illustrated further by the following Example, which is non-limiting.

EXAMPLE

[00105] Hydrogen Storage with Aluminum Formate, ALF: Experimental, Computational and Technoeconomic Studies.

[00106] Long-duration storage of hydrogen is involved in coupling renewable H_2 with stationary fuel cell power applications. Aluminum formate (ALF), which adopts the ReO_3-type structure, has remarkable H_2 storage performance at non-cryogenic (>120 K) temperatures and low pressures, e.g.., from 120 K to 160 K and from 10 bar to 20 bar. Here, H_2 adsorption performance is described for ALF over the 77 K to 296 K temperature range using gas isotherms, in-situ neutron powder diffraction, DFT calculations, as well as technoeconomic analysis (TEA) illustrating ALF's competitive performance for long-duration storage versus compressed hydrogen and leading metal-organic frameworks (MOFs). The TEA shows ALF's storage capacity when combined with a temperature/pressure swing process, which has advantages versus

compressed H_2 at a fraction of the pressure (15 bar versus 350 bar). Given ALF's performance in the 10 bar to 20 bar regimes under moderate cooling, it is useful for safe storage systems serving fuel cells.

[00107] Stationary hydrogen-powered fuel cells are being developed to deliver clean and flexible power. Renewable energy powered electrolysis can generate hydrogen but may involve days' worth of hydrogen storage to smooth renewable energy variability. Storage is also involved in cases where hydrogen is used as a backup power system, with a necessary target storage duration of 96 hours to meet the requirements set by the United States National Fire Protection Association. This presents a challenge, as compressed gas or cryogenic hydrogen storage is operationally expensive and inefficient at large scales for these storage durations, and salt caverns proposed for storage are not widely available and require pipelines to make them suitable for significantly larger applications. As such, work has been conducted to identify material-based solutions for hydrogen storage that operate at lower pressures and warmer temperatures.

[00108] Porous metal-organic frameworks (MOFs) can perform well in adsorbing H_2 within their porous structures, and via gas-framework interactions, facilitating high hydrogen storage capacities. However, a MOF's peak adsorption under equilibrium conditions is only one indicator, and a MOF can be evaluated across other factors, such as the constraints resulting from integration with electrolyzer and fuel cell systems. Fuel cells involve high-purity hydrogen at fast delivery rates and modest pressures, which MOFs are uniquely capable of achieving. Additionally, green H_2 generated by on-site electrolyzers tends to be warm ($\approx$ 320 K or above). Storing this warm H_2 under cryogenic temperatures (i.e., 77 K) could lead to expensive refrigeration costs. For example, for cooling processes under 248 K and 83K, the refrigeration cost for 1 MW of cooling load increases from 18.5 $/GJ to 360 $/GJ (2017 values), respectively.

[00109] Conventional MOFs for hydrogen storage required low temperatures to achieve high hydrogen uptake. Some MOFs (e.g., $Zn_4O(BDC)_3$ (MOF-5, BDC^{2-} = 1,4-benzenedicarboxylate), $Cu_3(BTC)_2$ (HKUST-1, BTC^{3-} = 1,3,5-benzenetricarboxylate, CdIF-13 (sod-Cd(benzimidazolate)$_2$)), show maximum hydrogen uptake under cryogenic temperature and high-pressure conditions, whereas

some emerging MOFs, such as Ni_2(*m*-dobdc) and V-btdd (*m*-dobdc^{4-} = 4,6-dioxido-1,3-benzenedicarboxylate; H_2btdd, bis(1*H*-1,2,3-triazolo[4,5-*b*],[4′,5′-*i*])dibenzo[1,4]dioxin), exhibit record deliverable H_2 at near-ambient temperatures and high-pressure conditions (i.e., above 100 bar). Ni_2(*m*-dobdc) can achieve a lower levelized cost of storage ($/kWh) relative to cryogenic storage, but not compared to compressed gas storage at 350 bar without Ni_2(*m*-dobdc) being made cheaply and able to retain relatively high hydrogen uptake (i.e., below 10 $/kg and above 15 g/kg excess uptake). Slower charging of the storage tank can reduce the cost of associated compression and refrigeration units, improving the promise of sorbent-based systems.

[00110] Adsorptive properties of low-cost MOF materials, aluminum formate, $Al(HCOO)_3$ (ALF) are appealing. ALF has an ReO_3-type structure and adsorbs CO_2 from dried CO_2-rich flue gas conditions with high CO_2/N_2 selectivity, to selectively adsorb CO_2 from any hydrocarbon mixture, including acetylene, and provides selective O_2 adsorption characteristics from O_2/N_2 mixtures above cryogenic temperatures. ALF also has attributes for industrially utilized materials, such as withstanding pelletization, being air-stable, and being derived from cheap commodity chemicals. ALF can be used for stationary hydrogen-powered fuel cell applications.

[00111] ALF displays remarkable H_2 storage performance above cryogenic temperatures (> 120 K), with the most promising performance between 120 K and 160 K. We discuss the H_2 adsorption performance of ALF over the temperature ranges from 77 K to 296 K via gas isotherms, the crystal-structure of ALF as it adsorbs D_2 gas, as resolved from in-situ neutron powder diffraction, DFT calculations that support the observed performance, and technoeconomic analysis illustrating ALF's price competitive performance versus leading MOFS and compressed hydrogen for long-term storage. For the technoeconomic analysis, we show how the storage capacity of ALF, when combined with a temperature/pressure swing process, has clear advantages versus compressed H_2 at a fraction of the pressure.

[00112] Gas isotherm measurements

[00113] FIG. 18 shows the excess gas adsorption/desorption isotherm measurements of ALF at various temperatures plotted as a function of grams of H_2 adsorbed versus kilograms (kg) of ALF. FIG. 19, FIG. 20, and FIG. 21 show the same

data plotted with other metrics, as well as the total adsorption plots, for comparison. As can be seen from FIG. 18, ALF shows excess adsorption of H_2 gas of ≈11 grams of H_2 per kg of ALF near 120 K and ≈25 bar of pressure. As temperature is increased, the maximum adsorption decreased, as is expected from thermodynamics. Each of the isotherms can be described as Type I isotherms, and from non-linear Langmuir fits of the excess isotherms (FIG. 22), the experimental heat of adsorption for the H_2 adsorption is 8.67 kJ/mol when treated with a single site Langmuir model.

[00114] The dual-site treatments provide similar heat of adsorption values between ≈ 8.5 kJ/mol and ≈ 9 kJ/mol as a function of loading. Given the dense, ultramicroporous nature of ALF (a material with pore sizes less than 10 Å) when compared to many large pore MOFs, the adsorption values at increased pressures trend closer to values for compressed hydrogen. FIG. 19, FIG. 20, and FIG. 21 shows observed volumetric H_2 storage densities for ALF versus theoretical compressed H_2 volumetric densities of a given pressure and temperature swing process ending at 5 bar and 296 K. As such, the large initial H_2 adsorption at temperatures between 120 K and 200 K and pressures beneath 50 bar offers promising performance for H_2 storage using ALF.

[00115] As temperature is decreased beneath 120 K (FIG. 1, FIG. 2, FIG. 21), the inherent kinetic effects of ALF grow more pronounced, manifesting as hysteresis between adsorption and desorption curves. We have observed this phenomenon for both CO_2 and O_2 adsorption with ALF, albeit at different temperatures given the distinct interactions each gas has with ALF. This kinetic behavior is not uncommon for microporous systems and has been observed in such systems as zeolite type A, and a non-ReO_3-type Mn(II)-formate. Both materials, much like ALF, display complex sorbate-framework interactions that impact adsorption kinetics. ALF has a gating temperature that depends on the nature of each specific gas adsorbed into ALF and exhibits dynamic opening of its pore aperture .

[00116] In-situ D_2-dosed neutron powder diffraction experiments on ALF were conducted at the POWGEN instrument at Oak Ridge National Laboratory. Experiments were conducted at 160 K under multiple pressures of D_2 gas (0 bar, 10 bar, 20 bar, 50 bar, 90 bar) to resolve how the structure of ALF filled and/or changed with D_2 gas. The 160 K temperature was chosen for the experiments as adsorption

was known to be both fast and in high enough quantities to ensure that reliable positions of the D_2 molecules could be located within the allotted experimental time frame. Furthermore, given the fast onset of H_2 adsorption at 120 K, conducting the experiments at 160 K also allowed incremental observation of the adsorption of D_2 into the structure of ALF to be done more precisely.

[00117] ALF adopts an ReO_3-type structure. It is akin to the perovskite structure, only instead of an *A*-site cation, there is a vacancy (void space). The structure of ALF is found in the $Im\bar{3}$ space group, and as a result, has two crystallographically distinct cavities, denoted as the small (SC) and large cavities (LC), which differ by how the hydrogens of the formates point toward, or away, from the center of each cavity, respectively. The pore volumes for the SC and LC at 300 K are 43(3) $Å^3$ and 79(9) $Å^3$, respectively. For CO_2 adsorption, the SC favors CO_2 adsorption relative to the LC because the hydrogen bonding from the formate hydrogens engages in a "hand-in-glove" interaction with CO_2. This contrasts what was observed for O_2 adsorption in ALF, where hydrogen bonding in the small cavity is found to be less significant, with a slight preference for the LC. This slight preference for the large cavity is observed here for D_2 adsorption.

[00118] FIG. 20 shows select results from the in-situ gas-dosed neutron powder diffraction experiments, including visualization of the D_2 positioning within the crystal structure of ALF obtained from Rietveld-derived chemical models. =FIG. 20(a) shows a representative Rietveld refinement fit of the data acquired for the highest dosed D_2 condition, 90 bar. This data set was used to confidently resolve the positions of the D_2 gas molecules adsorbed within ALF, which were then used for the lower pressure data sets. The Supporting Information shows the refinement fits obtained for the other pressures tested (0 bar, 10 bar, 20 bar, 50 bar). Specific to the refinements, the gas molecules were modelled as "super-atoms," given that D_2 is a quantum object, and the molecular dumbbell is orientationally averaged to produce a more spherical scattering center as is typically observed in the literature. An appropriate Rietveld refinement will use a single D atom, instead of a D_2 molecule, to describe a D_2 molecular position. In the refinements, each D super-atom was allowed a maximum occupancy of 2 to account for the modelling of a D_2 molecule.

[00119] FIG. 20(b) shows the refined amounts of D_2 adsorbed in ALF as derived from the Rietveld refinements over the range of pressures. The amounts graphed are the total amount adsorbed at each pressure, as well as the amount for each cavity. The occupancies in Figure 2(b) have been converted to grams of H_2 per kg of ALF, for direct comparison with the isotherm data in FIG. 19. The metrics in mmol of D_2 per g of ALF, and g of D_2 per kg of ALF, are also found in the Supporting Information (FIG. 37). FIG. 10, FIG. 12, FIG. 14, FIG. 16, and FIG. 18 show the crystallographic occupancies from the refinements prior to conversion. As can be appreciated, the power of the in-situ gas dosing neutron diffraction experiments is that the Rietveld refinements with such data provide real-space context as to how gases interact with an adsorbent. In this instance, we found that at all D_2 pressures tested, and given that ALF has two distinct cavities, the SC and LC, both cavities adsorbed D_2 gas at near equal amounts after equilibration when normalized for multiplicity. This is shown in FIG. 20(b) when comparing the D_2 occupancy of the LC versus the D_2 occupancy found in just one SC. There are three times as many SCs versus LCs within ALF, given the $Im\bar{3}$ symmetry.

[00120] Though D_2 is adsorbed into each of the cavities at near equal proportions, how the D_2 molecules fill within the two cavities is distinct. FIG. 20(c) and (d) illustrate how the D super-atoms are found within the SCs and LCs, respectively, as resolved from the Rietveld refinement with the data at 160 K and 90 bar D_2 pressure. The small cavity D super-atom was found to be best modelled with one position at the special position [0, 1/2 ,0], which is the center of the small cavity. Attempts were made to move the super-atom off this special position within the small cavity, which in principle could describe any preferential positioning within the cavity. However, no position away from the [0, 1/2, 0] position was found to statistically improve the fit or provide any other convincing indications of localization. Instead, the most stable and statistically consistent result was modelled with a super atom at the center of the cavity with a large isotropic Debye-Waller factor B_{eq} (refined and stable B_{eq} value of ≈14 $Å^2$). This result implies that the D_2 inside of the small cavity is on average localized at the center of the cavity, albeit likely somewhat dynamic under these conditions.

[00121] This result contrasts with what was found to be the case for the large cavity, where if the D super-atoms were modelled at the center of the large cavity, they had a similar refined B_{eq} of ≈14.2 Å^2 to that of the small cavity D super atom. However, if they were displaced from the special position to populate the surface of sphere inside of the large cavity, the B_{eq} values of the D super-atoms reduced and stabilized by an order of magnitude to ≈1.7 Å^2. This spherical surface modelling is shown in FIG. 20(d). This indicates that there is preferential adsorption of the D_2 gas towards the surfaces of the large cavity walls/ligands, as opposed to occupying the center of the cavity. The distinction in the localization of D_2 within the two cavities can be rationalized given that there is likely vibrational movement of the formates/formate hydrogens at these temperatures that would constantly perturb the location of the D_2 molecules when at the center of the small cavity. Given that the large cavity has no such formate hydrogens that point inward, the D_2 molecules could be expected to be comparatively undisturbed as they associate with the formate ligands O−C−O backbone through weak electrostatic and other dispersion forces. This model is further supported by a DFT derived heatmap for H_2 positional energy inside the cavities of ALF. The heatmap suggests the existence of a shallow energy landscape for H_2 towards the walls of the LC, contrasting with a clear localized low energy landscape for H_2 positioned at the center of the SC (FIG. 38). There is also agreement between the total hydrogen capacity of the pores compared to that expected from the 160 K adsorption isotherm.

[00122] Furthermore, in agreement with our diffraction and isotherm results, the DFT calculated H_2 heats of adsorption for each of the cavities are found to be 11.66 kJ/mol and 12.54 kJ/mol for the SC and LC, respectively. These similarly valued heat of adsorptions for the two cavities aligns well with what was seen from diffraction, which suggests that H_2 fills both cavities with comparable amounts, with a slight preference for the LC. The DFT calculated heat of adsorption values are also close to the isotherm-derived heat of adsorption of 8.67 kJ/mol (fitting from non-linear Langmuir fits to the adsorption data 120 K – 297 K, Figure S6). The optimal heat of adsorption for hydrogen storage materials at ambient conditions should be between 15 kJ/mol and 25 kJ/mol.

[00123] Materials for on-board H_2 use, including V-btdd, and Ni_2(*m*-dobdc), are judged by their high H_2 storage densities as close to room temperature as possible.

This contrasts with long duration H_2 storage materials, where H_2 storage density is not the most important factor, given that space is not limited as it would be in a vehicle. Instead, materials for long duration H_2 storage are judged by their general performance (adsorption per *T* and *P*), scalability, and cost. ALF distinguishes itself in this regard from most MOF materials proposed for long-duration H_2 storage by being derived from low-cost commodity chemicals and still achieving high H_2 uptakes at low working pressures and non-cryogenic temperatures. We evaluate the impact of these characteristics on the cost for an on-site, large-scale (10 MW) and long-duration (96 hours) stationary H_2 storage application to meet backup power needs (8 cycles per year). While the reported cycle lives for many MOFs are from 1000 to 5000 cycles, the effects of replacement and stability should be evaluated for future studies requiring more operation cycles. Low pressure operation is compelling, as a storage pressure between 10 bar to 25 bar is all that is needed for serving the pressure requirements of stationary fuel cells operating at 2 bar - 10 bar. Beyond economic considerations, operating storage systems at low pressures also greatly reduces the safety concerns and system complexity when dispensing H_2, providing lower system costs and fostering general public acceptance of the technology.

[00124] With regard to material costs, at high manufacturing rates, it has been suggested that emerging MOFs that are manufactured using abundant metals, such as nickel or zinc, can achieve a material cost of 10 $/kg of MOF. Lowering the MOF manufacture cost to the level of ≈2 $/kg, which is expected with ALF given that it is made from the abundant commodity chemical reagents aluminum hydroxide and formic acid (priced at 0.3-0.5 $/kg and 0.5-0.9 $/kg wholesale costs, respectively), provides a cost reduction with substantial promise. ALF avoids the use of comparatively complex organic reagents such as 2,5-dihydroxyterephthalic acid or metal salts such as nickel nitrate (priced at 2-20 $/kg and 3-15 $/kg, respectively, Supporting Information). Assuming a conservative material cost of 2 $/kg and based on the H_2 excess uptake with ALF (FIG. 19) and its other fundamental properties (density, specific heat, etc.), we find that a minimum levelized cost of storage is achieved at a working pressure near 15 bar (FIG. 24a). At this pressure and under moderate cooling (120 K), the modelled ALF (with packing density of 1429 kg/m^3) achieves approximately two-thirds of the system-level energy density of 350 bar compressed gas storage at ambient conditions (FIG. 24b). This represents a ≈ 95%

pressure reduction for comparable performance when using ALF. Furthermore, we again mention that ALF withstands pelletization and ball milling, making it promising to achieve high packing densities during deployment, which contributes to high system-level energy density.

[00125] If such low material costs can be achieved, ALF offers a levelized cost of storage that is lower than 350 bar compressed gas systems, despite its cooling requirement (FIG. 24a). This is true, even at a working temperature of 273 K; however, more pressure is required for ALF to achieve costs that are comparable with 350 bar compressed gas systems. A low material cost, such as ALF, would also put the capital cost of MOF on par with other system components, such as compressors and refrigerators (Supporting Information, Figure S19). We compare ALF to an emerging leader for H_2 storage, Ni_2(*m*-dobdc), to illustrate each material's optimal operation range based on their cost performance across 120 K - 293 K and 0 bar to 170 bar (FIG. 24c). The findings are remarkable as both ALF and Ni_2(*m*-dobdc) could achieve a lower levelized cost of storage than 350 bar compressed gas systems. This is the first study where sorbent-based hydrogen storage outperforms cryogenic and compressed gas technologies in a hydrogen storage application.

[00126] The unique adsorption attributes of ALF compared to contemporary MOFs provide new opportunities for future applications for H_2 storage (FIG. 24d). ALF's optimum conditions use moderate cooling and low pressures to achieve high storage, potentially making ALF suitable for applications where a precooled hydrogen stream requires storage, as may be the case for the capture of cryogenic boil-off gas capture.

[00127] Aluminum formate, ALF, adopts the ReO_3-type structure and adsorbs H_2 at non-cryogenic temperatures with an experimental heat of adsorption of ≈8.6 kJ/mol. From in-situ neutron diffraction analysis of D_2-dosed ALF, we show how both of ALF's cavities fill at comparable levels. Specifically, the large cavity of ALF has more localized D_2 molecules near the walls of the framework, whilst in the small cavity, D_2 molecules are located near the center. The adsorption isotherms show that the optimal performance of ALF is found at relatively low pressures (around 25 bar) where the total uptake is near 12g H_2 / kg of ALF at 120 K. ALF's H_2 adsorption performance

makes it advantageous compared to other reported MOFs for low pressure applications at intermediate temperatures.

[00128] From technoeconomic analysis, ALF is currently the only MOF (to date) to achieve cost parity with 350 bar compressed gas storage at a working pressure within the operation range for safe storage systems serving fuel cells. This is achieved at non-cryogenic temperatures, with the best cost performance found between 120 K and 160 K. Given its lower pressure adsorption performance, ALF can be used in H_2 storage/capture areas of interest, such as H_2 boil-off capture. ALF has practical attributes for industrially relevant processes. ALF is pelletizable in contrast to many large void space MOFs that often become amorphous upon pelletization. ALF is chemically robust, withstanding weeks at ambient air conditions without major degradation. ALF is made from cheap and ubiquitous commodity chemicals, wherein it faces fewer challenges in scalability compared to most other MOFs. Such characteristics provide sorbent-based hydrogen storage and market applications with sorbent behavior and suitable operating conditions. As cooling adds refrigeration costs, ALF will benefit from applications where low-pressure and cool or near ambient hydrogen is available and requires storage.

[00129] Experimental Section

[00130] Reflux synthesis of $Al(HCOO)_3$

[00131] The as-made $Al(HCOO)_3$ was synthesized using the reported procedure.[1] In a typical synthesis, formic acid (100 mL) and aluminum hydroxide (1.2 g, 0.015 mol) were refluxed in a 250 mL three-necked round-bottomed flask at 100 °C (373 K) for 48 h. After completing the reaction, excess formic acid was extracted by centrifugation, and the white solid was rinsed with a copious amount of ethanol and separated using vacuum filtration. The air-dried sample gave a yield of 95% white solid product of $Al(HCOO)_3(CO_2)_{0.75}(H_2O)_{0.25}(HCOOH)_{0.25}$/(guest included/as-made $Al(HCOO)_3$). Based on our chemical analysis, it is likely that the actual as-made compound is $Al(HCOO)_3(CO_2)_{0.75}(H_2O)_{0.50}$, with two molecules in the large cavities. Analytical CHN data for $AlC_{3.75}H_4O_8$ (molecular mass: 204 g/mol): calculated mass percentages C: 22.06%, H: 1.96% and observed C: 22.58%, H: 2.32%.

[00132] Activation of as-made Al(HCOO)3 to ALF

[00133] The air-dried, as-made $Al(HCOO)_3(CO_2)_{0.75}(H_2O)_{0.25}(HCOOH)_{0.25}$ (0.5 g, 2.16 mmol) was activated according to the following procedure: heated at 150 °C (423 K) for 24 h under high vacuum (1×10^{-4} mmHg) or heated in air/ambient conditions at 180 °C (453 K) for 24 h, yielding quantitative amounts of the guest-free $Al(HCOO)_3$ (ALF). Analytical CHN data for $AlC_3H_3O_6$ (molecular mass: 162.03 g/mol): calculated. C: 22.24%, H: 1.87%, and observed C: 21.23%, H: 1.93%.

[00134] Neutron powder diffraction (NPD) of ALF and D2-dosed ALF

[00135] Neutron diffraction measurements were performed on a 0.4 g activated sample of ALF powder at the Oak Ridge National Laboratory (ORNL). Data were collected at the high-resolution neutron powder diffractometer, POWGEN using frame 2 (wavelength = 1.5 Å). The sample was loaded into an aluminum sample can in a He environment glove box and sealed with a lid for gas loading. After mounting the sample into a closed cycle refrigerator (CCR), the sample was reactivated at elevated temperatures under vacuum to remove possible residual helium.

[00136] For the D_2 dosing data sets, a syringe pump was used in constant pressure mode to maintain the assigned static pressure (and boost the D_2 pressure from the cylinder when needed). A calibrated gas dosing manifold setup with an attached pressure gauge was used to deliver the gas to the sample stick/holder and confirm the D_2 pressure applied on the sample. The sample was equilibrated for 10 mins before data collection.

[00137] Powder Diffraction Data Rietveld Refinements

[00138] Diffraction data collected on ALF was analyzed using the TOPAS 6 software suite.

[00139] To locate the positions of the D_2 molecules with the highest degree of certainty, the 160 K, 90 bar data set was used. The D_2 molecules were modelled as D super-atoms. These D super-atom positions, as well as thermal parameters, were carried over and fixed for lower dosing refinements.

[00140] H2 gas isotherms on ALF

[00141] Prior to the sorption study, all samples were activated under a dynamic vacuum (≈ 10^{-3} mmHg) for 12 hours at 110 ºC (383 K). The sample masses are 290.5 mg for ALF. After each measurement, the sample was heated to 323 K and pumped for several hours.

[00142] Volumetric gas adsorption measurements were performed using a custom developed fully computer-controlled Sieverts apparatus as discussed previously. Briefly, the fully computer-controlled Sievert apparatus operates in a sample temperature range of 20 K to 500 K and a pressure range of 0 bar to 100 bar. In the volumetric method, gas is admitted from a dosing cell with known volume to the sample cell in a controlled manner; the gas pressure and temperature are controlled and recorded.

[00143] Some unique features of the setup are as follows; the instrument has multiple gas inlets including He, N_2, H_2, which enables the first nitrogen pore volume and surface measurements followed by He-cold volume determination and finally the gas adsorption measurements without needing to move the sample from the cell. Two high precision pressure gauges with parts-per-billion resolution and typical accuracy of 0.05% (20 psia (≈1.38 bar) and 500 psia (≈34.47 bar), respectively) were used to precisely measure the pressure. For isotherm measurements below room temperature, the sample temperature was controlled using a closed cycle refrigerator (CCR). The difference between the actual sample temperature and the control set point is within 1 K over the whole operating temperature range. The connection between the sample cell and the dose cell is through 1/8" capillary high-pressure tubing, which provided a sharp temperature interface between the sample temperature and the dose temperature (i.e., room temperature). The cold volumes for the empty cell were determined using He as a function of pressure at every temperature before the real sample measurement and were used to calculate the sample adsorption.

[00144] Since the adsorbed amount is deducted from the raw P-V-T data using a real gas equation of state, a critically important issue is the accuracy of the chosen equation of state (EOS) in terms of describing the real gas behavior within the desired temperature and pressure range. Using an empty cell as a reference, we found that the MBWR EOS best describes the real gas behavior of He, N_2, H_2. Therefore, in all our isotherm data reduction, the NIST MBWR EOS is used. [NIST Standard

Reference Database 23: NIST Reference Fluid Thermodynamic and Transport Properties Database].

[00145] Measured Isosteric Heat of Adsorption Q_{st}, single site Langmuir

[00146] Langmuir adsorption models can be used to quantify the amount of adsorbate adsorbed onto a material as a function of partial pressure at a given temperature. The following assumptions are made to do such a single site quantification: every binding site is identical; there are no interactions between adsorbed molecules, and there are no interactions in the gas phase.

[00147] The identical assumption can be inferred from understanding of the system, as well as the behavior of the system and whether the fit appears appropriate.

[00148] Isotherm data at multiple temperatures was used to extract the heat of adsorption (Q_{st}) as a function of the adsorbed amount. The Q_{st} was calculated after fitting data sets using the non-linear single site Langmuir equation:

$$Q_e = \frac{q_{max} C_e b}{1 + bC_e}$$

where Q_e = observed uptake, q_{max} is maximum uptake, C_e is pressure, and b is the Langmuir constant.

[00149] Dual-site Langmuir analysis and upper and lower bound pore volume determination.

[00150] We calculated porosity of ALF (i.e., pore volume and surface area) using the code PoreBlazer using He as the probe. The pore volume calculated by He-probe is directly related to the dead volume measured by He-gas in our Sievert gas adsorption experiments. FIG. 30 summarizes calculated pore volume and surface area by He probe. The calculated pore volume and surface area for N_2 is zero in agreement with experiment, as ALF is selective against N_2, and therefore N_2 is inappropriate for pore volume analysis.

[00151] Our calculations using a He-probe indicate that we have two pores with diameter of 3.5 Å and 4.5 Å, as shown in FIG. 31. This is in good agreement with the structure obtained from neutron data. We note that ≈1/3 of the pore volume is from

the large cavity (LC) and ≈ 2/3 of the pore volume is due from the small cavity (blue line in the plot shows the cumulative pore volume normalized to unity). Our calculations indicate that the pore limiting diameter (PLD) is ≈ 2 Å, which is responsible for slow kinetics at a given blocking temperature for each gas adsorbed into ALF. We note that in the conventional unit cell (standardized .cif of ALF, SG: *Im*-3 (204)), we have large cages centered at (0,0,0) and (1/2,1/2,1/2) (light green spheres) and small cages (blue spheres) centered at (1/2,0,0),(0,1/2,0), (0,0,1/2), (1/2,1/2,0),(1/2,0,1/2), and (0,1/2,1/2). (FIG. 31)

[00152] To further understand experimental pore volume of ALF, we performed a N_2 isotherm at 77 K and obtained zero adsorption. This is a result of very small cage openings, consistent with our calculated PLD. We therefore attempted to estimate the pore volume using CO_2 adoption at 271 K, where at P = 32.9 bar, the liquid and gas phase of CO_2 coexists. However, given slow kinetics of CO_2 adsorption in ALF at 271 K, the desorption curve does not follow the adsorption curve (FIG. 32). Hence, the amount of CO_2 adsorption is likely lower than actual adsorption if we were not limited by kinetic considerations. Nevertheless, using the density of liquid CO_2 at this pressure and temperature, we estimate the pore volume of ALF as 0.09 cc/g, which should be considered as the lower limit for the actual pore volume of ALF.

[00153] In estimating the total adsorption and then Q_{st}, we consider two cases; in the first case we take the pore volume of ALF as 0.195 cc/g from the He-probe calculation as the upper limit. In the worst-case scenario, we use the CO_2 determined pore volume of 0.09 cc/g as the lower limit. As is shown in Figures S10 and S11 (parameters in FIG. 34 and FIG. 36), the Q_{st} obtained from the total adsorption of H_2 using either 0.09 cc/g or 0.195 cc/g pore volumes does not change calculated Q_{st} considerably, and is ≈ 9 kJ/mol.

[00154] The dual-site Langmuir model equation is:

$$Q_e = \frac{q_{max1} C_e b_1}{1 + b_1 C_e} + \frac{q_{max2} C_e b_2}{1 + b_2 C_e}$$

[00155] Heat capacity from differential scanning calorimetry and general TGA/DSC

[00156] Thermogravimetric analysis (TGA) coupled to differential scanning calorimetry (DSC) was carried out with a NETZSCH STA 449 F1 Jupiter.

[00157] To measure heat capacity, TGA-DSC was performed at a heating rate of 10 °C/min under nitrogen atmosphere with 20 mL/min flow rate over a temperature range of 190 K to 297 K. A three-cycle scan was carried out, which included runs for baseline correction, standard reference material (sapphire), and activated ALF. The sample weight used was ≈10 mg. The experimental and data processing procedure followed work by Mu and Walton.

[00158] For the reported TGA/DSC (FIG. 44), the same instrument was used, with a heating rate of 5°C/min under He atmosphere with 20 mL/min flow rate.

[00159] Techno-economic analysis

[00160] Modelling hydrogen storage for stationary power and for conducting techno-economic analysis (TEA) was used for both the MOFs and compressed H_2 storage. Experimentally measured material density, heat of adsorption, and H_2 uptakes at temperature and pressure conditions shown in FIG. 19 were used as the inputs for ALF. The energy and power consumption were determined based on macroscopic energy balance between the charged and discharged states, followed by economic analysis based on established cost-performance relations and protocols to calculate the levelized cost of storage. In this study, we added land cost estimation using 60,000 $/acre (1 acre = 4046.86 m^2) based on average listings for U.S. industrial lands in 2022. FIG. 42 summarizes the main economic parameters used in the TEA and the market listings found for the key MOF synthesis ingredients used in this study for ALF and Ni_2(*m*-dobdc). The ingredient listings were used to justify qualitative and relative MOF cost comparisons reported in literature.

[00161] Density functional theory calculations

[00162] Density functional theory (DFT) calculations were performed using the *Vienna ab initio* Simulation *Package* (VASP) with the projected augmented wave (PAW) pseudopotentials, and the following electrons were treated explicitly: H $1s^1$, C $2s^2 2p^2$, O $2s^2 2p^4$ and Al $3s^2 3p^1$. The exchange-correlation functional was calculated using the generalized gradient approximation (GGA) and the van der Waals

interactions were treated using the Grimme's method (DFT+D3). A plane wave kinetic energy cutoff of 520 eV and a 3×3×3 Monkhorst-Pack k-point mesh was used. Structural relaxations were performed until the interatomic forces less than 0.01 eV/Å. The adsorption energy of adsorbate H_2 inside $Al(HCOO)_3$, was calculated as:

$$E_{adsorption} = (E[Al(HCOO)_3, nM] - E[Al(HCOO)_3] - nE[M])/n$$

where E is the DFT total energies and n is the number of the adsorbate molecule in the cubic unit cell. The total energy of adsorbate molecule was calculated by putting a single molecule at the center of a 15×15×15 $Å^3$ box. The position energy of H_2 $Al(HCOO)_3$ was calculated by putting an adsorbate molecule at the center of the small and large cavities, aligned along [100] direction and moved along a translation vector t = (x, y, z) where x, y, and z = −0.1, −0.05, 0, 0.05, and 0.1 in fractional units. Then one of the hydrogen atoms in H_2 was kept fixed (FIG. 38).

[00163] Specific heat calculations using Quantum Espresso

[00164] A full structural optimization (lattice parameters and atomic optimization) using *ab initio* Quantum Espresso package was performed, alongside PAW potentials with revPBE functional and grimme-d3 corrections for vdW-interactions. Kinetic energy cutoff was set to 50 Ry for wavefunctions and 400 Ry for charge density. The k-space integration was performed with 3x3x3 k-points in the Brillouin zone. FIG. 39 lists the optimized lattice parameters and the atomic positions obtained, which are in excellent agreement with experimental data (within a few percent). The experimental fractional coordinates are given in parenthesis in FIG. 39.

[00165] Specific heat calculations derived from Gamma-phonons (calculated by finite-displacement approach (i.e., 0.01 Ang.) were performed using the optimized conventional cell. The obtained gamma phonons were calculated using conventional cell which corresponds to two q-phonons at the primitive cell. Due to large size of the conventional cell, this is understood to be sufficient to estimate the heat capacity of ALF as a function of temperature. Thermal expansion and the effect of the temperature on the phonon energies were omitted from calculations.

[00166] The processes described herein may be embodied in, and fully automated via, software code modules executed by a computing system that includes

one or more general purpose computers or processors. The code modules may be stored in any type of non-transitory computer-readable medium or other computer storage device. Some or all the methods may alternatively be embodied in specialized computer hardware. In addition, the components referred to herein may be implemented in hardware, software, firmware, or a combination thereof.

[00167] Many other variations than those described herein will be apparent from this disclosure. For example, depending on the embodiment, certain acts, events, or functions of any of the algorithms described herein can be performed in a different sequence, can be added, merged, or left out altogether (e.g., not all described acts or events are necessary for the practice of the algorithms). Moreover, in certain embodiments, acts or events can be performed concurrently, e.g., through multi-threaded processing, interrupt processing, or multiple processors or processor cores or on other parallel architectures, rather than sequentially. In addition, different tasks or processes can be performed by different machines and/or computing systems that can function together.

[00168] Any logical blocks, modules, and algorithm elements described or used in connection with the embodiments disclosed herein can be implemented as electronic hardware, computer software, or combinations of both. To clearly illustrate this interchangeability of hardware and software, various illustrative components, blocks, modules, and elements have been described above generally in terms of their functionality. Whether such functionality is implemented as hardware or software depends upon the particular application and design constraints imposed on the overall system. The described functionality can be implemented in varying ways for each particular application, but such implementation decisions should not be interpreted as causing a departure from the scope of the disclosure.

[00169] The various illustrative logical blocks and modules described or used in connection with the embodiments disclosed herein can be implemented or performed by a machine, such as a processing unit or processor, a digital signal processor (DSP), an application specific integrated circuit (ASIC), a field programmable gate array (FPGA) or other programmable logic device, discrete gate or transistor logic, discrete hardware components, or any combination thereof designed to perform the functions described herein. A processor can be a

microprocessor, but in the alternative, the processor can be a controller, microcontroller, or state machine, combinations of the same, or the like. A processor can include electrical circuitry configured to process computer-executable instructions. In another embodiment, a processor includes an FPGA or other programmable device that performs logic operations without processing computer-executable instructions. A processor can also be implemented as a combination of computing devices, e.g., a combination of a DSP and a microprocessor, a plurality of microprocessors, one or more microprocessors in conjunction with a DSP core, or any other such configuration. Although described herein primarily with respect to digital technology, a processor may also include primarily analog components. For example, some or all of the signal processing algorithms described herein may be implemented in analog circuitry or mixed analog and digital circuitry. A computing environment can include any type of computer system, including, but not limited to, a computer system based on a microprocessor, a mainframe computer, a digital signal processor, a portable computing device, a device controller, or a computational engine within an appliance, to name a few.

[00170] The elements of a method, process, or algorithm described in connection with the embodiments disclosed herein can be embodied directly in hardware, in a software module stored in one or more memory devices and executed by one or more processors, or in a combination of the two. A software module can reside in RAM memory, flash memory, ROM memory, EPROM memory, EEPROM memory, registers, hard disk, a removable disk, a CD-ROM, or any other form of non-transitory computer-readable storage medium, media, or physical computer storage known in the art. An example storage medium can be coupled to the processor such that the processor can read information from, and write information to, the storage medium. In the alternative, the storage medium can be integral to the processor. The storage medium can be volatile or nonvolatile.

[00171] While one or more embodiments have been shown and described, modifications and substitutions may be made thereto without departing from the spirit and scope of the invention. Accordingly, it is to be understood that the present invention has been described by way of illustrations and not limitation. Embodiments herein can be used independently or can be combined.

[00172] All ranges disclosed herein are inclusive of the endpoints, and the endpoints are independently combinable with each other. The ranges are continuous and thus contain every value and subset thereof in the range. Unless otherwise stated or contextually inapplicable, all percentages, when expressing a quantity, are weight percentages. The suffix (s) as used herein is intended to include both the singular and the plural of the term that it modifies, thereby including at least one of that term (e.g., the colorant(s) includes at least one colorants). Option, optional, or optionally means that the subsequently described event or circumstance can or cannot occur, and that the description includes instances where the event occurs and instances where it does not. As used herein, combination is inclusive of blends, mixtures, alloys, reaction products, collection of elements, and the like.

[00173] As used herein, a combination thereof refers to a combination comprising at least one of the named constituents, components, compounds, or elements, optionally together with one or more of the same class of constituents, components, compounds, or elements.

[00174] All references are incorporated herein by reference.

[00175] The use of the terms “a,” “an,” and “the” and similar referents in the context of describing the invention (especially in the context of the following claims) are to be construed to cover both the singular and the plural, unless otherwise indicated herein or clearly contradicted by context. It can further be noted that the terms first, second, primary, secondary, and the like herein do not denote any order, quantity, or importance, but rather are used to distinguish one element from another. It will also be understood that, although the terms first, second, etc. are, in some instances, used herein to describe various elements, these elements should not be limited by these terms. For example, a first current could be termed a second current, and, similarly, a second current could be termed a first current, without departing from the scope of the various described embodiments. The first current and the second current are both currents, but they are not the same condition unless explicitly stated as such.

[00176] The modifier about used in connection with a quantity is inclusive of the stated value and has the meaning dictated by the context (e.g., it includes the

degree of error associated with measurement of the particular quantity). The conjunction or is used to link objects of a list or alternatives and is not disjunctive; rather the elements can be used separately or can be combined together under appropriate circumstances.

What is claimed is:

1. A metal-organic framework comprising a porous ReO_3-type aluminum formate, a congener of the porous ReO_3-type aluminum formate, or a combination comprising at least one of the foregoing metal-organic frameworks.

2. The metal-organic framework of claim 1, wherein the metal-organic framework has an X-ray powder diffraction pattern that comprises 2θ peaks at 10.98°, 15.55°, 19.07°, 22.05°, 24.70°, 27.10°, 29.31°, 31.89°, 33.35°, and 35.21 at 300 K with a unit cell lattice parameter of 11.39 Å, space group Im-3 (204) for X-rays at a wavelength 1.5406 Å.

3. The metal-organic framework of claim 1, wherein the metal-organic framework is $X_{1-n}Y_nZ_3$,

wherein:

X is a metal;

Y is a metal, and Y is different than X;

Z is selected from the group consisting of HCOO-*, RCOO-*, H_2PO_2, and NO_2, wherein * is a point of atachment;

R is a C1 to C6 alkyl group; and

n is a real number from 0 to 1.

4. The metal-organic framework of claim 3, wherein X has a +3 oxidation state.

5. The metal-organic framework of claim 3 , wherein X comprises Al, Fe, Mn, Y, Sc, Ga, In, Ti, Fe, Mn, V, Cr, Co, Tl, Bi, Ru, Os, Re, Ir, Rh, Ce, La, Pr, Nd, Sm, Eu,

Gd, Tb, Dy, Ho, Er, Tm, Yb, Lu, or a combination comprising at least one of the foregoing metals.

6. The metal-organic framework of claim 3, wherein X comprises a plurality of different metals.

7. The metal-organic framework of claim 3, wherein X is Al.

8. The metal-organic framework of claim 3, wherein Y has a +3 oxidation state.

9. The metal-organic framework of claim 3, wherein Y comprises Al, Fe, Mn, Y, Sc, Ga, In, Ti, Fe, Mn, V, Cr, Co, Tl, Bi, Ru, Os, Re, Ir, Rh, Ce, La, Pr, Nd, Sm, Eu, Gd, Tb, Dy, Ho, Er, Tm, Yb, Lu, or a combination comprising at least one of the foregoing metals.

10. The metal-organic framework of claim 3, wherein Y comprises a plurality of different metals.

11. The metal-organic framework of claim 3, wherein Y is Fe.

12. The metal-organic framework of claim 3, wherein Z is HCOO-*.

13. The metal-organic framework of claim 1, wherein n is from 0 to 0.99.

14. The metal-organic framework of claim 13, wherein n is from 0.25 to 0.85.

15. The metal-organic framework of claim 1, wherein the metal-organic framework is selected from the group consisting of $Al(HCOO)_3$, $Al_{0.75}Fe_{0.25}(HCOO)_3$; $Al_{0.5}Fe_{0.5}(HCOO)_3$; $Al_{0.25}Fe_{0.75}(HCOO)_3$; $Al_{0.15}Fe_{0.85}(HCOO)_3$; $V(HCOO)_3$; and $V_{0.3}Al_{0.7}(HCOO)_3$.

16. The metal-organic framework of claim 1, wherein the metal-organic framework absorbs molecular hydrogen at a temperature from 0 K to 300 K at a pressure from 0 bar to 700 bar.

17. The metal-organic framework of claim 1, wherein the metal-organic framework selectively adsorbs molecular hydrogen in a composition comprising the molecular hydrogen and a polyatomic component, such that the metal-organic framework adsorbs the molecular hydrogen in an absence of adsorbing other components of the composition.

18. The metal-organic framework of claim 17, wherein the polyatomic component comprises a hydrocarbon, CO_2, or a combination comprising at least one of the foregoing polyatomic components.

19. The metal-organic framework of claim 18, wherein the hydrocarbon comprises methane.

20. A hydrogen fuel member for storing molecular hydrogen, the hydrogen fuel member comprising:

a molecular hydrogen physisorber that comprises a metal-organic framework; and

a storage container in which is disposed the molecular hydrogen physisorber.

21. The hydrogen fuel member of claim 20, wherein the metal-organic framework comprises a porous ReO_3-type aluminum formate, a congener of the porous ReO_3-type aluminum formate, or a combination comprising at least one of the foregoing metal-organic framework.

22. The hydrogen fuel member of claim 20, wherein the metal-organic framework has an X-ray powder diffraction pattern that comprises 2θ peaks at 10.98°, 15.55°, 19.07°, 22.05°, 24.70°, 27.10°, 29.31°, 31.89°, 33.35°, and 35.21 at 300 K with a unit cell lattice parameter of 11.39 Å, space group Im-3 (204) for X-rays at a wavelength 1.5406 Å.

23. The hydrogen fuel member of claim 20, wherein the metal-organic framework is $X_{1-n}Y_nZ_3$,

wherein:

X is a metal;

Y is a metal, and Y is different than X;

Z is selected from the group consisting of HCOO-*, RCOO-*, H_2PO_2, and NO_2, wherein * is a point of atachment;

R is a C1 to C6 alkyl group; and

n is a real number from 0 to 1.

24. The hydrogen fuel member of claim 23, wherein X has a +3 oxidation state.

25. The hydrogen fuel member of claim 23, wherein X comprises Al, Fe, Mn, Y, Sc, Ga, In, Ti, Fe, Mn, V, Cr, Co, Tl, Bi, Ru, Os, Re, Ir, Rh, Ce, La, Pr, Nd, Sm, Eu, Gd, Tb, Dy, Ho, Er, Tm, Yb, Lu, or a combination comprising at least one of the foregoing metals.

26. The hydrogen fuel member of claim 23, wherein X comprises a plurality of different metals.

27. The hydrogen fuel member of claim 23, wherein X is Al.

28. The hydrogen fuel member of claim 23, wherein Y has a +3 oxidation state.

29. The hydrogen fuel member of claim 23, wherein Y comprises Al, Fe, Mn, Y, Sc, Ga, In, Ti, Fe, Mn, V, Cr, Co, Tl, Bi, Ru, Os, Re, Ir, Rh, Ce, La, Pr, Nd, Sm, Eu, Gd, Tb, Dy, Ho, Er, Tm, Yb, Lu, or a combination comprising at least one of the foregoing metals.

30. The hydrogen fuel member of claim 23, wherein Y comprises a plurality of different metals.

31. The hydrogen fuel member of claim 23, wherein Y is Fe.

32. The hydrogen fuel member of claim 23, wherein Z is HCOO-*.

33. The hydrogen fuel member of claim 20, wherein n is from 0 to 0.99.

34. The hydrogen fuel member of claim 33, wherein n is from 0.25 to 0.85.

35. The hydrogen fuel member of claim 20, wherein the metal-organic framework is selected from the group consisting of $Al(HCOO)_3$, $Al_{0.75}Fe_{0.25}(HCOO)_3$; $Al_{0.5}Fe_{0.5}(HCOO)_3$; $Al_{0.25}Fe_{0.75}(HCOO)_3$; $Al_{0.15}Fe_{0.85}(HCOO)_3$; $V(HCOO)_3$; and $V_{0.3}Al_{0.7}(HCOO)_3$.

36. The hydrogen fuel member of claim 20, wherein the metal-organic framework absorbs molecular hydrogen at a temperature from 0 K to 300 K at a pressure from 0 bar to 700 bar.

37. The hydrogen fuel member of claim 20, wherein the metal-organic framework selectively adsorbs molecular hydrogen in a composition comprising the molecular hydrogen and a polyatomic component, such that the metal-organic framework adsorbs the molecular hydrogen in an absence of adsorbing other components of the composition.

38. The hydrogen fuel member of claim 37, wherein the polyatomic component comprises a hydrocarbon, CO_2, or a combination comprising at least one of the foregoing polyatomic components.

39. The hydrogen fuel member of claim 38, wherein the hydrocarbon comprises methane.

40. A process for storing molecular hydrogen, the process comprising:

adsorbing molecular hydrogen in hydrogen fuel member,

wherein the hydrogen fuel member comprises:

a molecular hydrogen physisorber that comprises a metal-organic framework; and

a storage container in which is disposed the molecular hydrogen physisorber.

41. The process of claim 40, further comprising: separating the molecular hydrogen in a composition comprising the molecular hydrogen and a polyatomic component, such that the metal-organic framework selectively adsorbs the molecular hydrogen in an absence of adsorbing other components of the composition.

42. The process of claim 41, wherein separating the molecular hydrogen in the composition comprises contacting the metal-organic framework with the composition and selectively adsorbing the molecular hydrogen over the other components of the composition.

43. The process of claim 42, wherein the polyatomic component comprises a hydrocarbon, CO_2, or a combination comprising at least one of the foregoing polyatomic components.

44. The process of claim 43, wherein the hydrocarbon comprises methane.

45. The process of claim 42, wherein contacting the metal-organic framework with the composition comprises subjecting the metal-organic framework to a flow of gas of the composition that includes an isotope of molecular hydrogen.

46. The process of claim 45, wherein the isotope of the molecular hydrogen comprises hydrogen, deuterium, or a combination comprising at least one of the foregoing isotopes.

47. The process of claim 40, further comprising activating or reducing an amount of molecular hydrogen adsorbed on the metal-organic framework by subjecting the metal-organic framework to a temperature from 90 K to 450 K or a reduced pressure for a period of time sufficient to release a selected amount of the molecular hydrogen.

48. The process of claim 40, further comprising:

desorbing molecular hydrogen from the metal-organic framework in the storage container to obtain free molecular hydrogen; and

releasing the free molecular hydrogen from the storage container.

49. The process of claim 40, further comprising activating the metal-organic framework by:

providing unactivated metal-organic framework; and

subjecting the unactivated metal-organic framework to a selected temperature under reduced pressure for a selected period of time to obtain an activated metal-organic framework.

50. The process of claim 40, wherein the metal-organic framework comprises a porous ReO_3-type aluminum formate, a congener of the porous ReO_3-type aluminum formate, or a combination comprising at least one of the foregoing metal-organic framework.

51. The process of claim 40, wherein the metal-organic framework has an X-ray powder diffraction pattern that comprises 2θ peaks at 10.98°, 15.55°, 19.07°, 22.05°, 24.70°, 27.10°, 29.31°, 31.89°, 33.35°, and 35.21 at 300 K with a unit cell lattice parameter of 11.39 Å, space group Im-3 (204) for X-rays at a wavelength 1.5406 Å.

52. The process of claim 40, wherein the metal-organic framework is $X_{1-n}Y_nZ_3$,

wherein:

X is a metal;

Y is a metal, and Y is different than X;

Z is selected from the group consisting of HCOO-*, RCOO-*, H_2PO_2, and NO_2, wherein * is a point of atachment;

R is a C1 to C6 alkyl group; and

n is a real number from 0 to 1.

53. The process of claim 52, wherein X has a +3 oxidation state.

54. The process of claim 52, wherein X comprises Al, Fe, Mn, Y, Sc, Ga, In, Ti, Fe, Mn, V, Cr, Co, Tl, Bi, Ru, Os, Re, Ir, Rh, Ce, La, Pr, Nd, Sm, Eu, Gd, Tb, Dy, Ho, Er, Tm, Yb, Lu, or a combination comprising at least one of the foregoing metals.

55. The process of claim 52, wherein X comprises a plurality of different metals.

56. The process of claim 52, wherein X is Al.

57. The process of claim 52, wherein Y has a +3 oxidation state.

58. The process of claim 52, wherein Y comprises Al, Fe, Mn, Y, Sc, Ga, In, Ti, Fe, Mn, V, Cr, Co, Tl, Bi, Ru, Os, Re, Ir, Rh, Ce, La, Pr, Nd, Sm, Eu, Gd, Tb, Dy, Ho, Er, Tm, Yb, Lu, or a combination comprising at least one of the foregoing metals.

59. The process of claim 52, wherein Y comprises a plurality of different metals.

60. The process of claim 52, wherein Y is Fe.

61. The process of claim 52, wherein Z is HCOO-*.

62. The process of claim 52, wherein n is from 0 to 0.99.

63. The process of claim 62, wherein n is from 0.25 to 0.85.

64. The process of claim 52, wherein the metal-organic framework is selected from the group consisting of $Al(HCOO)_3$, $Al_{0.75}Fe_{0.25}(HCOO)_3$; $Al_{0.5}Fe_{0.5}(HCOO)_3$; $Al_{0.25}Fe_{0.75}(HCOO)_3$; $Al_{0.15}Fe_{0.85}(HCOO)_3$; $V(HCOO)_3$; and $V_{0.3}Al_{0.7}(HCOO)_3$.

65. The process of claim 52, wherein the metal-organic framework absorbs molecular hydrogen at a temperature from 0 K to 300 K at a pressure from 0 bar to 700 bar.

66. The process of claim 52, wherein the metal-organic framework selectively adsorbs molecular hydrogen in a composition comprising the molecular hydrogen and a polyatomic component, such that the metal-organic framework adsorbs the molecular hydrogen in an absence of adsorbing other components of the composition.

67. The process of claim 66, wherein the polyatomic component comprises a hydrocarbon, CO_2, or a combination comprising at least one of the foregoing polyatomic components.

68. The process of claim 67, wherein the hydrocarbon comprises methane.

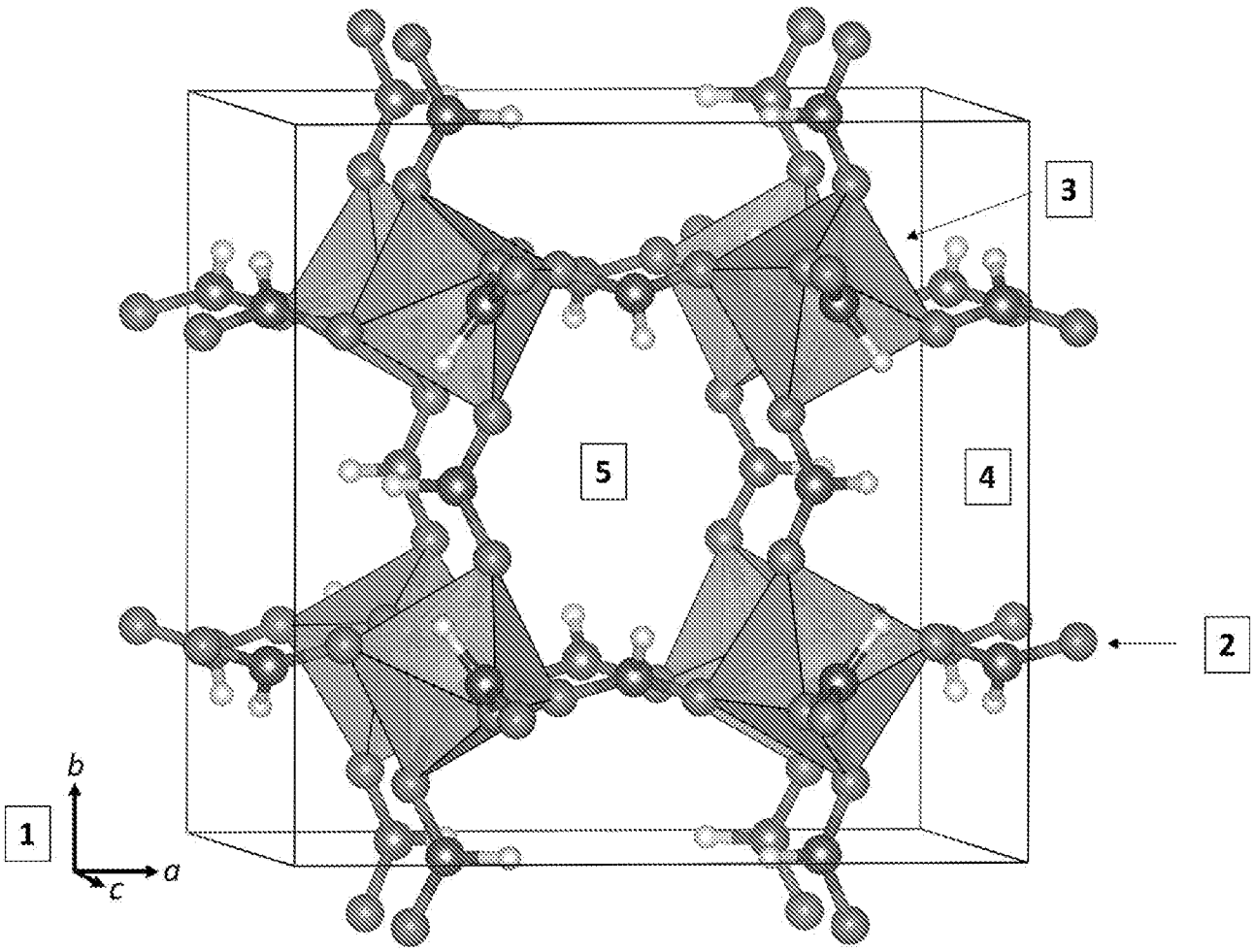

FIG. 1

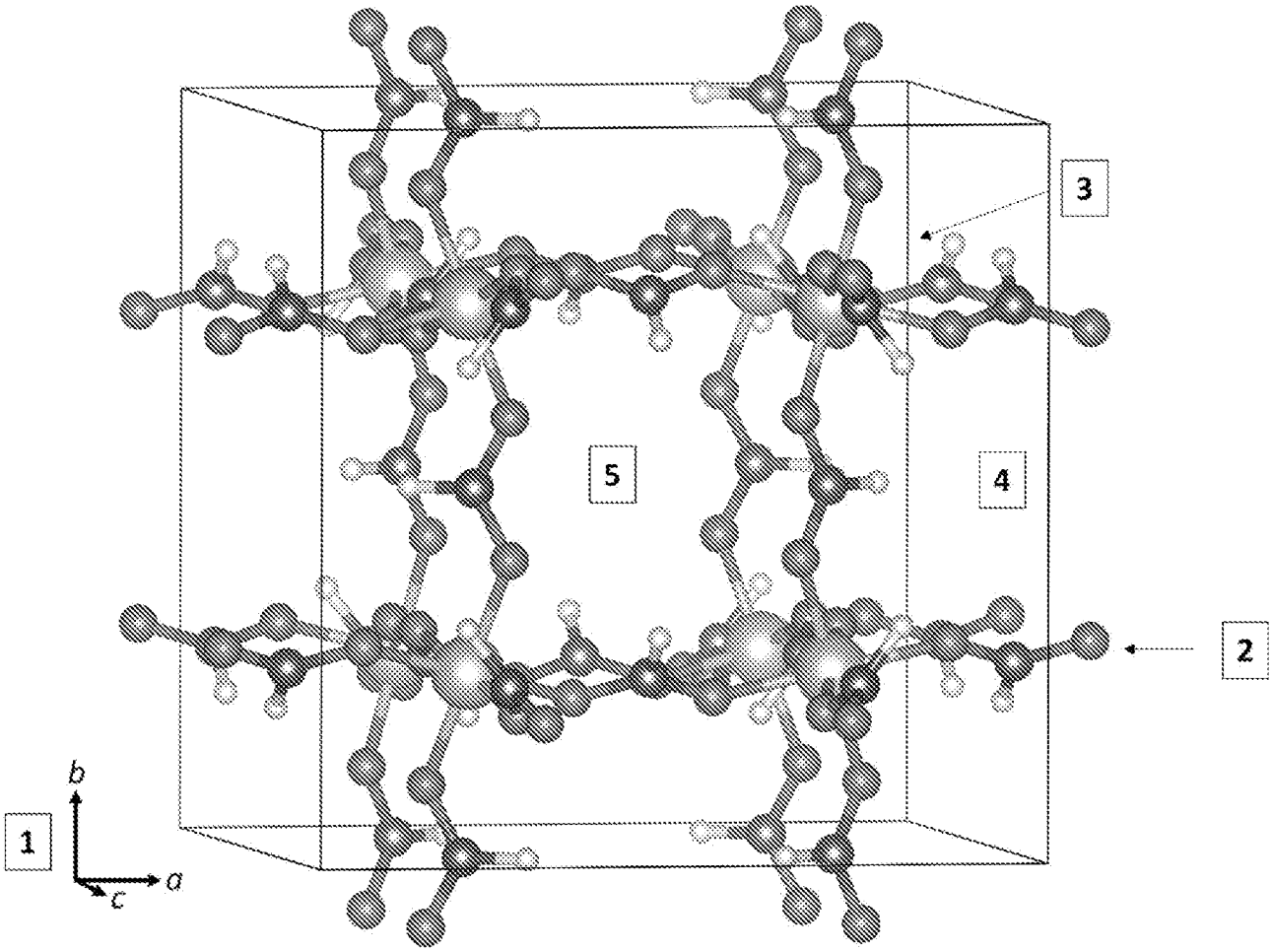

FIG. 2

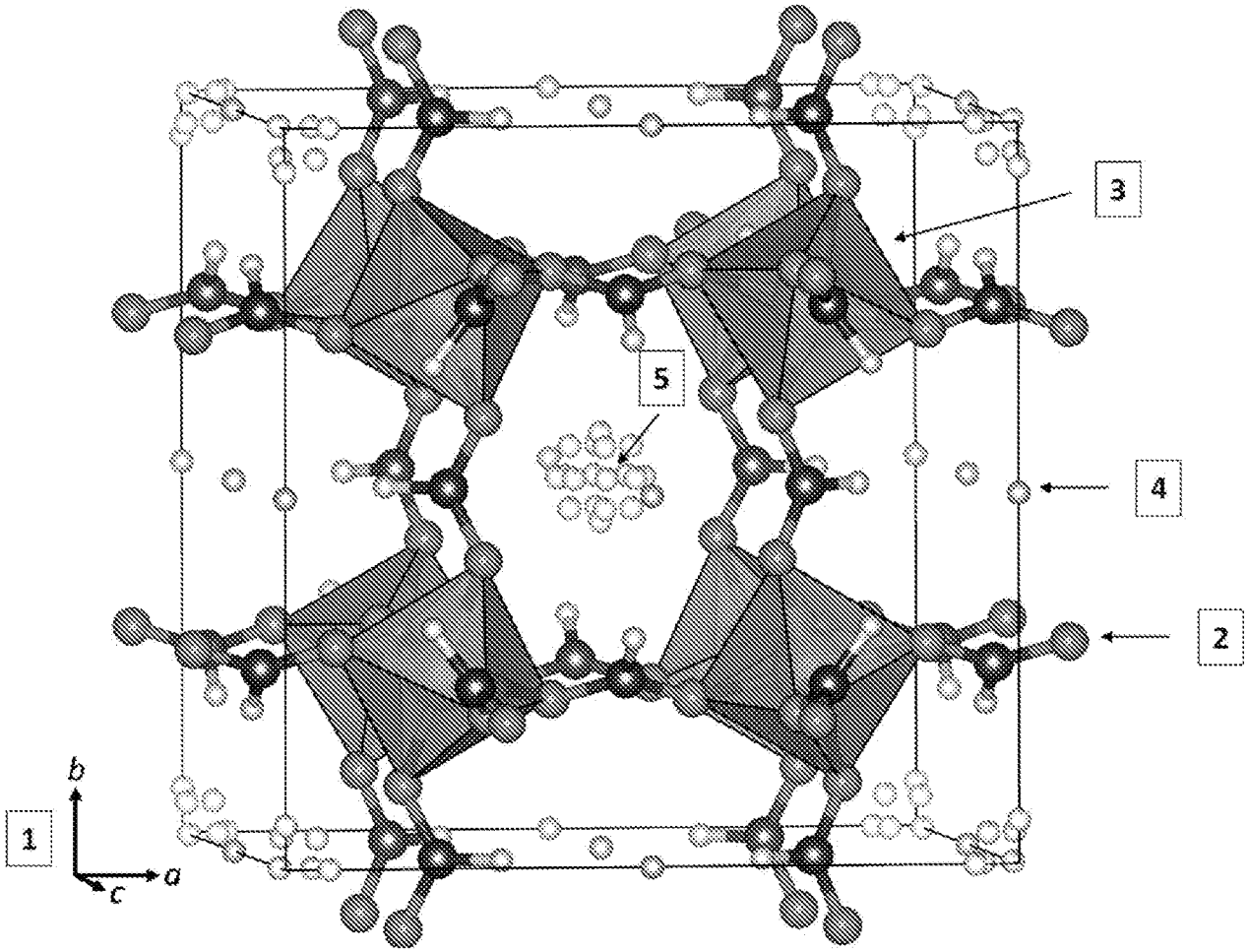

FIG. 3

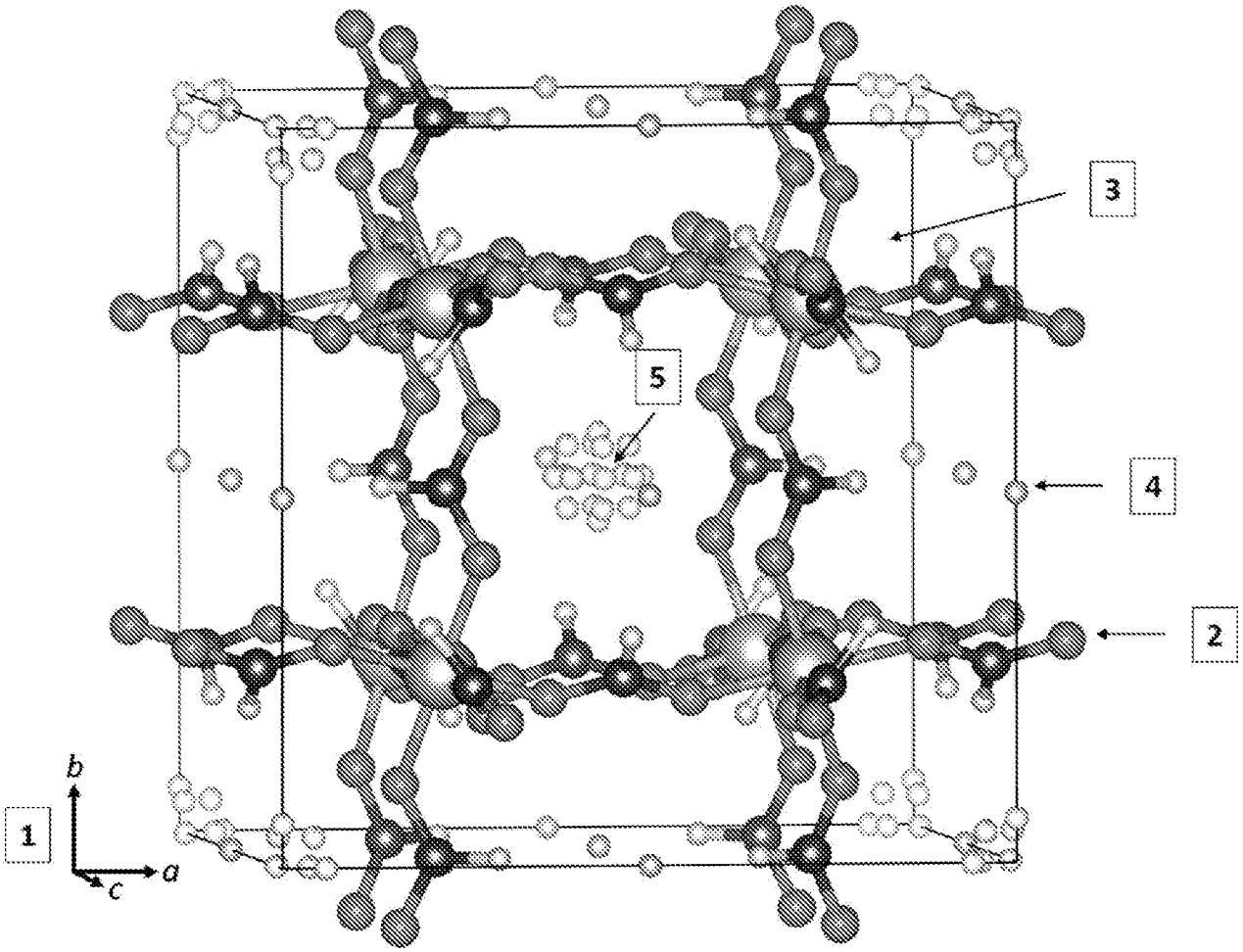

FIG. 4

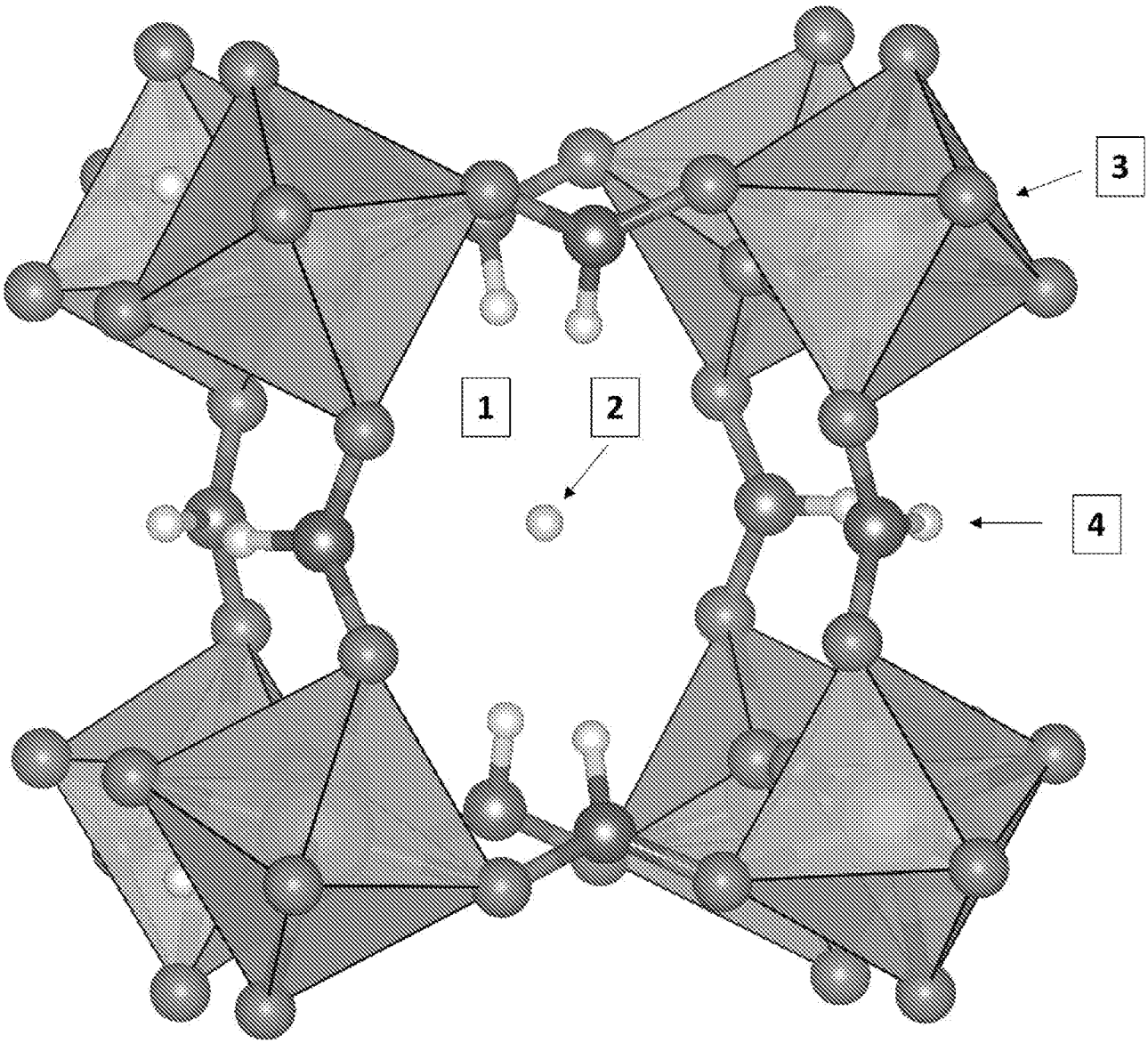

FIG. 5

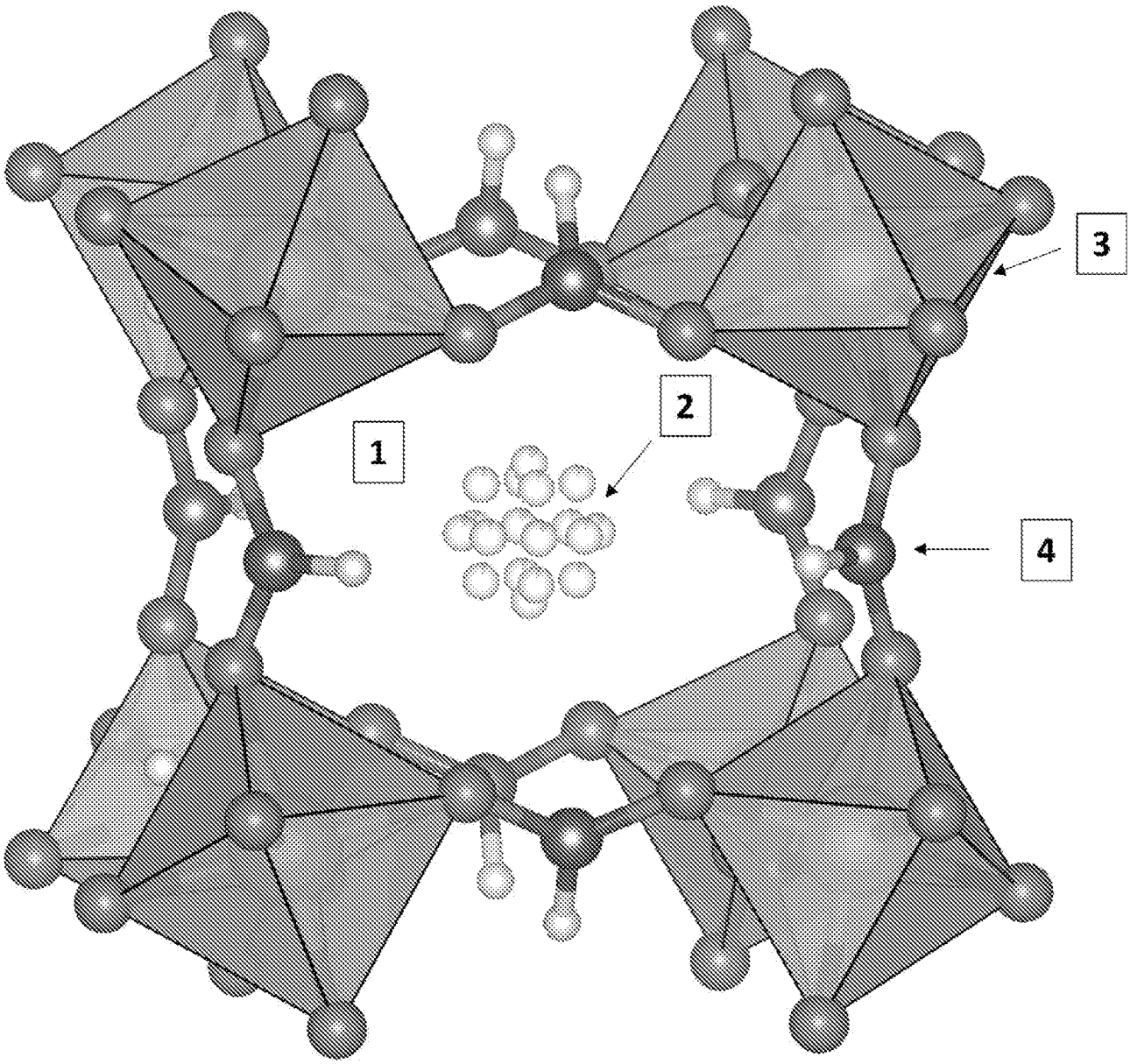

FIG. 6

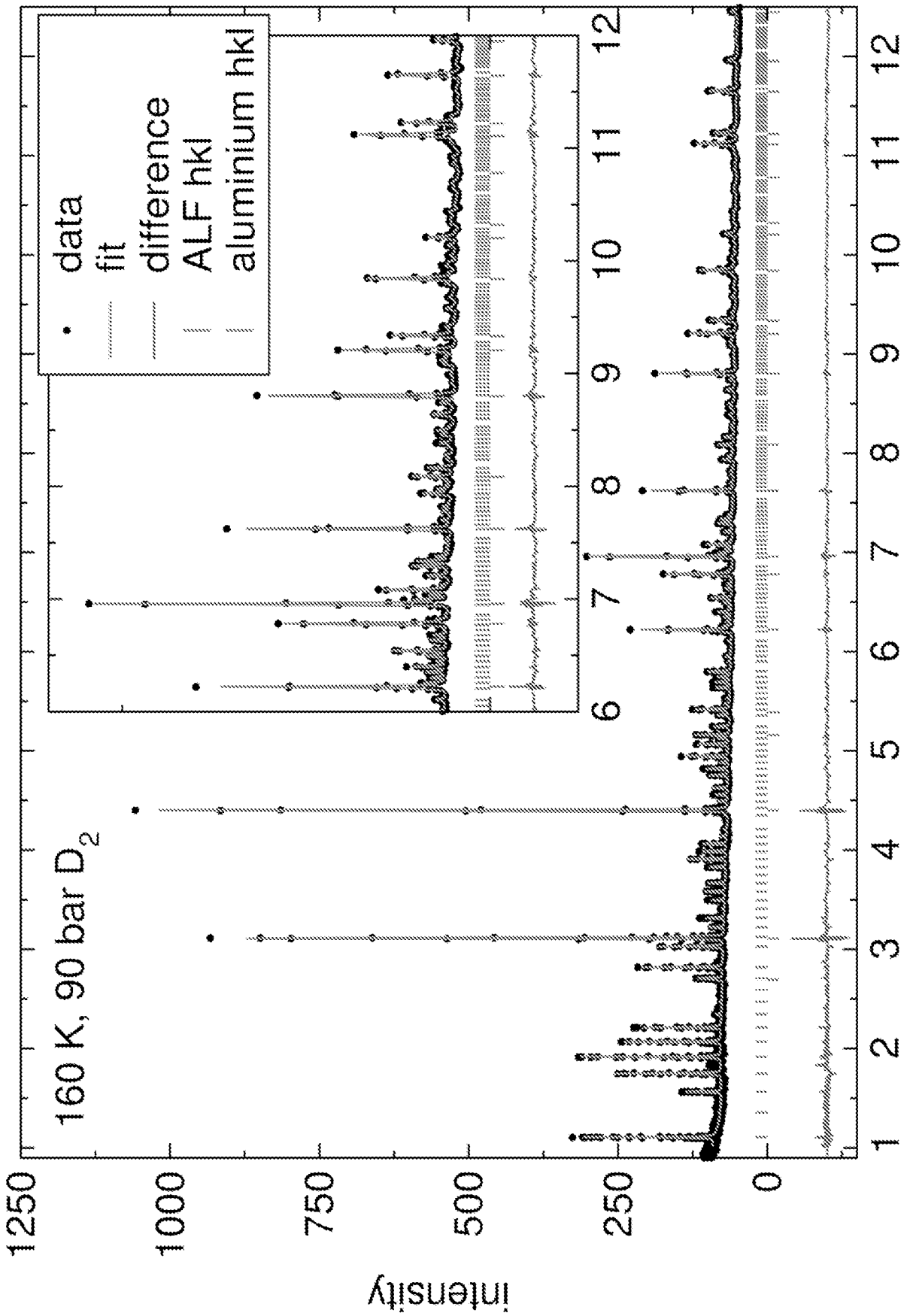
160 K, 90 bar D_2
data
fit
difference
ALF hkl
aluminium hkl
intensity
Q ($Å^{-1}$)
0
250
500
750
1000
1250
1
2
3
4
5
6
7
8
9
10
11
12

FIG. 7

atom #	element	label	x	y	z	Occ.	B	Site	Sym.
1	Al	Al	0.25	0.25	0.25	1	0.2	8c	.-3.
2	C	C1	0.2581(4)	0.2430(3)	0	1	0.653(3)	24g	m..
3	H	H1	0.799(1)	0.6773(9)	0	1	4.0(2)	24g	m..
4	O	O1	0.903(2)	0.7116(2)	0.2001(2)	1	0.73(3)	48h	1
5	D	D1	0	0.5	0	1.26(5)	14.2(7)	6b	mmm..
6	D	D2	0.0421(2)	0.0421(2)	0	0.077(7)	1.7(7)	24g	m..
7	D	D2_2	0.0595(4)	0	0	0.077(7)	1.7(7)	12d	mm2..

FIG. 8

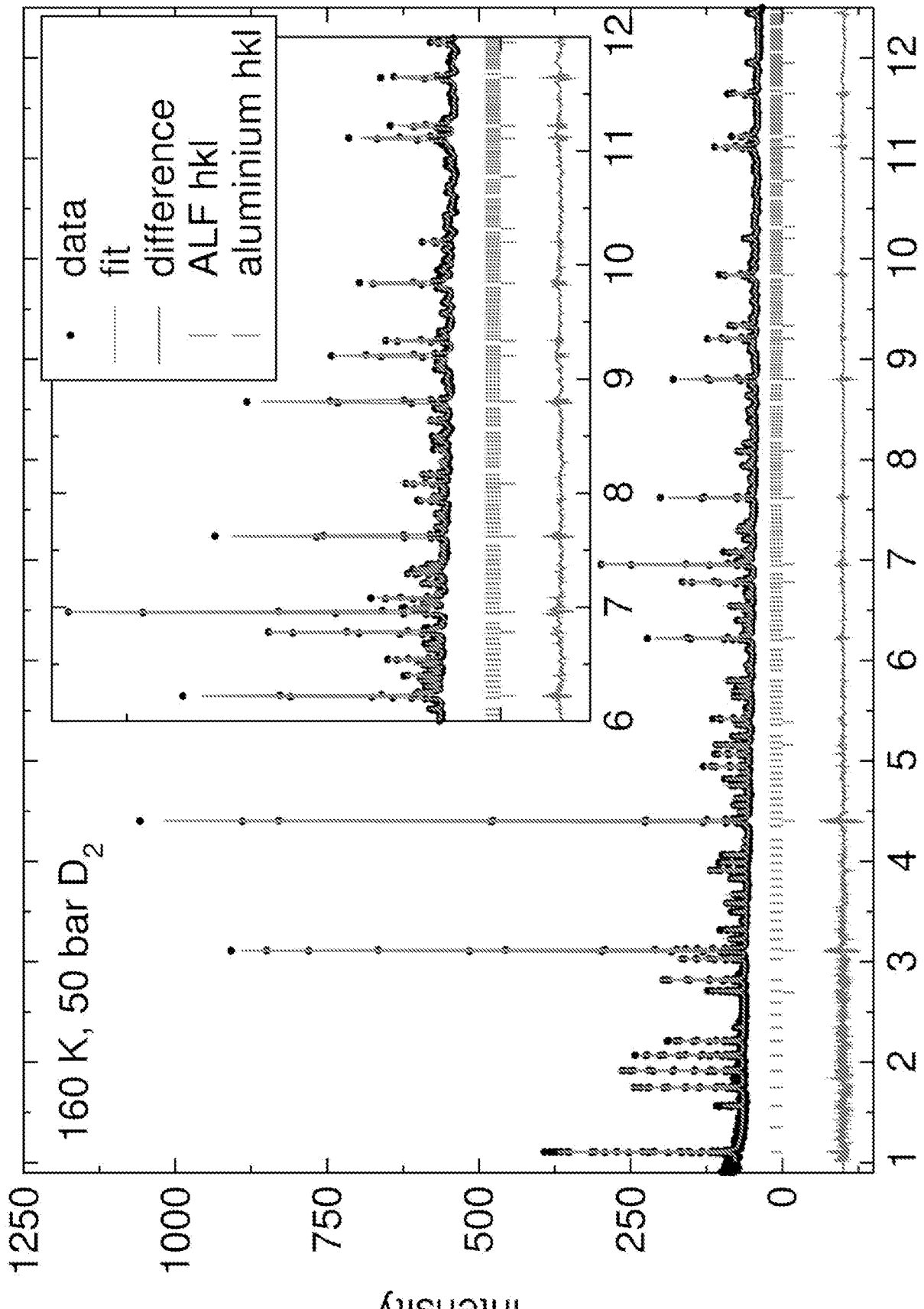
160 K, 50 bar D_2
data
fit
difference
ALF hkl
aluminium hkl
intensity
Q (Å^{-1})
0
250
500
750
1000
1250
1
2
3
4
5
6
7
8
9
10
11
12

FIG. 9

atom #	element	label	x	y	z	Occ.	B	Site	Sym.
1	Al	Al	0.25	0.25	0.25	1	0.2	8c	.-3.
2	C	C1	0.2579(4)	0.2428(3)	0	1	0.71(3)	24g	m..
3	H	H1	0.799(1)	0.6775(9)	0	1	4.2(2)	24g	m..
4	O	O1	0.9033(2)	0.7116(2)	0.1999(2)	1	0.75(3)	48h	1
5	D	D1	0	0.5	0	1.13(5)	14.2(7)	6b	mmm..
6	D	D2	0.0421(2)	0.0421(2)	0	0.067(8)	1.7(7)	24g	m..
7	D	D2_2	0.0595(4)	0	0	0.067(8)	1.7(7)	12d	mm2..

FIG. 10

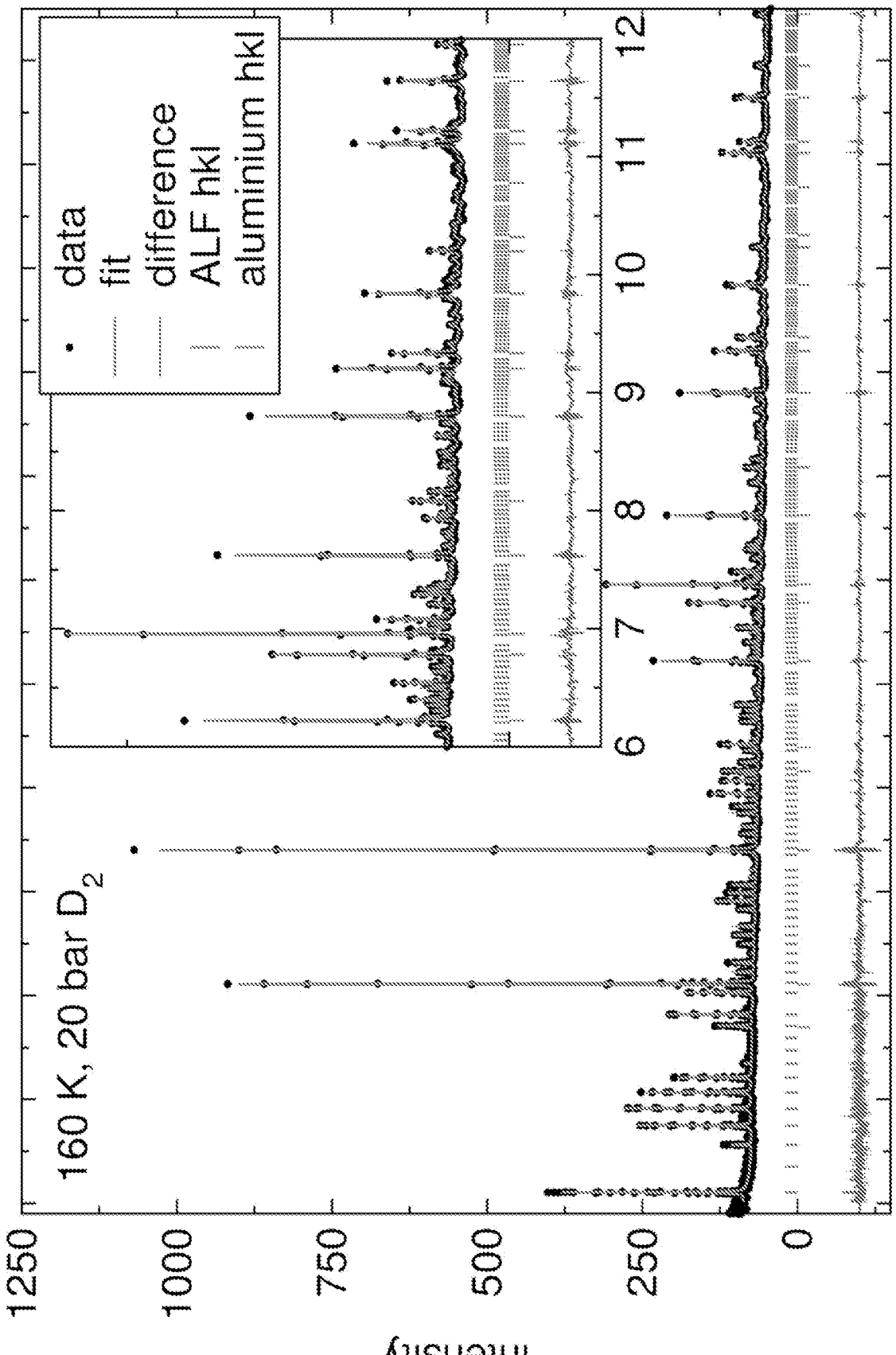
160 K, 20 bar D_2
data
fit
difference
ALF hkl
aluminium hkl
intensity
Q ($Å^{-1}$)
0
250
500
750
1000
1250
1
2
3
4
5
6
7
8
9
10
11
12

FIG. 11

atom #	element	label	x	y	z	Occ.	B	Site	Sym.
1	Al	Al	0.25	0.25	0.25	1	0.2	8c	.-3.
2	C	C1	0.2580(3)	0.2426(3)	0	1	0.69(4)	24g	m..
3	H	H1	0.800(1)	0.6780(9)	0	1	4.3(2)	24g	m..
4	O	O1	0.9035(2)	0.7114(2)	0.1998(2)	1	0.75(3)	48h	1
5	D	D1	0	0.5	0	0.83(5)	14.2(7)	6b	mmm . .
6	D	D2	0.0421(2)	0.0421(2)	0	0.059(8)	1.7(7)	24g	m..
7	D	D2_2	0.0595(4)	0	0	0.059(8)	1.7(7)	12d	mm2 . .

FIG. 12

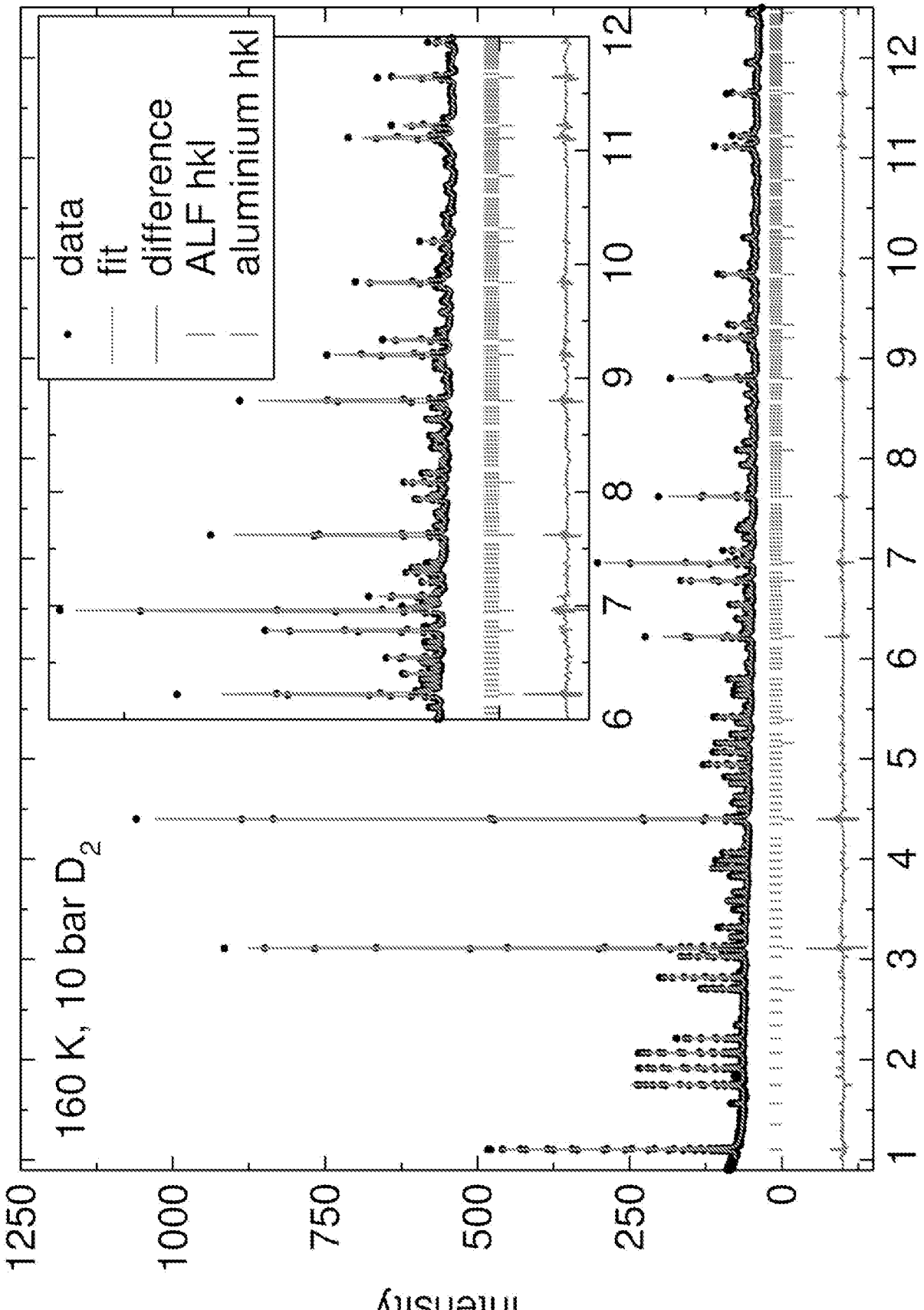
160 K, 10 bar D_2
data
fit
difference
ALF hkl
aluminium hkl
intensity
Q (Å^{-1})
0
250
500
750
1000
1250
1
2
3
4
5
6
7
8
9
10
11
12

FIG. 13

atom #	element	label	x	y	z	Occ.	B	Site	Sym.
1	Al	Al	0.25	0.25	0.25	1	0.2	8c	.-3.
2	C	C1	0.2579(4)	0.2429(3)	0	1	0.73(3)	24g	m..
3	H	H1	0.801(1)	0.6788(9)	0	1	4.0(2)	24g	m..
4	O	O1	0.9034(2)	0.7113(2)	0.1997(3)	1	0.74(3)	48h	1
5	D	D1	0	0.5	0	0.43(5)	14.2(7)	6b	mmm..
6	D	D2	0.0421(2)	0.0421(2)	0	0.031(7)	1.7(7)	24g	m..
7	D	D2_2	0.0595(4)	0	0	0.031(7)	1.7(7)	12d	mm2..

FIG. 14

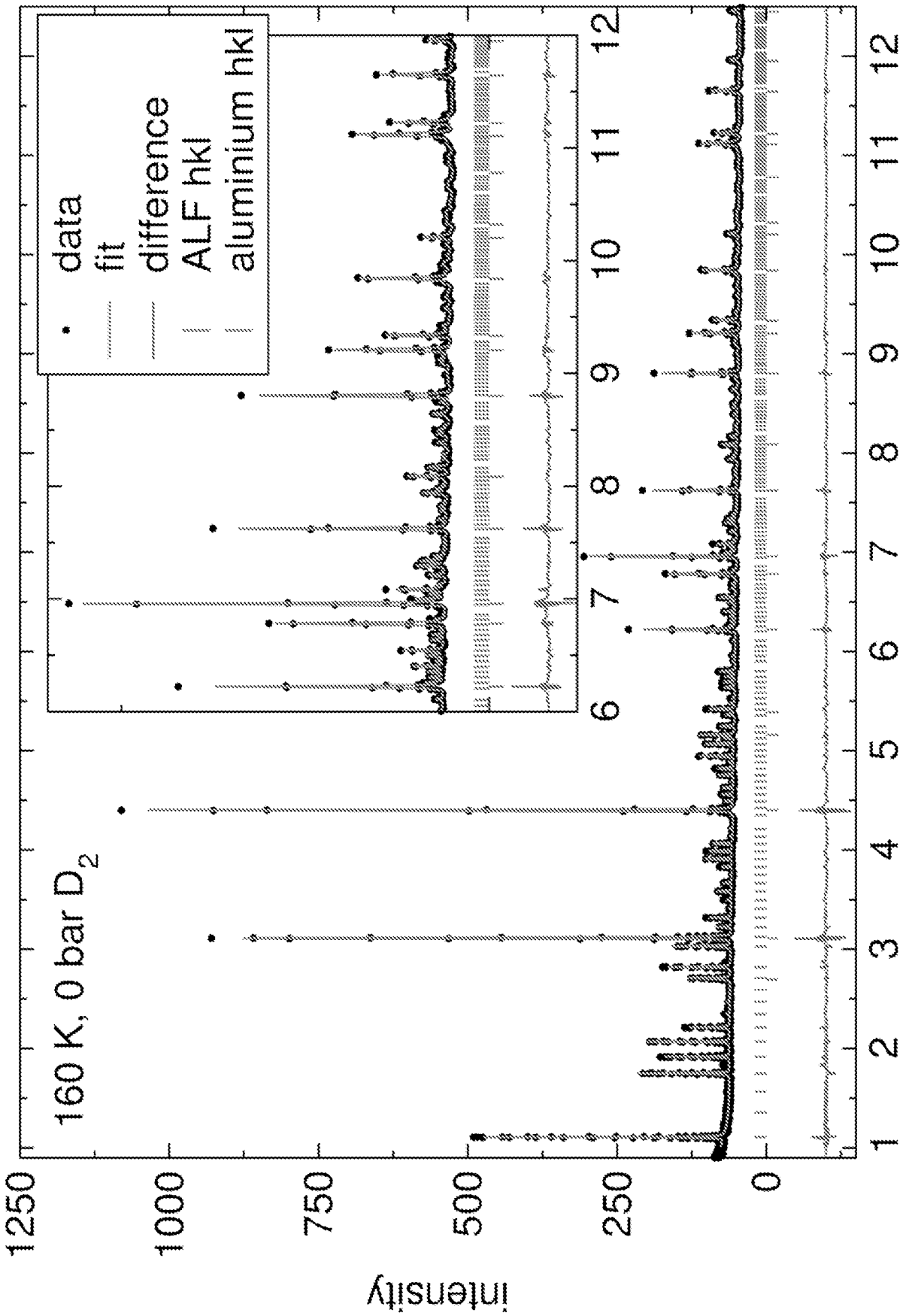
160 K, 0 bar D_2
data
fit
difference
ALF hkl
aluminium hkl
intensity
Q (Å^{-1})
0
250
500
750
1000
1250
1
2
3
4
5
6
7
8
9
10
11
12

FIG. 15

atom #	element	label	x	y	z	Occ.	B	Site	Sym.
1	Al	Al	0.25	0.25	0.25	1	0.2	8c	.-3.
2	C	C1	0.2600(4)	0.2410(4)	0	1	0.44(5)	24g	m..
3	H	H1	0.810(1)	0.683(1)	0	1	4.4(2)	24g	m..
4	O	O1	0.9035(2)	0.7110(3)	0.2000(3)	1	0.73(5)	48h	1

FIG. 16

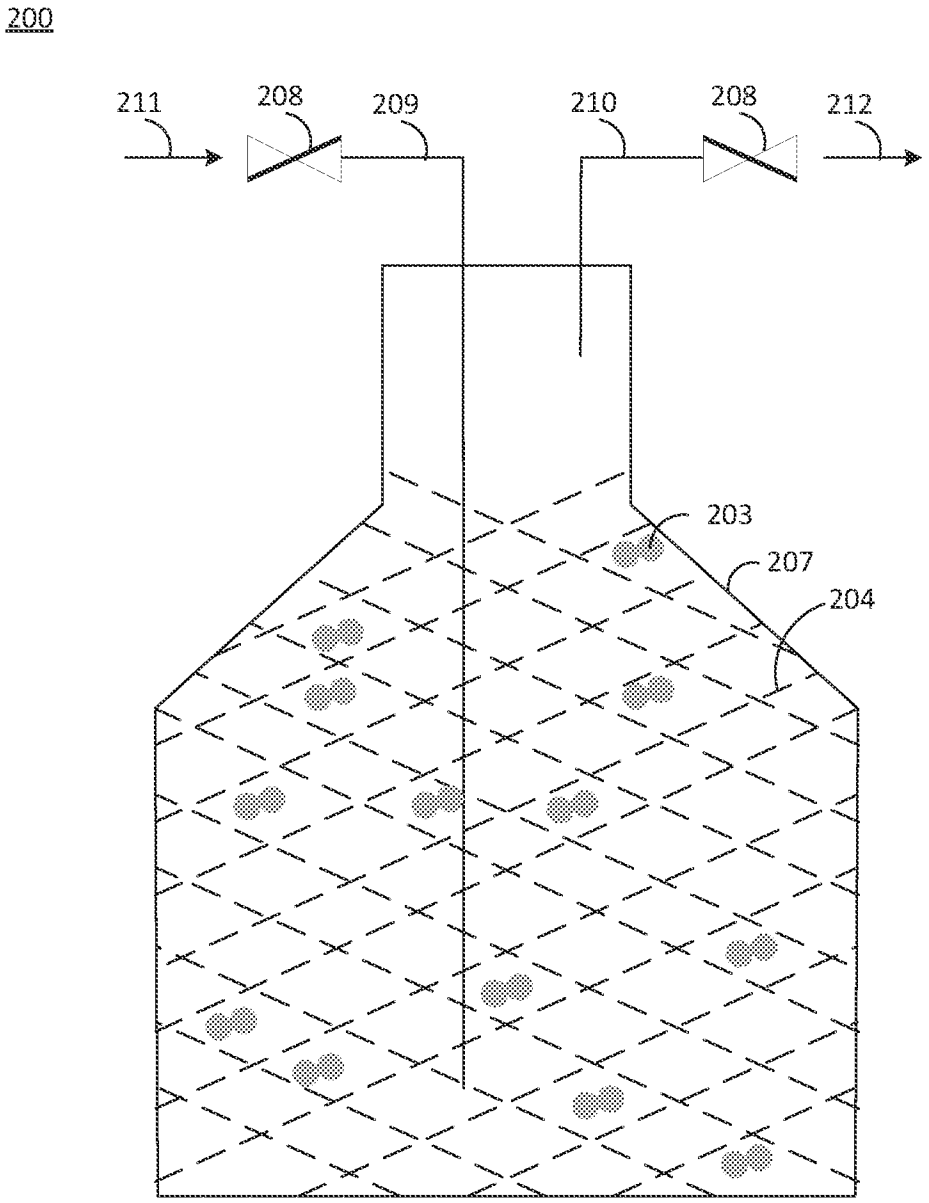

FIG. 17

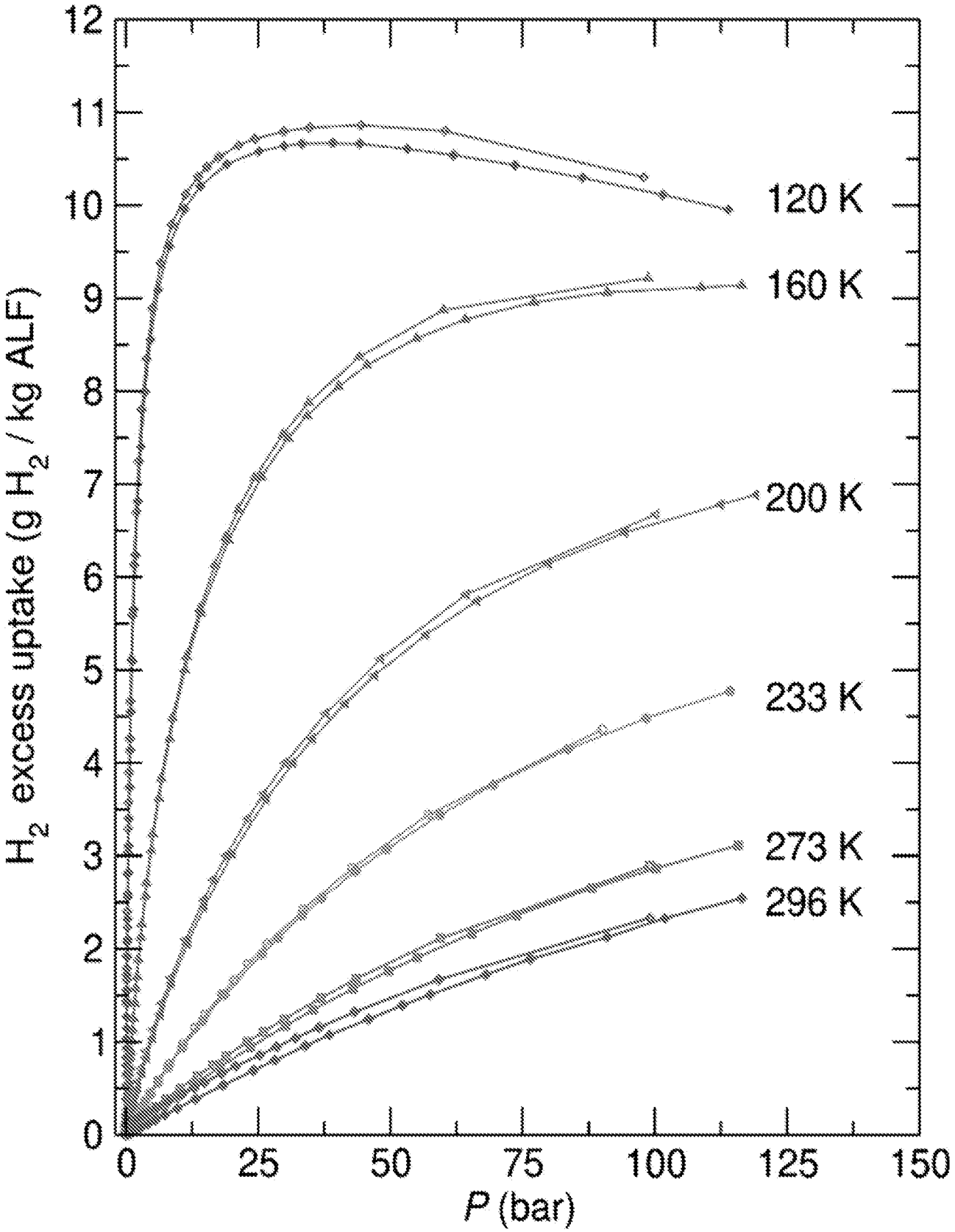
12
11
10
9
8
7
6
5
4
3
2
1
0
0
25
50
75
100
125
150
H_2 excess uptake (g H_2 / kg ALF)
P (bar)
120 K
160 K
200 K
233 K
273 K
296 K

FIG. 18

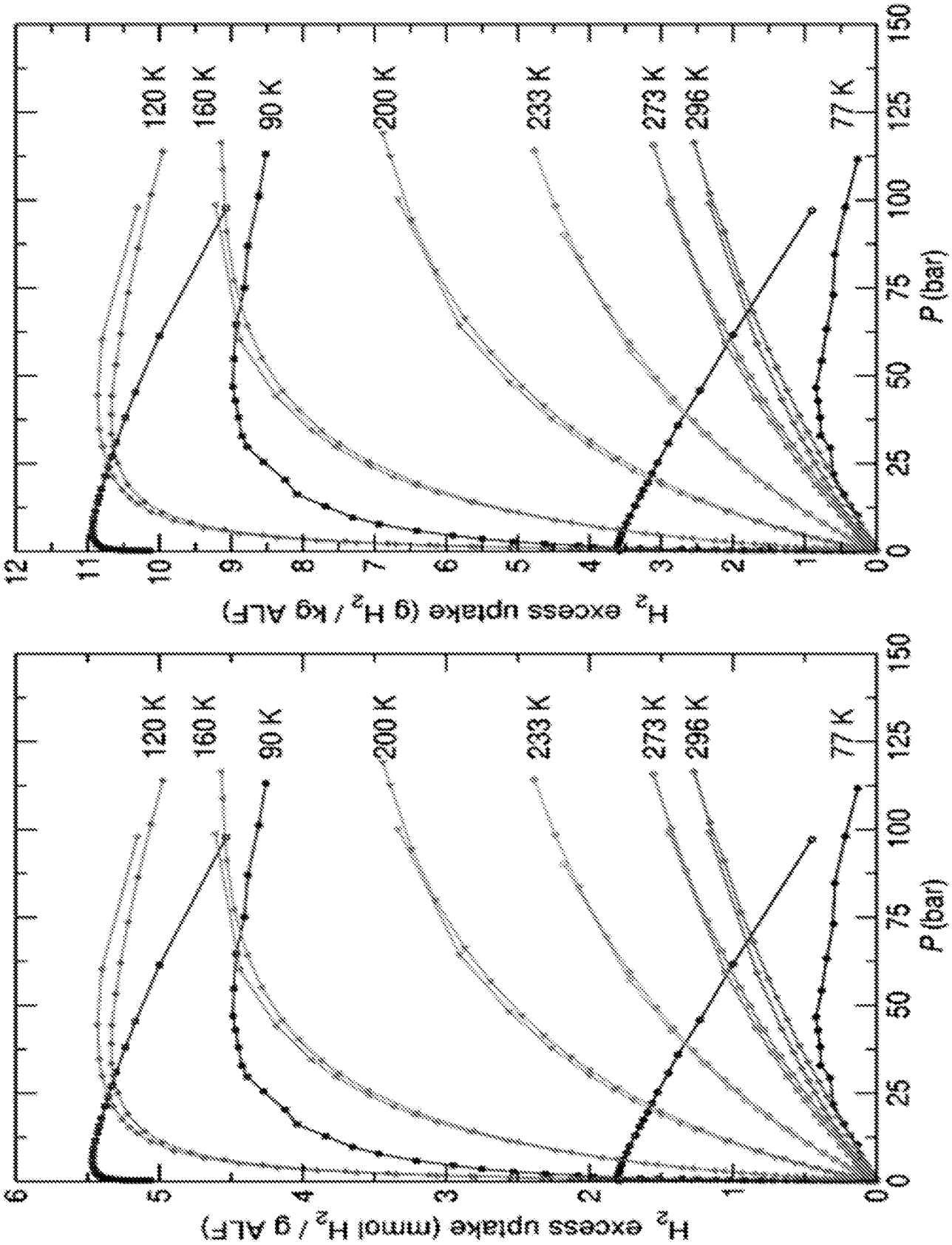
H2 excess uptake (g H2 / kg ALF)
H2 excess uptake (mmol H2 / g ALF)
P (bar)
120 K
160 K
90 K
200 K
233 K
273 K
296 K
77 K

FIG. 19

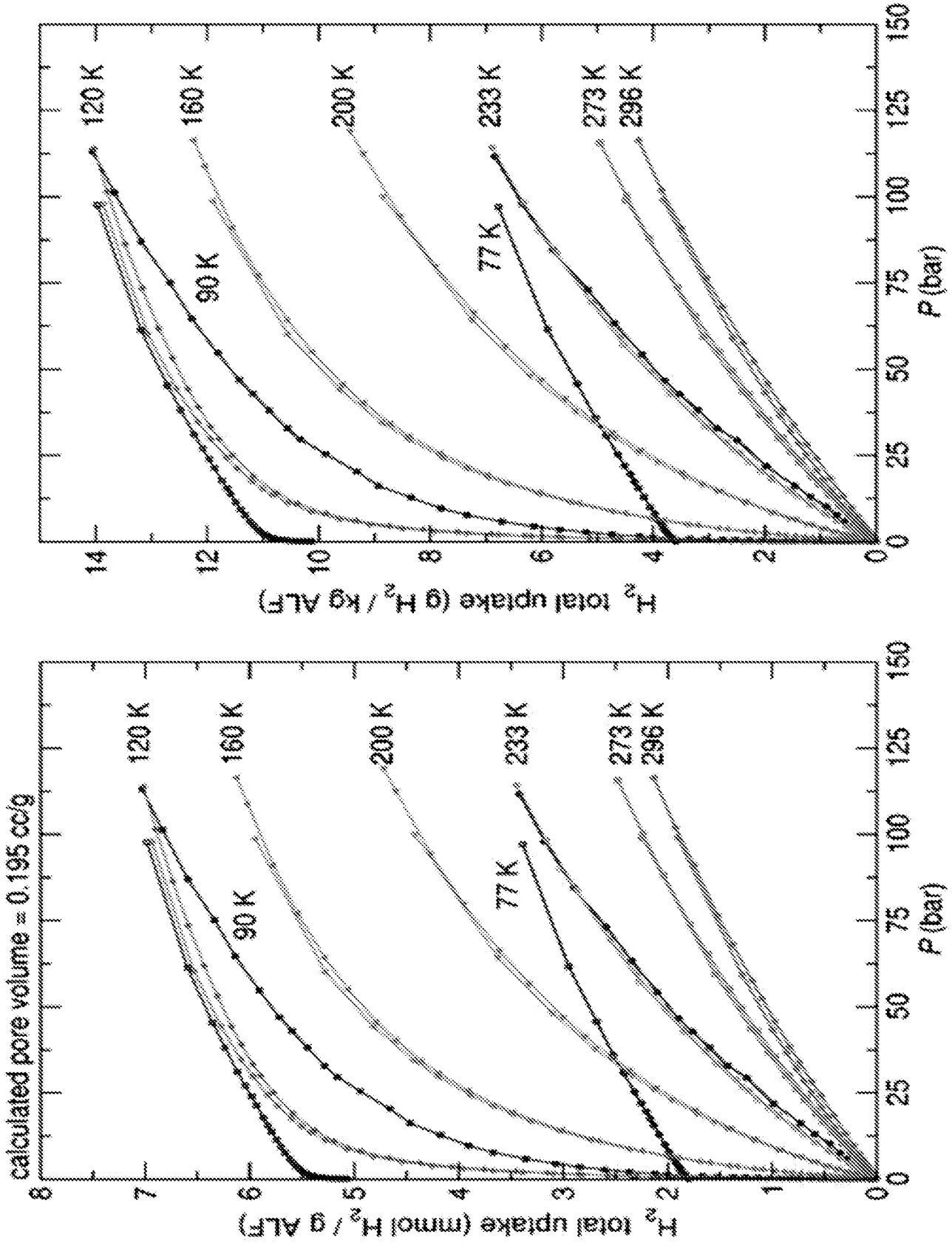
calculated pore volume = 0.195 cc/g
H2 total uptake (mmol H2 / g ALF)
H2 total uptake (g H2 / kg ALF)
P (bar)
120 K
160 K
200 K
233 K
273 K
296 K
90 K
77 K

FIG. 20

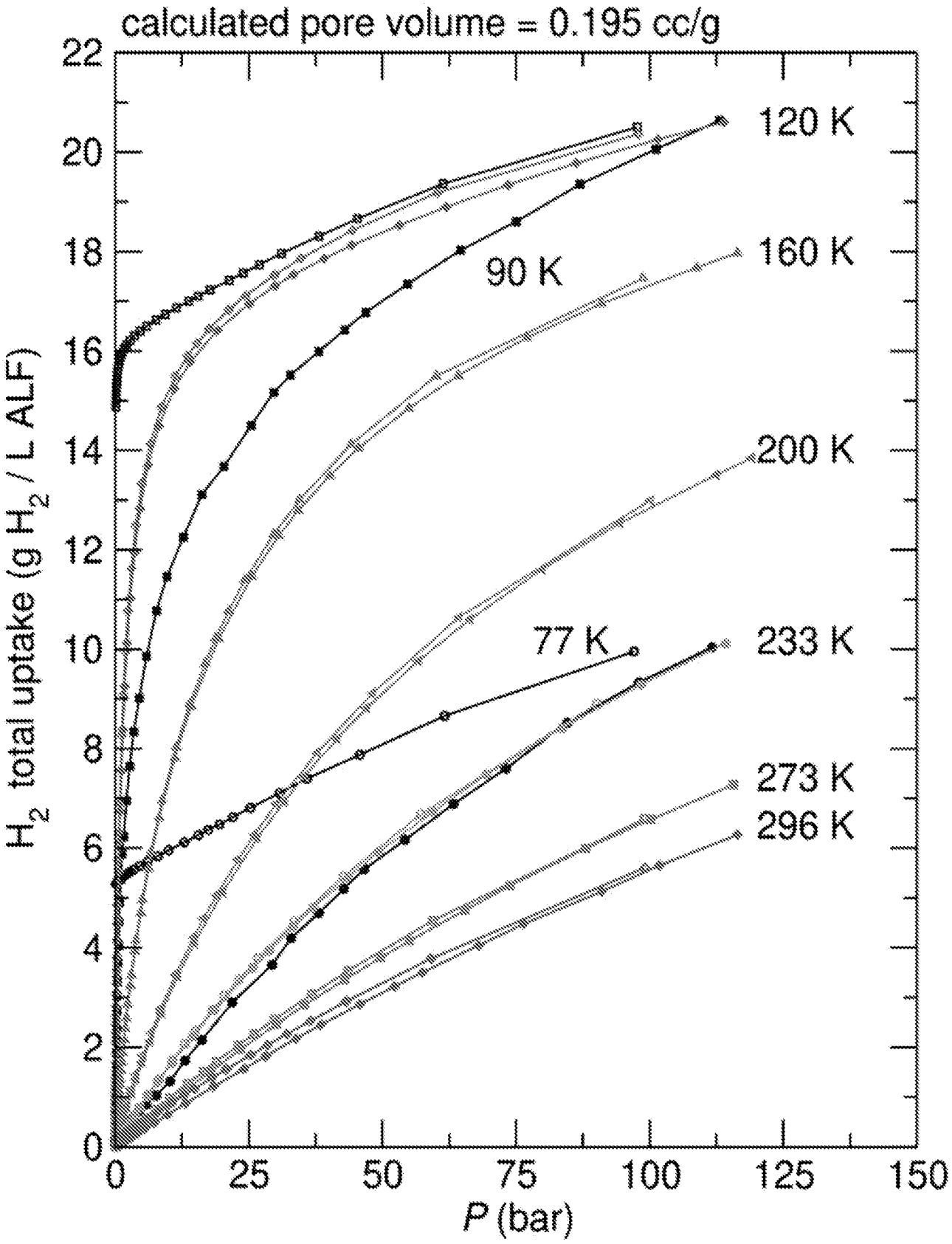
calculated pore volume = 0.195 cc/g
H2 total uptake (g H2 / L ALF)
P (bar)
0
2
4
6
8
10
12
14
16
18
20
22
0
25
50
75
100
125
150
120 K
160 K
90 K
200 K
77 K
233 K
273 K
296 K

FIG. 21

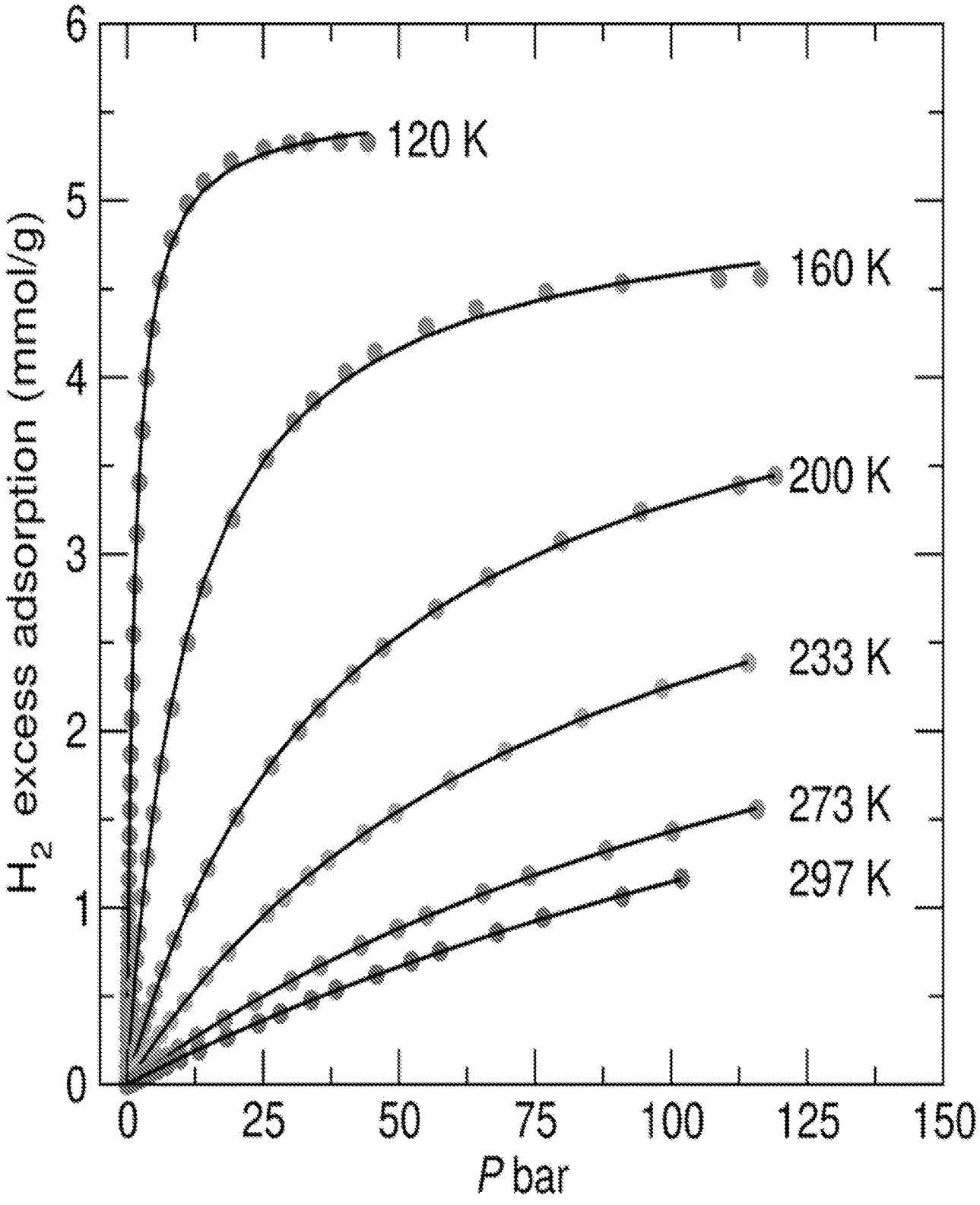
6
5
4
3
2
1
0
H_2 excess adsorption (mmol/g)
120 K
160 K
200 K
233 K
273 K
297 K
0
25
50
75
100
125
150
P bar

FIG. 22

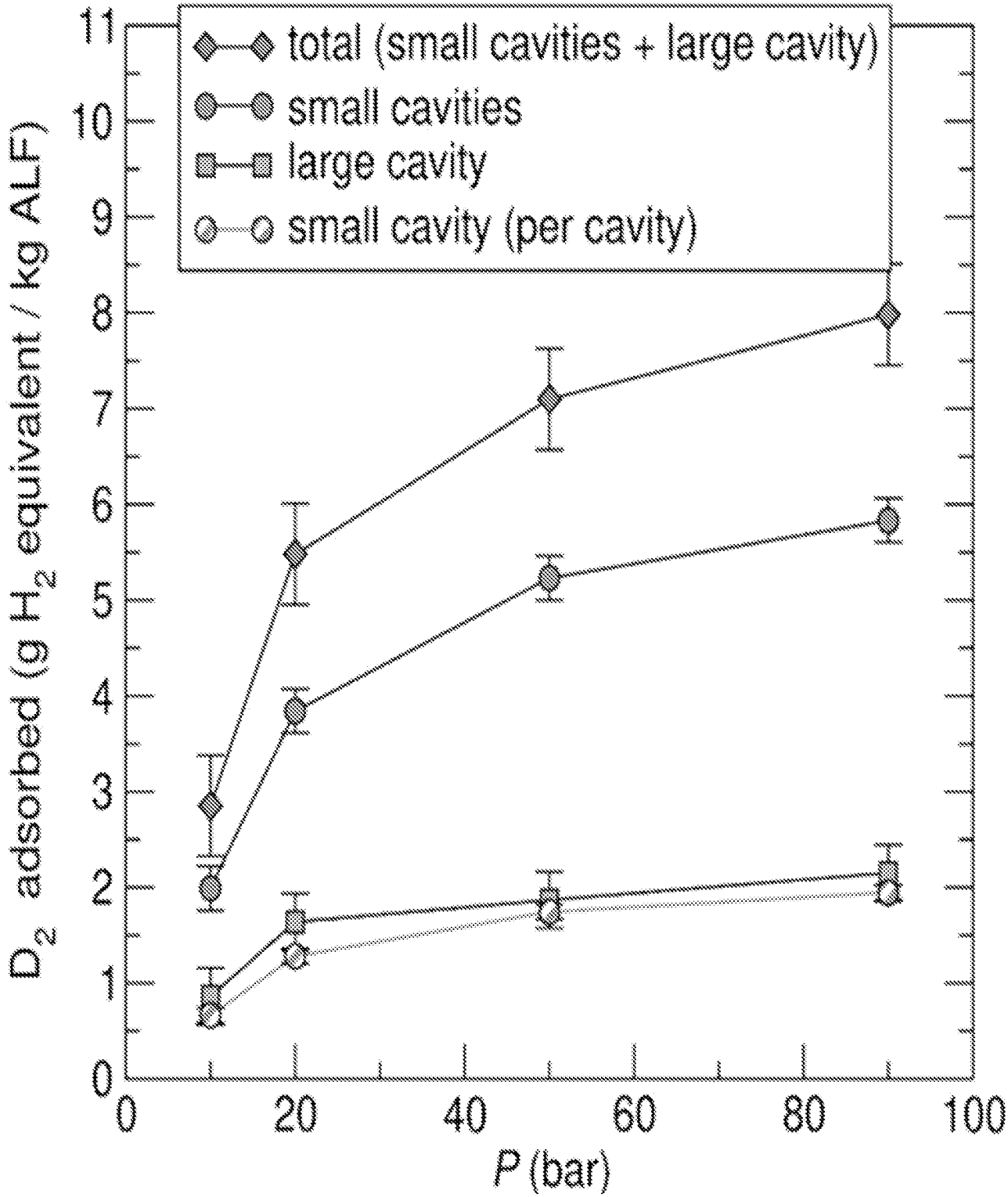
total (small cavities + large cavity)
small cavities
large cavity
small cavity (per cavity)
D_2 adsorbed (g H_2 equivalent / kg ALF)
0
1
2
3
4
5
6
7
8
9
10
11
0
20
40
60
80
100
P (bar)

FIG. 23

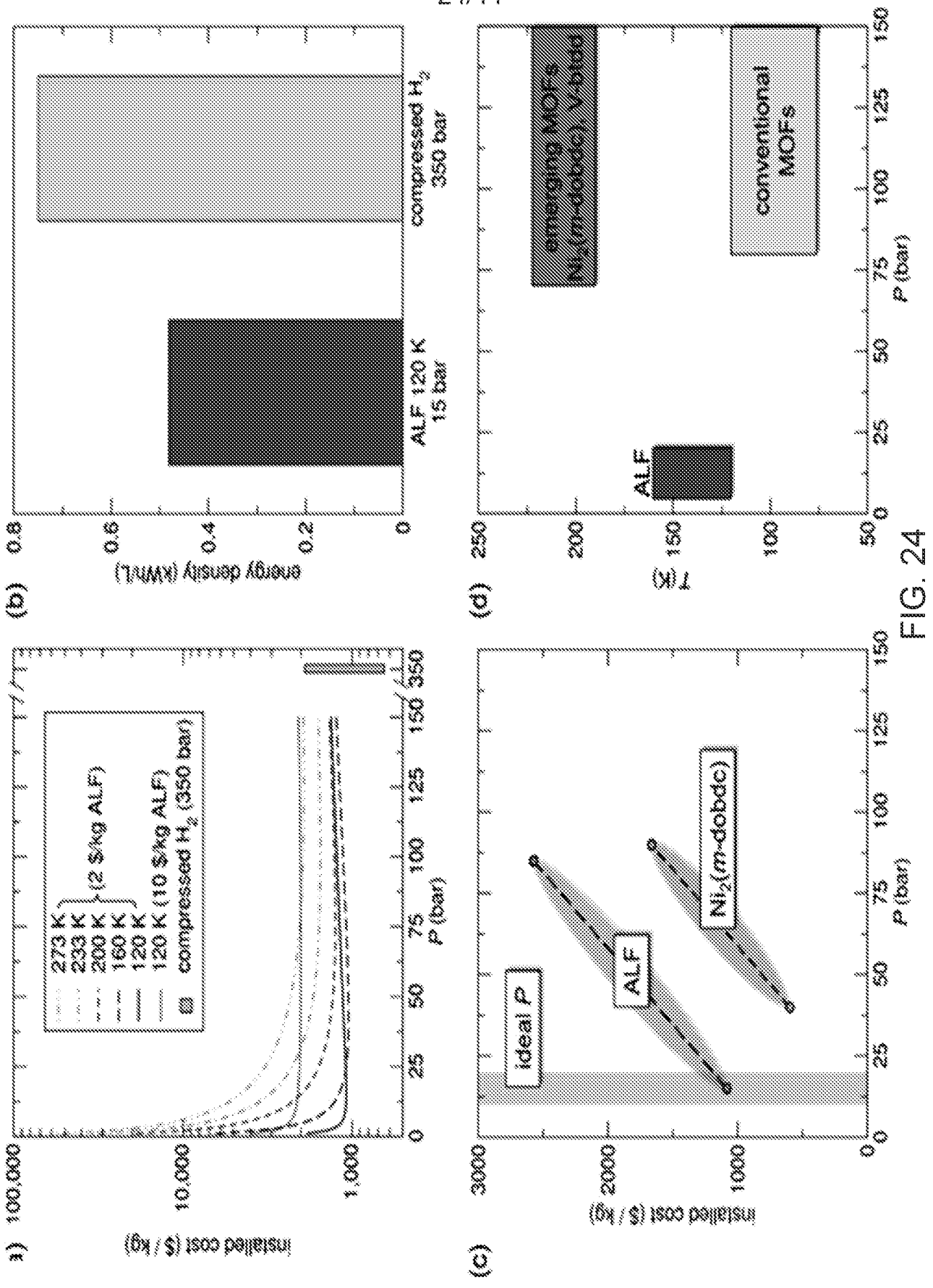
(a)
(b)
(c)
(d)
installed cost ($ / kg)
P (bar)
273 K
233 K
200 K
160 K
120 K
120 K (10 $/kg ALF)
compressed H2 (350 bar)
(2 $/kg ALF)
energy density (kWh/L)
ALF 120 K
15 bar
compressed H2
350 bar
ideal P
ALF
Ni2(m-dobdc)
T (K)
emerging MOFs
Ni2(m-dobdc), V-pted
conventional
MOFs

FIG. 24

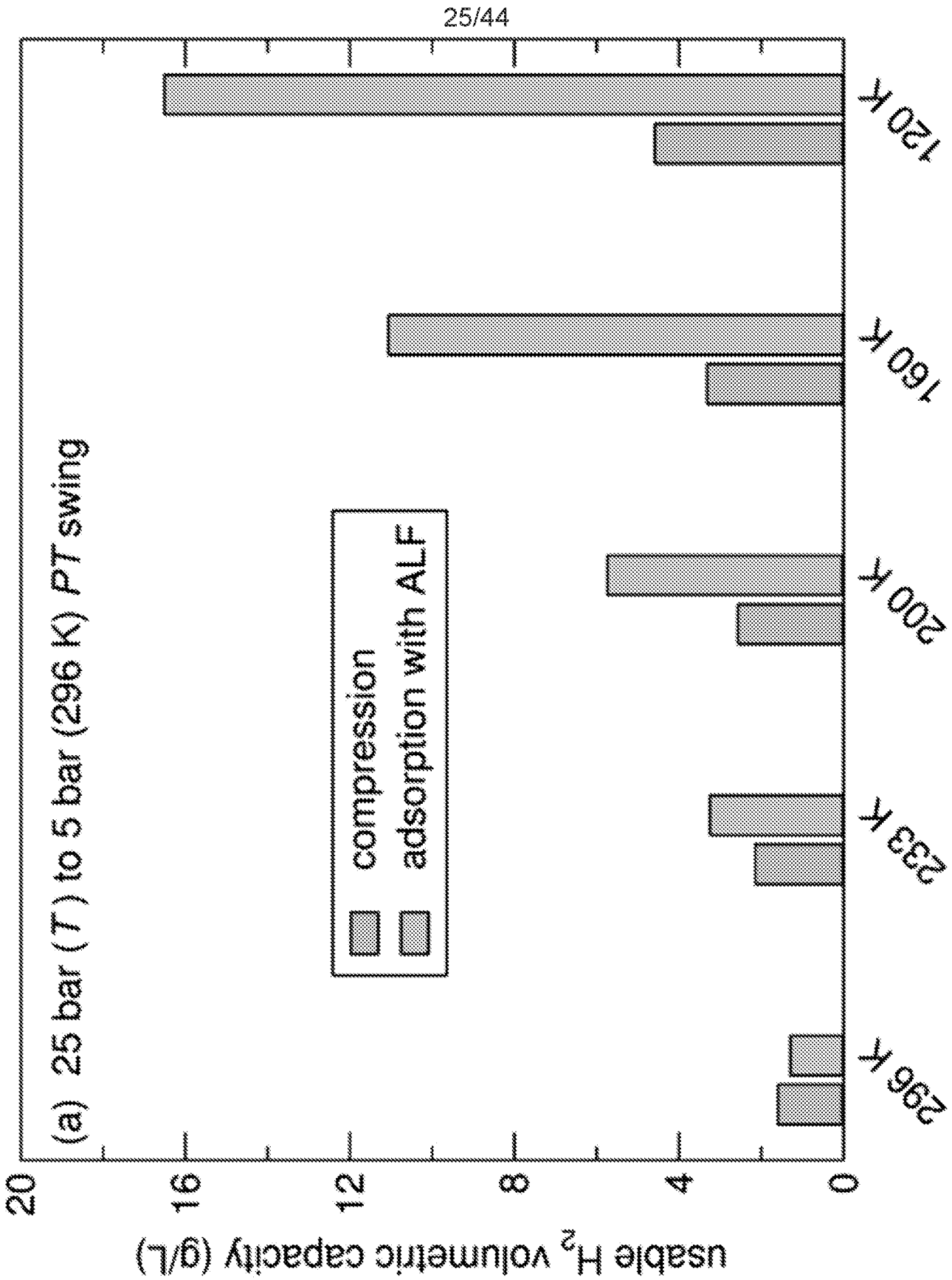
(a) 25 bar (T) to 5 bar (296 K) PT swing
compression
adsorption with ALF
120 K
160 K
200 K
233 K
296 K
0
4
8
12
16
20
usable H2 volumetric capacity (g/L)

FIG. 25

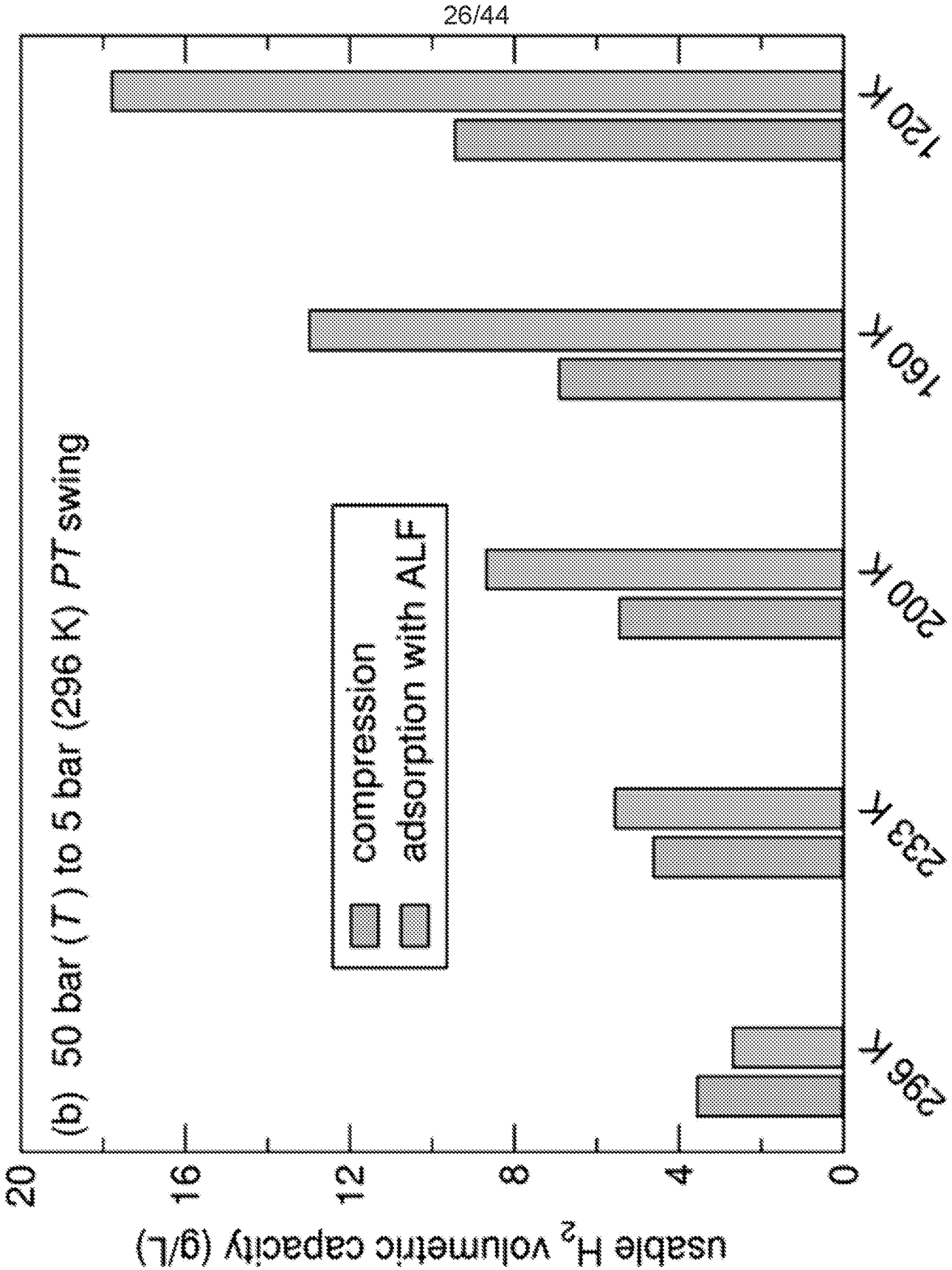
(b) 50 bar (T) to 5 bar (296 K) PT swing
compression
adsorption with ALF
120 K
160 K
200 K
233 K
296 K
0
4
8
12
16
20
usable H2 volumetric capacity (g/L)

FIG. 26

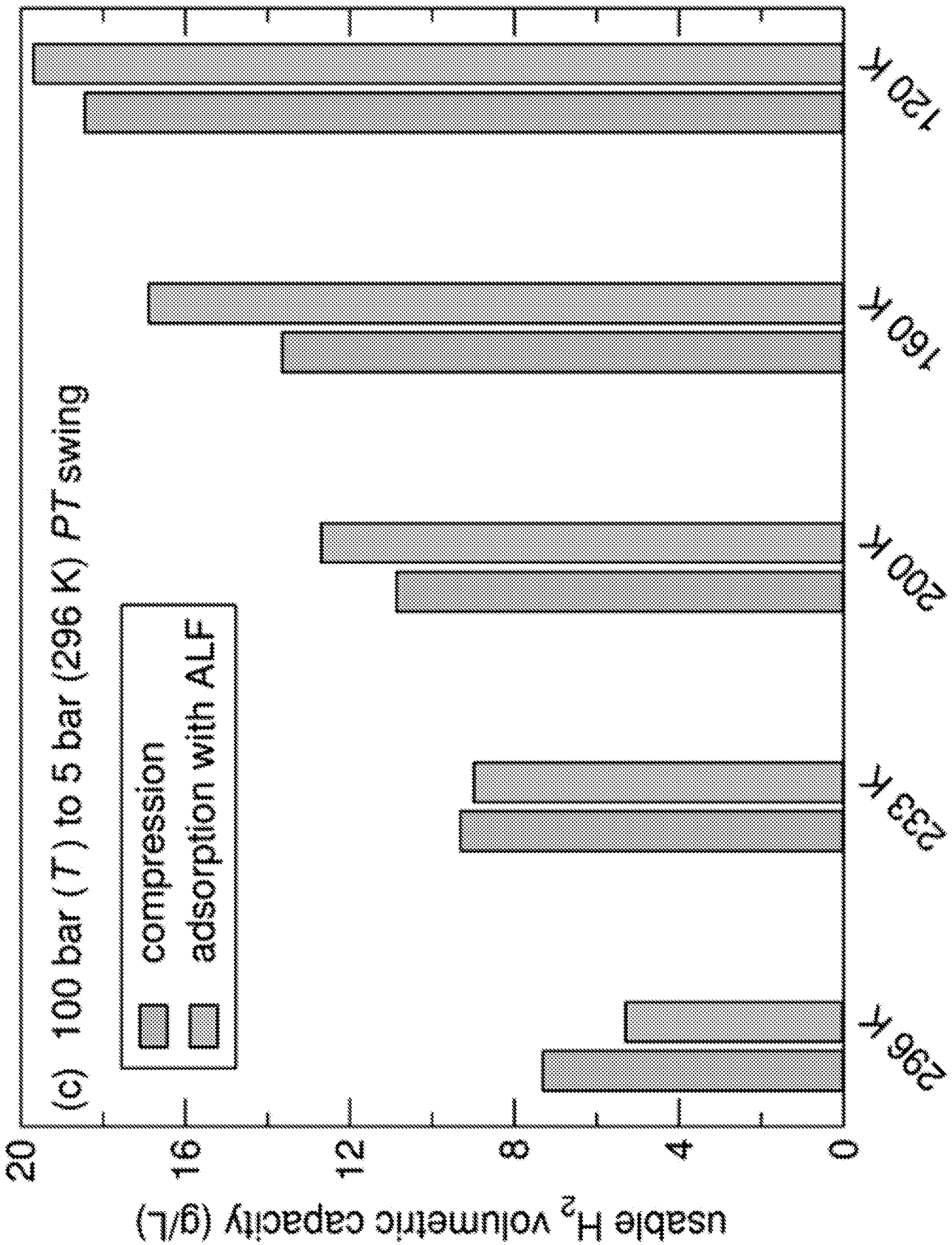
(c) 100 bar (T) to 5 bar (296 K) PT swing
compression
adsorption with ALF
usable H2 volumetric capacity (g/L)
0
4
8
12
16
20
120 K
160 K
200 K
233 K
296 K

FIG. 27

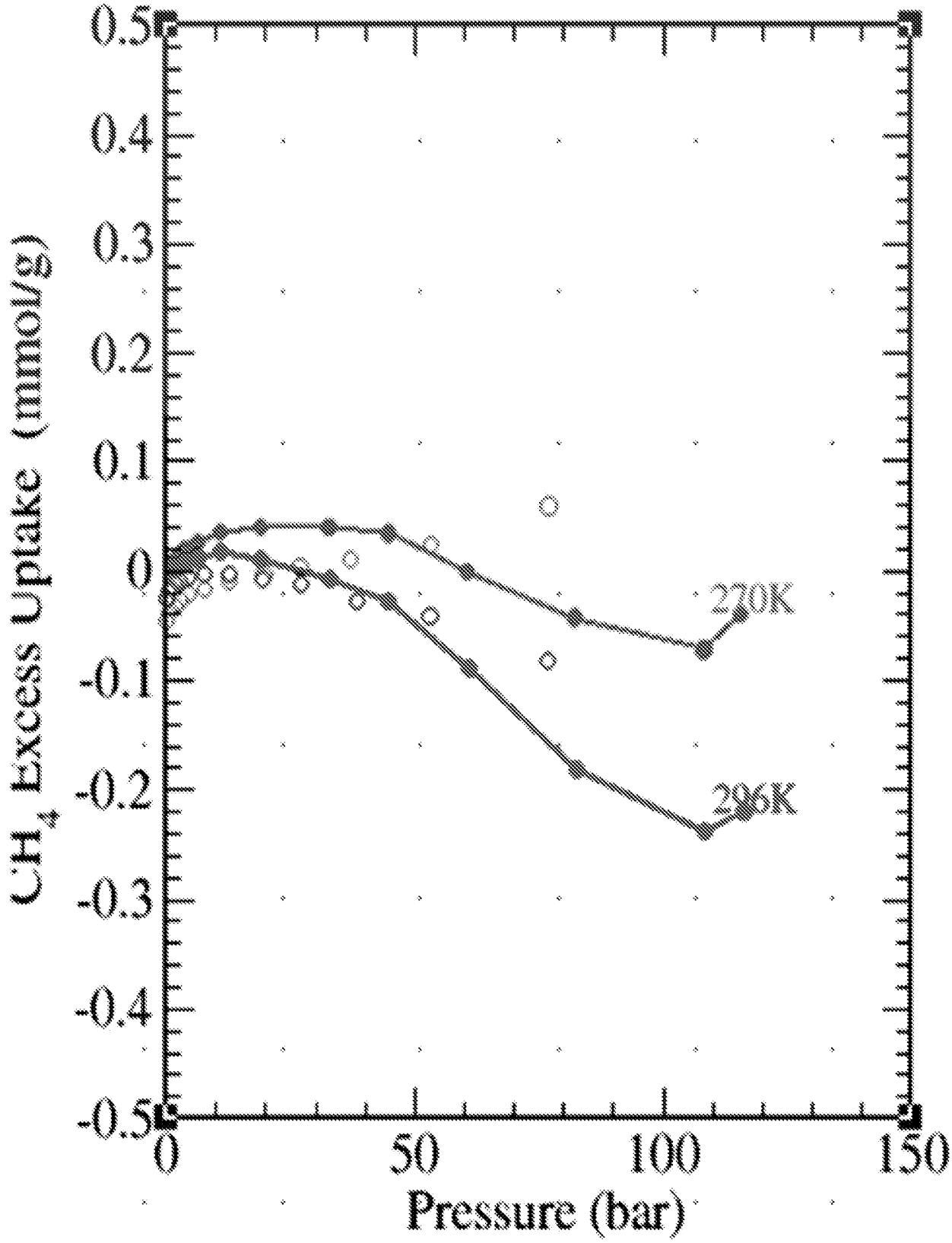
0.5
0.4
0.3
0.2
0.1
0
-0.1
-0.2
-0.3
-0.4
-0.5
0
50
100
150
CH4 Excess Uptake (mmol/g)
Pressure (bar)
270K
296K

FIG. 28

Temperature	b	q_{max} (mmol/g)
120 K	0.734451	5.548472
160 K	0.090133	5.087957
200 K	0.024276	4.638544
233 K	0.011965	4.140648
273 K	0.006104	3.778141
296 K	0.003887	4.096019

FIG. 29

ALF (property)	Value
Formula (conv. cell)	Al C_3 H_3 O_6 (Z = 8)
Molecular weight	1295.86 g/mol
Density	1.46 g/cc
Pore Limiting Diameter (PLD)	1.97 Å
Largest Cavity Diameter (LCD)	4.54 Å
Total Surface Area (He-probe)	11.71 m^2/g
Pore Volume (He-probe)	0.195 cc/g

FIG. 30

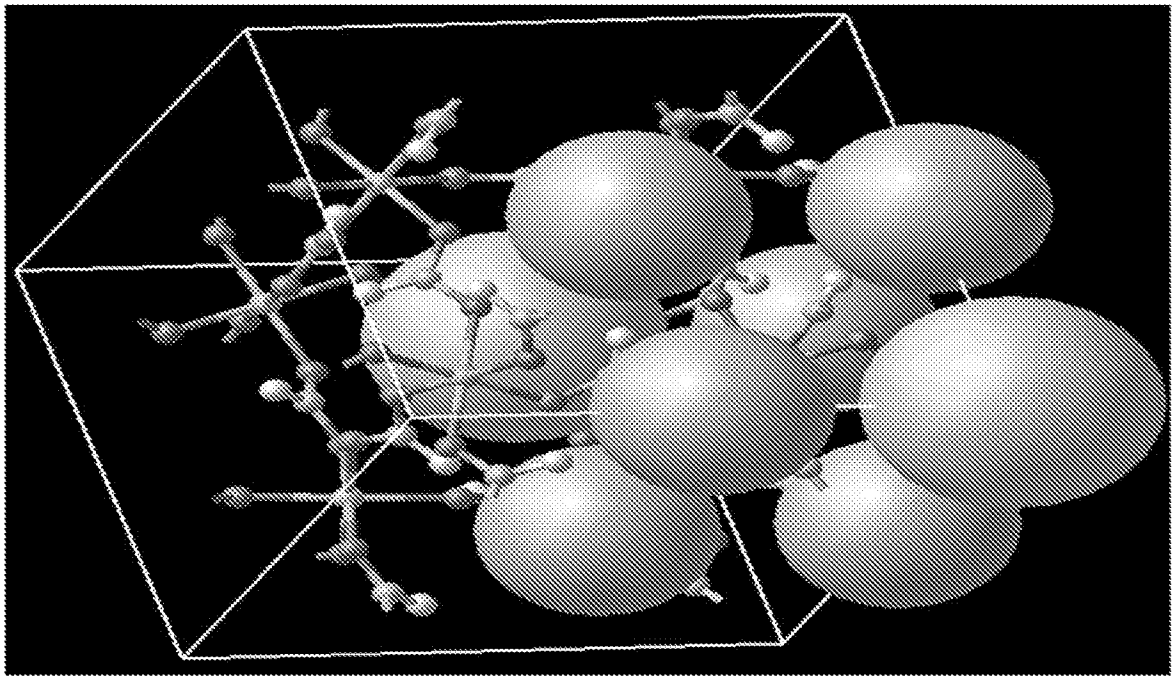

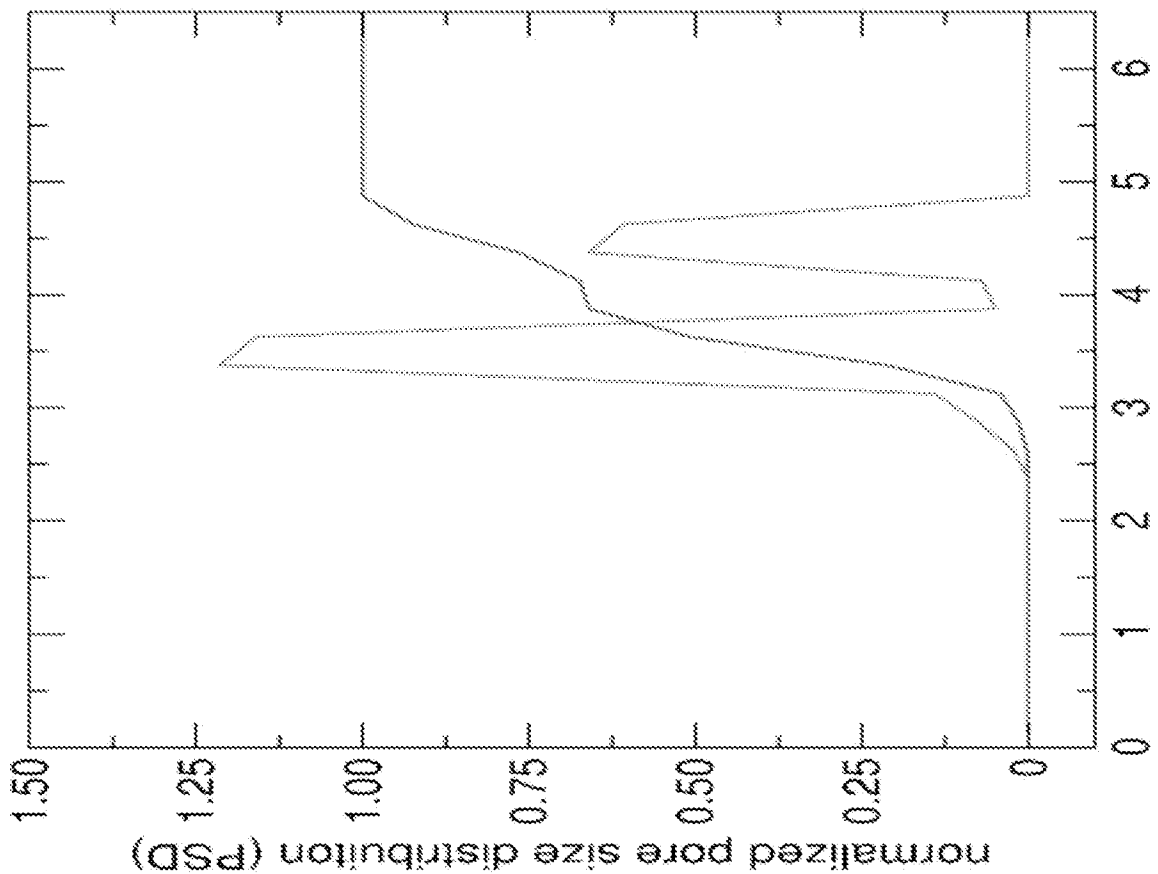
normalized pore size distribution (PSD)
1.50
1.25
1.00
0.75
0.50
0.25
0
0
1
2
3
4
5
6
pore size diameter (Å)

FIG. 31

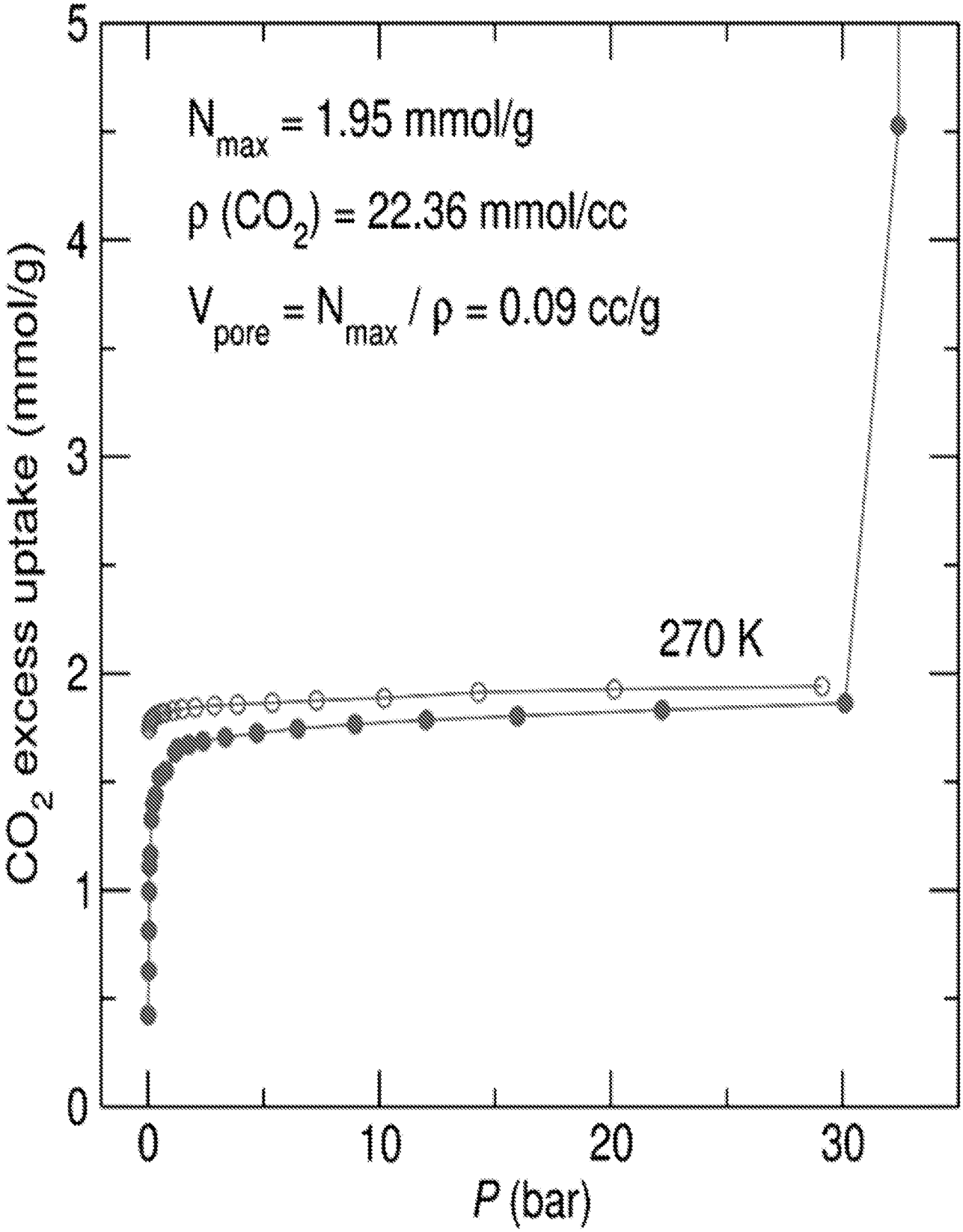
N_{max} = 1.95 mmol/g
ρ (CO_2) = 22.36 mmol/cc
V_{pore} = N_{max} / ρ = 0.09 cc/g
270 K
CO_2 excess uptake (mmol/g)
0
1
2
3
4
5
0
10
20
30
P (bar)

FIG. 32

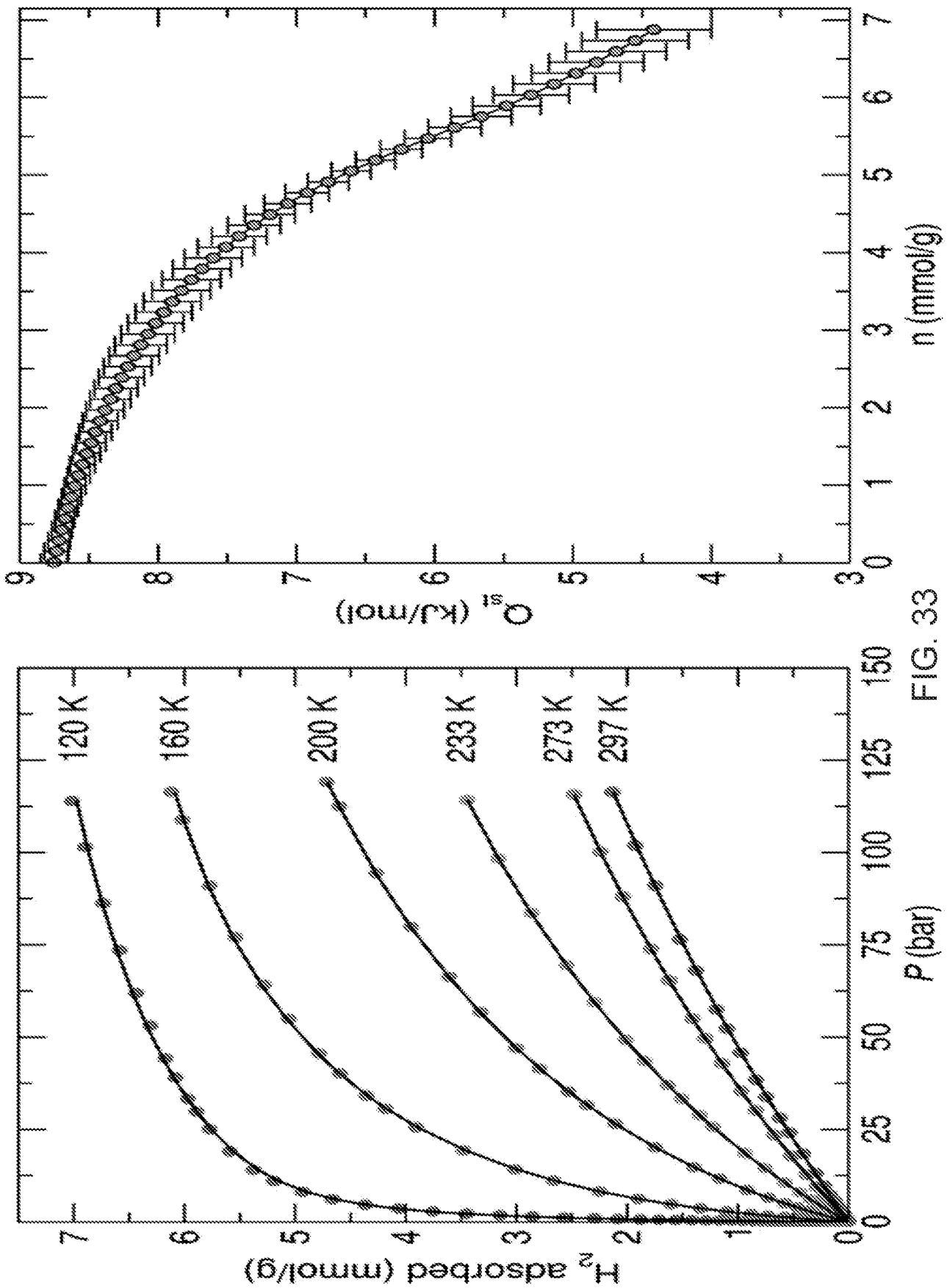
Q_{st} (kJ/mol)
n (mmol/g)
H_2 adsorbed (mmol/g)
P (bar)
120 K
160 K
200 K
233 K
273 K
297 K

FIG. 33

Temp. (K)	Q_{max1}	b_1	Q_{max2}	b_2
120.0	5.4222	0.7625	3.0401	0.0099
160.0	2.7171	0.1553	4.9665	0.0207
200.0	1.3421	0.0524	6.8491	0.0091
233.0	0.8046	0.0247	7.4360	0.0054
273.0	0.7114	0.0039	7.2895	0.0039
296.0	1.6337	0.0025	7.7907	0.0025

FIG. 34

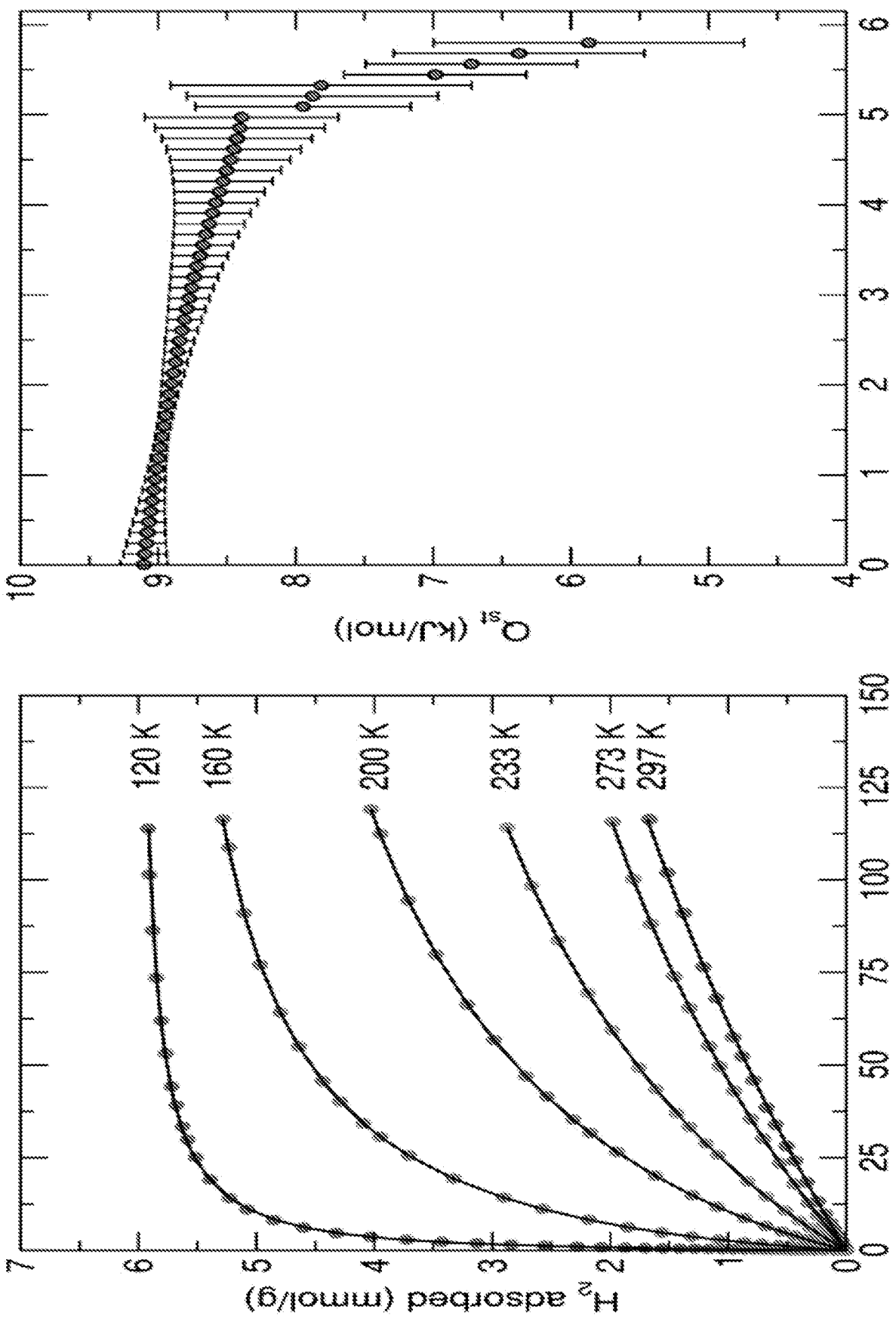
Q_{st} (kJ/mol)
10
9
8
7
6
5
4
0
1
2
3
4
5
6
n (mmol/g)
H_2 adsorbed (mmol/g)
7
6
5
4
3
2
1
0
0
25
50
75
100
125
150
P (bar)
120 K
160 K
200 K
233 K
273 K
297 K

FIG. 35

Temp. (K)	Q_{max1}	b_1	Q_{max2}	b_2
120.0	5.0399	0.8142	1.0072	0.1002
160.0	1.3381	0.2295	4.7369	0.0463
200.0	0.6616	0.0718	5.4136	0.0146
233.0	0.1789	0.0446	5.5224	0.0085
273.0	0.0000	0.0102	5.6180	0.0047
296.0	0.8114	0.0027	6.2745	0.0027

FIG. 36

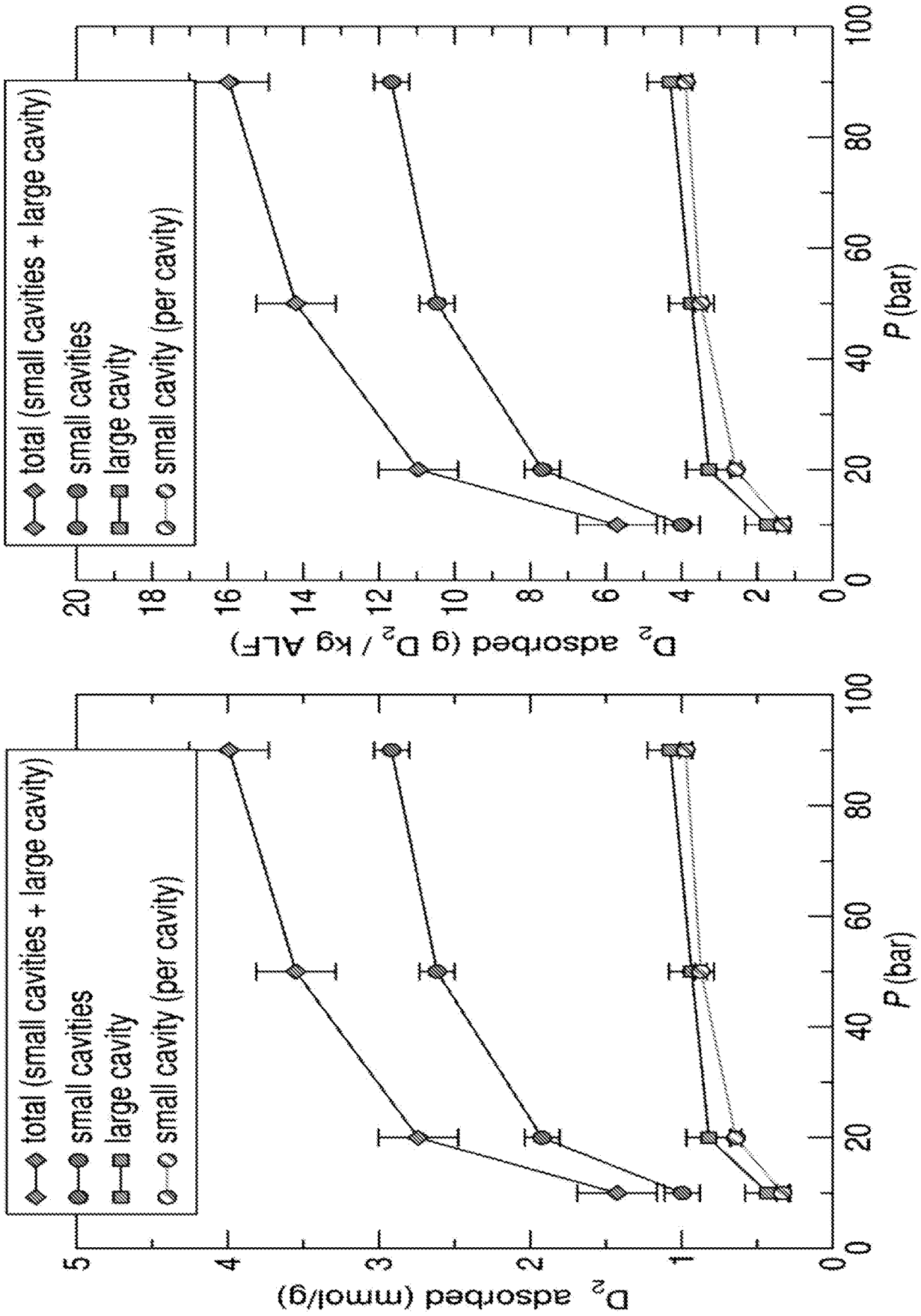
total (small cavities + large cavity)
small cavities
large cavity
small cavity (per cavity)
D2 adsorbed (mmol/g)
P (bar)
D2 adsorbed (g D2 / kg ALF)
P (bar)

FIG. 37

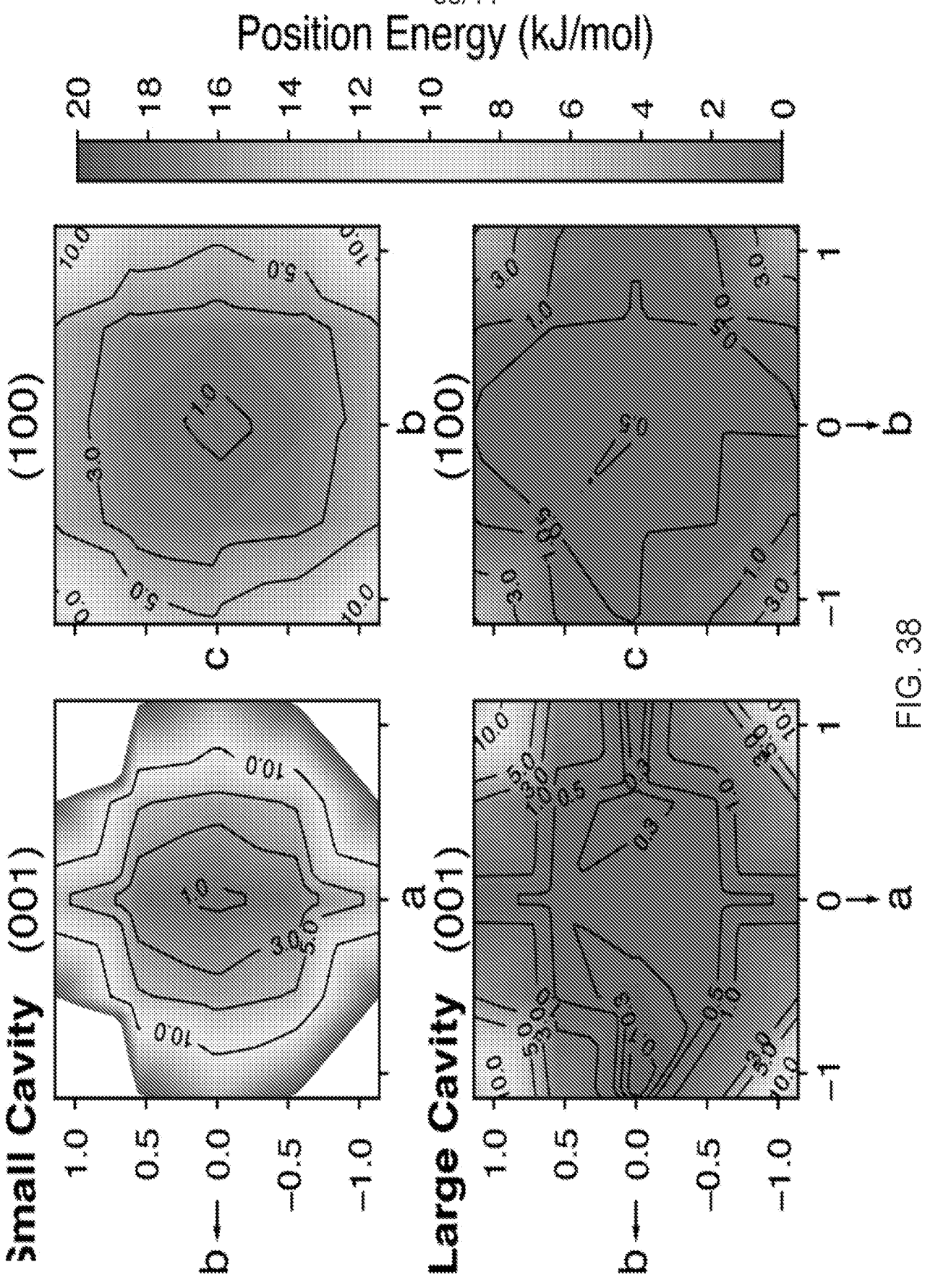
Position Energy (kJ/mol)
20
18
16
14
12
10
8
6
4
2
0
Small Cavity (001)
Large Cavity (001)
(100)
(100)
a
b
c
1.0
0.5
0.0
−0.5
−1.0
0
1
−1

FIG. 38

Element	x	y	z
Al	0.25	0.25	0.25
C	0.26077 (0.2600)	0.24217 (0.2410)	0
H	0.792702 (0.8101)	0.67796 (0.6830)	0
O	0.903299 (0.90352)	0.709581 (0.7110)	0.197318 (0.2000)

FIG. 39

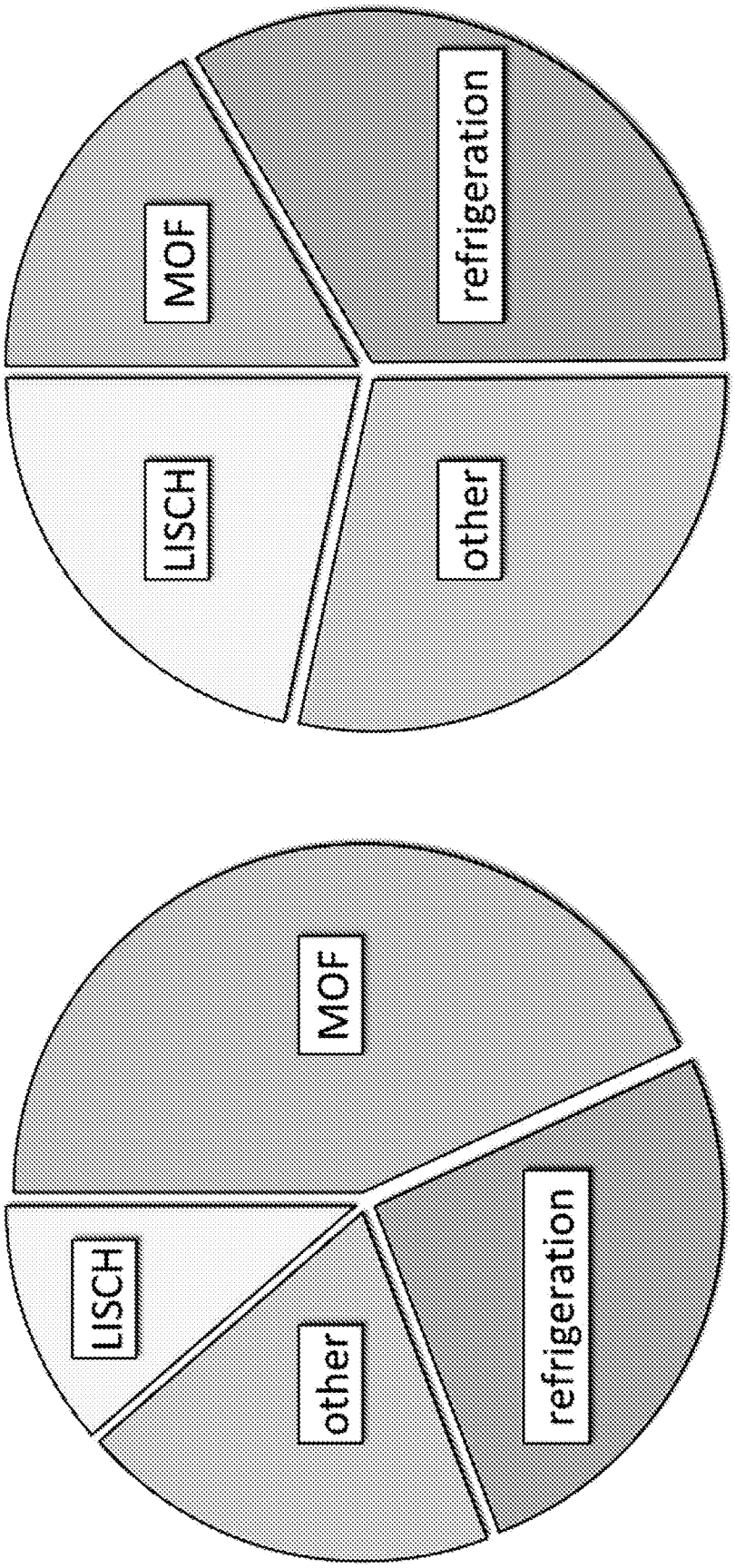
refrigeration
MOF
other
LISCH
MOF
refrigeration
other
LISCH

FIG. 40

Temperature	b	q_{max} (mmol/g)
120 K	0.734451	5.548472
160 K	0.090133	5.087957
200 K	0.024276	4.638544
233 K	0.011965	4.140648
273 K	0.006104	3.778141
296 K	0.003887	4.096019

FIG. 41

Compound	Wholesale cost range as of 04/2023 ($/kg)
Aluminum hydroxide	0.3 - 0.5
Formic acid	0.5 - 0.9
2,5-dihydroxyterephthalic acid	2 - 20
Nickel nitrate	3 - 15

FIG. 42

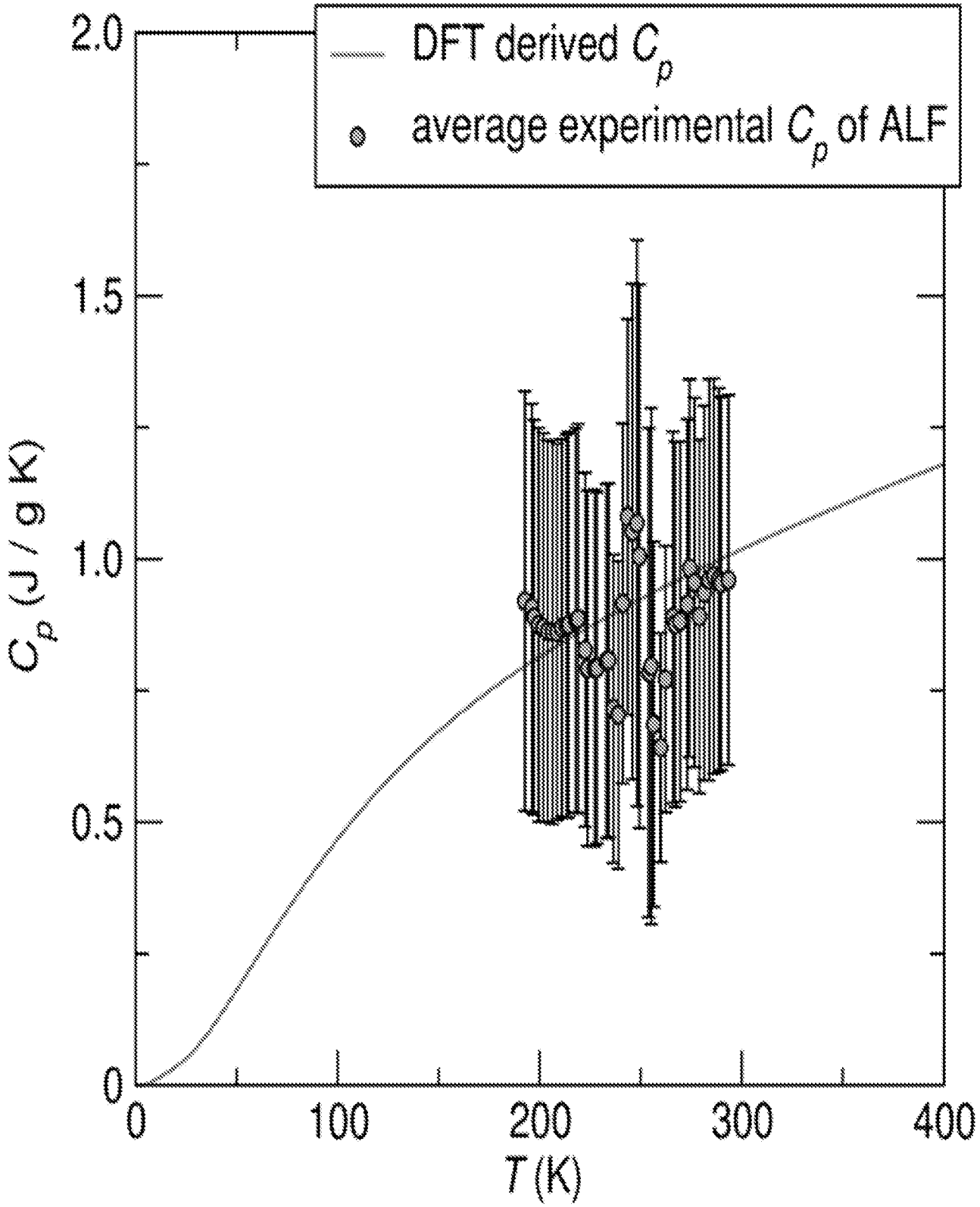
DFT derived C_p
average experimental C_p of ALF
C_p (J / g K)
2.0
1.5
1.0
0.5
0
0
100
200
300
400
T (K)

FIG. 43

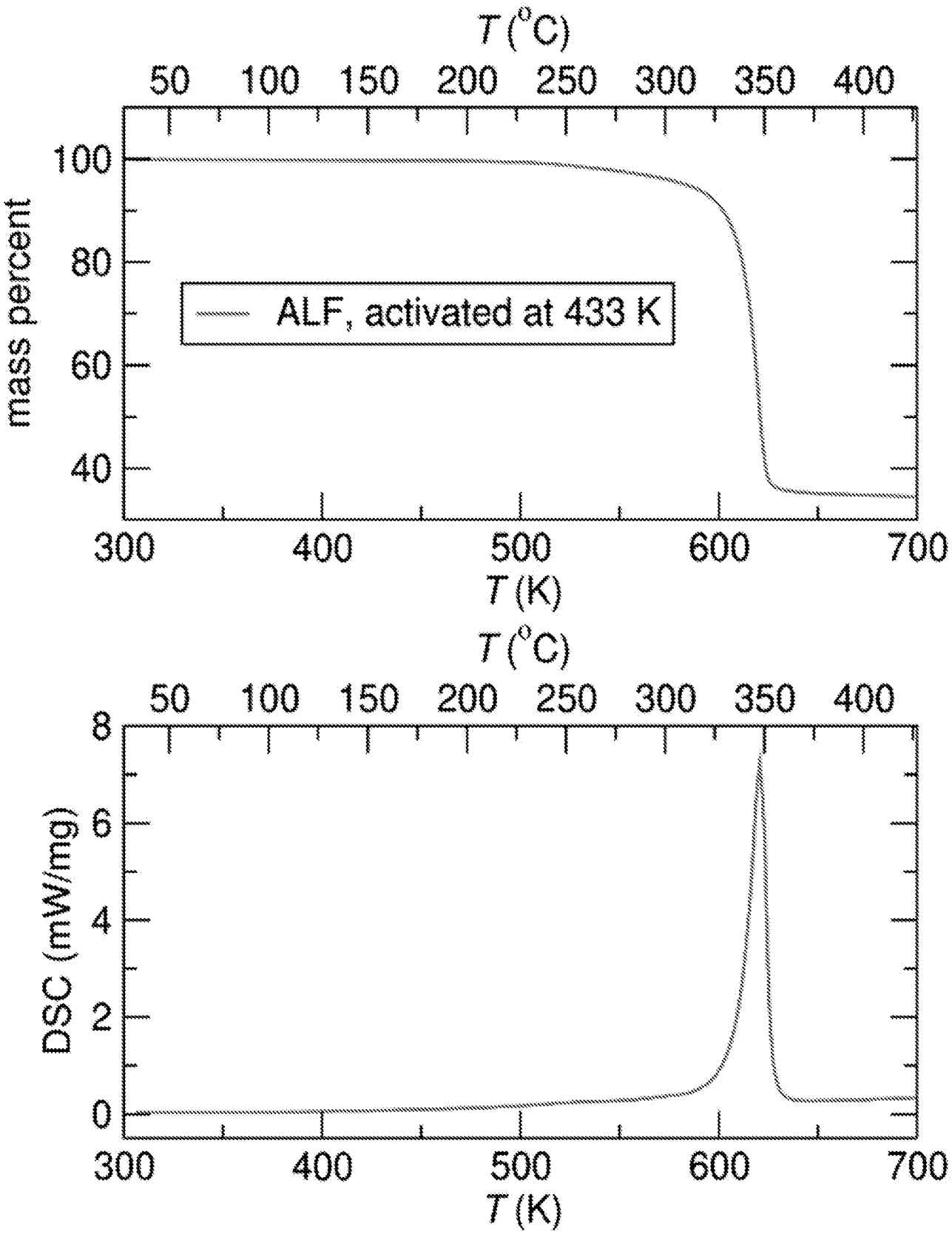
T (°C)
50 100 150 200 250 300 350 400
mass percent
100
80
60
40
ALF, activated at 433 K
300 400 500 600 700
T (K)
T (°C)
50 100 150 200 250 300 350 400
DSC (mW/mg)
8
6
4
2
0
300 400 500 600 700
T (K)

FIG. 44

INTERNATIONAL SEARCH REPORT

International application No
PCT/US2024/013659

A. CLASSIFICATION OF SUBJECT MATTER

INV. B01J20/22 B01D53/02 B01J20/28 C01B3/00 C01B3/50
C07F5/06 F17C11/00 B01D59/00
ADD.

According to International Patent Classification (IPC) or to both national classification and IPC

B. FIELDS SEARCHED

Minimum documentation searched (classification system followed by classification symbols)
B01J C01C B01D C01B C07F F17C

Documentation searched other than minimum documentation to the extent that such documents are included in the fields searched

Electronic data base consulted during the international search (name of data base and, where practicable, search terms used)
EPO-Internal, WPI Data

C. DOCUMENTS CONSIDERED TO BE RELEVANT

Category*	Citation of document, with indication, where appropriate, of the relevant passages	Relevant to claim No.
X	WO 2022/260592 A2 (NAT UNIV SINGAPORE [SG]; AGENCY SCIENCE TECH & RES [SG]) 15 December 2022 (2022-12-15) cited in the application	1-15
A	claims 1-20 figures 1-11,14-18,20-55 tables 1,2 examples 1,2,5,6	21-35, 45,46, 50-64

X	US 2008/184885 A1 (KIM KIMOON [KR] ET AL) 7 August 2008 (2008-08-07)	1
A	claims 1-7	21-35, 45,46, 50-64

	-/--	

[x] Further documents are listed in the continuation of Box C.

[x] See patent family annex.

* Special categories of cited documents :

"A" document defining the general state of the art which is not considered to be of particular relevance

"E" earlier application or patent but published on or after the international filing date

"L" document which may throw doubts on priority claim(s) or which is cited to establish the publication date of another citation or other special reason (as specified)

"O" document referring to an oral disclosure, use, exhibition or other means

"P" document published prior to the international filing date but later than the priority date claimed

"T" later document published after the international filing date or priority date and not in conflict with the application but cited to understand the principle or theory underlying the invention

"X" document of particular relevance;; the claimed invention cannot be considered novel or cannot be considered to involve an inventive step when the document is taken alone

"Y" document of particular relevance;; the claimed invention cannot be considered to involve an inventive step when the document is combined with one or more other such documents, such combination being obvious to a person skilled in the art

"&" document member of the same patent family

Date of the actual completion of the international search	Date of mailing of the international search report
31 May 2024	13/06/2024

Name and mailing address of the ISA/	Authorized officer
European Patent Office, P.B. 5818 Patentlaan 2 NL - 2280 HV Rijswijk Tel. (+31-70) 340-2040, Fax: (+31-70) 340-3016	Kaluza, Nicoleta

2

Form PCT/ISA/210 (second sheet) (April 2005)

INTERNATIONAL SEARCH REPORT

International application No
PCT/US2024/013659

C(Continuation). DOCUMENTS CONSIDERED TO BE RELEVANT

Category*	Citation of document, with indication, where appropriate, of the relevant passages	Relevant to claim No.
X	US 2003/148165 A1 (MULLER ULRICH [DE] ET AL) 7 August 2003 (2003-08-07)	1,16-20, 36-44, 47-49, 65-68
A	claims 1-7 paragraph [0038] examples 1,2	21-35, 45,46, 50-64

X	SHET SACHIN P ET AL: "A review on current trends in potential use of metal-organic framework for hydrogen storage", INTERNATIONAL JOURNAL OF HYDROGEN ENERGY, ELSEVIER, AMSTERDAM, NL, vol. 46, no. 21, 7 February 2021 (2021-02-07), pages 11782-11803, XP086521447, ISSN: 0360-3199, DOI: 10.1016/J.IJHYDENE.2021.01.020 [retrieved on 2021-02-07]	20, 36-44, 47-49, 65-68
A	table 1 Potential of MOF for hydrogen storage; page 11786 Stability of MOFs; page 11791, right-hand column - page 11792, left-hand column Opportunities for MOF in H2 storage; page 11798	21-35, 45,46, 50-64

X	EVANS HAYDEN A ET AL: "Perovskite-related ReO-type structures", NATURE REVIEWS MATERIALS, NATURE PUBLISHING GROUP UK, LONDON, vol. 5, no. 3, 22 January 2020 (2020-01-22), pages 196-213, XP037055427, DOI: 10.1038/S41578-019-0160-X [retrieved on 2020-01-22] Metal-organic frameworks; page 206, right-hand column - page 209, right-hand column	1-3,7, 12,15

T	HAYDEN A. EVANS: "Hydrogen Storage with Aluminum Formate, ALF: Experimental, Computational, and Technoeconomic Studies", JOURNAL OF THE AMERICAN CHEMICAL SOCIETY, [Online] vol. 145, no. 40, 28 September 2023 (2023-09-28), pages 22150-22157, XP093168559, ISSN: 0002-7863, DOI: 10.1021/jacs.3c08037 Retrieved from the Internet: URL:https://pubs.acs.org/doi/pdf/10.1021/jacs.3c08037> [retrieved on 2024-05-27] the whole document	1-68

2

INTERNATIONAL SEARCH REPORT

Information on patent family members

International application No
PCT/US2024/013659

Patent document cited in search report	Publication date	Patent family member(s)	Publication date
WO 2022260592 A2	15-12-2022	AU 2022290228 A1	04-01-2024
		CA 3221541 A1	15-12-2022
		EP 4352013 A2	17-04-2024
		WO 2022260592 A2	15-12-2022
US 2008184885 A1	07-08-2008	KR 20080073134 A	08-08-2008
		US 2008184885 A1	07-08-2008
		WO 2008096985 A1	14-08-2008
US 2003148165 A1	07-08-2003	CA 2391755 A1	01-08-2003
		CN 1617761 A	18-05-2005
		DE 20210139 U1	12-06-2003
		EP 1471997 A1	03-11-2004
		IS 7375 A	29-07-2004
		JP 2005525218 A	25-08-2005
		KR 20040096545 A	16-11-2004
		MX PA04007326 A	26-11-2004
		TW I304279 B	11-12-2008
		US 2003148165 A1	07-08-2003
		WO 03064030 A1	07-08-2003